Sensitive Measurement of Waterborne Parasites and Cell Culture Mycoplasma with Cantilever Sensor

A Thesis

Submitted to the Faculty

of

Drexel University

by

Sen Xu

in partial fulfillment of the

requirements for the degree

of

Doctor of Philosophy

December 2010

DEDICATION

To my parents and loved ones.

ACKNOWLEDGEMENTS

I would like to thank my advisor, Dr. Raj Mutharasan, for his guidance and support throughout the project. Without his input, this dissertation would not have been possible. I look up to him as a role model, not only in scientific research, but also in daily life.

Additional thanks to my committee members, Dr. Cameron Abrams, Dr. Richard Cairncross, Dr. Chuck Haas and Dr. Margaret Wheatley for their insights and valuable suggestions.

I would also like to extend my thanks all the lab partners for their helpful and constructive discussions; they are: Harsh Sharma, Ramji Lakshmanan, Blake Johnson, Yanjun Ding, Angela Leung, Kishan Rijal, David Maraldo and Pranam Shetty. During my study in Drexel, I have also received help from fellow graduate students. I would like to thank them all as well. I would also like to thank Dan Luu for technical support and fabrication assistance. Fundings from the government agencies (EPA and NSF) are also appreciated.

Finally, I would like to thank my parents and my sister for their love and care. They are the source of my strength.

TABLE OF CONTENTS

LIST OF TABLES

LIST OF FIGURES

Abstract

Sensitive Measurement of Waterborne Parasites and Cell Culture Mycoplasma with Cantilever Sensor

Sen Xu

Raj Mutharasan, Ph.D., Advisor

The objective of the research presented in this dissertation is to develop rapid and sensitive assays for waterborne parasites and mycoplasma contamination detection, as well as assess viability of these targets using piezoelectric excited millimeter-sized cantilever (PEMC) sensor.

Molecular and traditional culture methods in current use are time-consuming and laborious. PEMC sensor is a novel type of mass-sensitive sensor that enables rapid detection in liquid at high sensitivity. Typically it was functionalized with specific antibodies and exposed to the target analytes in a flow apparatus. When analytes bind to the antibody, mass of the sensor increases and causes decrease of sensor's resonant frequency. Real-time monitoring of resonant frequency changes was used for low concentration analytes detection. Limit of detection (LOD) for *C. parvum* was found to be 5 oocysts/mL, for *G. lamblia* was found to be 10 cysts/mL in buffers and in complex matrixes (milk, tap water and river water). LOD for mycoplasma (*Acholeplasma laidlawii*) was found to be 1,000 CFU/mL in cell culture samples. Detection was confirmed with second antibody binding or low pH release or scanning electron

microscope. Operating in complex matrixes showed lower sensor response and slower binding kinetics, which are attributed to the hindering of antigen transport and masking of antibody sites by alien material. A novel method was developed for cell viability assessment using a dye that accumulates in viable cells and not in dead cells. PEMC sensor was successfully used for sensing mass change caused by 2',7'-bis(2-carboxyethyl)-5,6-carboxyfluorescein (BCECF) accumulation in viable *E. coli* cells.

At a fundamental level, a novel measurement method based on monitoring sensor impedance magnitude was shown to be feasible. Impedance magnitude of the sensor was monitored not at resonant frequency, but at a fixed frequency near the initial resonant frequency. Results showed that impedance monitoring at a fixed frequency provides measurement equivalent to resonant frequency, with superior signal-to-noise ratio. Minute liquid density changes and antigen-antibody interactions were measured using this approach. This alternate approach lends itself to a simplified implementation for either a single sensor or a bank of multiple sensors. Because of its simplicity, the method would be suitable for high-throughput systems where multiple sensors are used simultaneously.

CHAPTER 1 : INTRODUCTION

1.1. Background

Detection of biological entities is of great importance in medical diagnostics, environmental monitoring, food safety, as well as biothreat detection. Traditional methods such as colony and plate counting, polymerase chain reaction (PCR) and enzyme-linked immunosorbent assay (ELISA) have been widely used for such purpose. These methods have good accuracy and sensitivity, as well as reliability. However, several drawbacks, such as tedious procedures, long turn-around time (timely decision cannot be made) and unavailability for easy field deployment plague them. These factors are the motivation for alternative methods development for rapid biological detection.

Over the past ten years, biosensors have drawn a great deal of attentions due to their simplicity, low cost, short time for time-to-results (TTR), sensitivity and selectivity. A typical biosensor contains three main components: a biorecognition element, a transducer and a read-out system [1]. The biosensors reported in the literature can be broadly divided based on transduction mechanism used; namely, optical, electrochemical, electromechanical and others. In a typical biosensor, the biorecognition element is a receptor, antibody, ssDNA, or another entity that provides molecular recognition. It is immobilized on the sensor surface and its interaction with the target analyte (pathogens, toxins, proteins, DNAs, etc.) is transduced into a measureable signal. In general, the transduced signal is proportional to the strength of interaction, often interpreted as binding.

Sensing platforms that do not require labeling steps are attractive in biological applications as labeling introduces variability and reduces avidity. Label-free methods are

intrinsically superior due to lower uncertainty caused by labeling. Since labeling occurs at various sites, the response of each labeled biomolecule may not be equal, and this leads to variability and uncertainty in the results at ultralow concentration of target. This is not of concern at higher concentration. Label-free detection reduces both time and effort required in assay development while at the same time practical issues related to shelf life and photo-quenching are avoided. Although a large number of sensor designs and methods for label-free detection have been described in the literature, only a few are commercially available. Among them surface plasmon resonance (SPR) and quartz crystal microbalance (QCM) are attractive techniques and have been applied widely for biological applications.

Cantilever biosensor is another label-free method suitable for biological detection, and holds great promise for rapid high-throughput assays due to its extraordinarily high sensitivity and scalability(Goeders 2008, Lavrik 2004, Raiteri 2001, Waggoner 2007). Recent research has demonstrated feasibility of detecting biological entities in liquid in picogram (10^{-12} g) to femtogram (10^{-15} g) range, and sensitivity at concentrations of nM (10^{-9} M) to fM (10^{-15} M) [2, 3]. Detection of oligonucleotides [4, 5], proteins [6-8], pathogens [9, 10] and other biological entities [11] have been widely investigated using both bending- and resonant-mode cantilever sensors. In our laboratory, a piezoelectric-excited millimeter-sized cantilever (PEMC) sensor was developed for highly sensitive detection of pathogens, toxin, proteins [12], biomolecules [13] and DNA hybridization [3] in a flow arrangement.

The overall goal of the research described in this dissertation is to examine PEMC sensor for sensitive detecting and quantifying waterborne parasites in real world media

and mycoplasma in cell culture samples at very low concentration, as well as developing a measurement method for high-throughput assays. In addition, examination of cell viability is to be explored.

1.2. Objectives

Waterborne parasites, *Cryptosporidium parvum* and *Giardia lamblia*, impose great health concern due to their common existence in source water and their hardy nature. Cell lines in research laboratories and industrial bioreactors are often infected with mycoplasmas, which require long time for positive detection. In this research, PEMC sensor, which is label-free and ultrasensitive, was examined for detecting waterborne parasites as well as mycoplasmas. Cell viability measurement on the sensor surface was examined for developing virulent pathogens detection method using *E. coli* as surrogate.

The specific objectives of my study are described as follows.

1. Can impedance at a fixed frequency be used as an alternative measurement parameter for PEMC sensor that would be suitable for high-throughput applications?
2. What is the limit of detection (LOD) for PEMC sensor for detection of waterborne parasites (*C. parvum* and *G. lamblia*) in both buffer and complex matrixes (milk, tap water and river water)?
3. Can a PEMC sensor be used at high flow rates (1-20 mL/min) for rapid processing of one liter river water samples?

4. Can a PEMC sensor based method be useful for sensitive and selective detection of targets that have low avidity antibodies? An example is mycoplasma.
5. Can a PEMC sensor be used for rapid cell viability measurement?

1.3. Contributions

The main contributions of this research are:

1. Impedance method is as effective as resonant frequency measurement for cantilever sensor. This will provide potential cost advantage when large group of sensors are used at the same time. Effectiveness of using impedance method for minute density change and *E. coli* O157:H7 detection were reported in *Sensors and Actuators B: Chemical* 143 (2009) 144-151 and *Sensors and Actuators B: Chemical* 145 (2010) 601-604. Details in Chapter 3.
2. Developed cantilever-based assay for rapid detection of *C. parvum* in PBS and in 25% milk samples at as low as 5 oocysts/mL. Demonstrated correlations between *C. parvum* concentration and sensor response to a second antibody and was reported in *Analytica Chimica Acta* 669 (2010) 81-86. Details in Chapter 4.
3. Developed cantilever-based assay for rapid detection of *G. lamblia* in finished and source waters at as low as 10 cysts/mL. Evaluated flow rate effect on *G. lamblia* attachment and sensor response. These results were reported in *Environmental Science and Technology* 44 (2010) 1736-1741. Details in Chapter 5.

4. Successfully demonstrated 1 cysts/mL detection feasibility for *G. lamblia* in a one liter sample at 5.0 mL/min. Details in Chapter 5.
5. Developed cantilever-based assay for rapid detection of mycoplasma contamination (*Acholeplasma laidlawii*) in cell culture samples at 1,000 CFU/mL and achieved four orders higher sensitivity than ELISA method, which was reported in *Biotechnology and Bioengineering* 105 (2010) 1069-1077. Details in Chapter 6.
6. Assessed viability of *E. coli* cells on cantilever sensor surface using a fluorescence dye (2',7'-bis(2-carboxyethyl)-5,6-carboxyfluorescein, acetoxymethyl ester, BCECF-AM). Confirmed cell viability using the growth method on the sensor surface. This study was reported in *Analytical Chemistry* (2010). Details in Chapter 7.

CHAPTER 2 : BIOSENSORS BACKGROUND AND LITERATURE REVIEW

2.1. Biosensors

Biological contaminants, if left undetected, can detrimentally impact both public safety and economy. The Environmental Protection Agency (EPA) has identified a list of microbiological contaminants that are known or anticipated to occur in public water systems and it is called the contaminant candidate list (CCL) [14]. In bioprocess industry, it is recommended for routine detection of mycoplasma contaminations to ensure biological products quality. Culture and colony counting methods, polymerase chain reaction and immuno-based laboratory methods provide highly accurate and reproducible results widely used for both qualitative and quantitative identification of microbial contaminants. Although these methods provide selective and reliable measurements, they have several shortcomings, including the need for trained personnel and extended time to obtain results. As a consequence, timely management decisions are not made. Hence, there is a need for rapid and inexpensive methods for pathogen detection. In the last ten years a great deal of research on the development of biosensors for biological detection has occurred in an attempt to meet this challenge. This chapter will examine some of the current biosensor technologies used for detection of pathogens, viruses and toxins, as well as summarize commercially available platforms.

The definition of a biosensor, by the recommendation of the International Union of Pure and Applied Chemistry (IUPAC) in 1999, is a self-contained integrated device capable of providing selective quantitative or semi-quantitative analytical information using a biological recognition element. From the IUPAC definition, a biosensor consists

of three main components: the biorecognition molecule that recognizes and binds the target of interest with high selectivity, the transducer that converts the binding reaction into a measurable signal, and the output system which amplifies and displays the signal in a useful form. Figure 2.1 shows a schematic representation of these three components. Compared to conventional analytical and culture methods, biosensors offer significant advantages of being rapid, cost-effective and field portable. These features have attracted a great deal of interest in developing biosensors for biological detection and environmental monitoring. Several reviews on biosensors for environmental applications have been recently published [15-17].

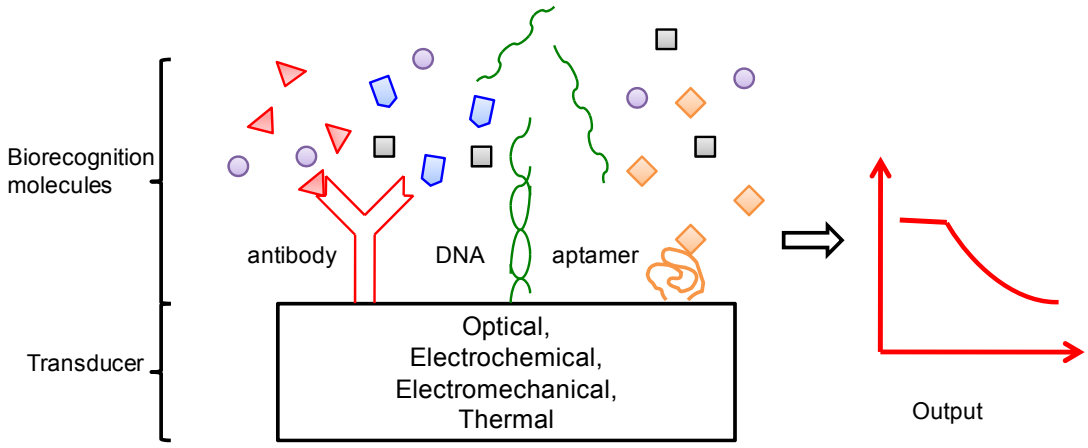

Figure 2-1. Components of a biosensor. Analytes attach to the transducer surface via biorecognition molecules. The binding of analytes is converted into a measurable electrical signal. The output system amplifies and displays the signal in a useful form.

In this chapter, the emphasis is on biosensors mechanism and surface chemistry. Biosensors are grouped according to the signal transduction used, and the most extensively investigated methods that exhibit effective performance are presented in

detail. Common methods of immobilizing biorecognition molecules in fabricating a biosensor are also presented.

2.2. Transduction mechanism of biosensors

Among the various transduction mechanisms investigated, three main methods have received most of the attention from biosensor researchers. They are *optical*, *electrochemical* and *electromechanical*. Other techniques, such as thermal and magnetic methods, have been less extensively investigated and are not included in this chapter.

2.2.1 Optical biosensors

Optical techniques are the most widely investigated method due to their speed, sensitivity and advantage of measuring non-destructively. Fluorescence- and chemiluminescence-based methods require labeled reagents. However, sensors that use optical resonance and interference do not require labeled reagents as they rely on refractive index (RI) changes that occur due to association or dissociation of target analytes.

2.2.1.1 Fluorescence and chemiluminescence

Fluorescence-based detection requires fluorescent agents that emit light at specific wavelengths when excited by a lower wavelength source. The enhancement or attenuation of the optical signal can indicate a binding reaction. For detection, antibodies or oligonucleotides are labeled with fluorescent molecules such as fluorescein isothiocyanate (FITC). Advancements in fluorescence detection have enabled both single

molecule detection [18] and single-nucleotide mismatch discrimination [19]. Fluorescence detection can also be combined with established methods such as PCR and ELISA for designing sensitive assays. Although the sensitivity of fluorescence methods is very high, as in single molecule detection, fluorescent labeling may interfere with the function of the biomolecules, thus changing kinetics or specificity of binding.

Nanomaterials, such as quantum dots (QDs) and nanoparticles have been employed for fluorescence assays and have shown high detection sensitivity. Changes in the optical properties of nanoparticles due to target binding can be used for detecting DNA hybridization and the presence of target protein at ultralow concentrations [20, 21]. QDs have been widely used as fluorescent dyes and probes for biomolecules. They have the potential to replace conventional fluorescent reagents in bioassays due to their broad excitation spectra, sharp emission spectra, and easily tunable emission properties.

Chemiluminescence (CL) or bioluminescence is the emission of light resulting from a chemical reaction. In electrochemiluminescence (ECL), which is widely used for sensing, the luminescence is initiated and controlled by electrode voltage. The advantage of CL over fluorescence methods is the absence of a light source and the associated electronics. CL measurement has advanced rapidly in recent years due to advancements in electronic sensing devices such as the charged coupled detector (CCD) which has been widely applied in the analysis of inorganic, organic and biological compounds. In addition, CL sensors can be coupled with gas or liquid chromatography, or capillary electrophoresis to provide additional analytical data.

2.2.1.2 Surface plasmon resonance (SPR)

A surface plasmon wave (SPW) is an electromagnetic wave that occurs along the boundary between two media with opposite signs of dielectric constants, such as a metal and a dielectric. The propagation constant of the plasmon (β_{sp}) is given by [22]:

$$\beta_{sp} = \frac{2\pi}{\lambda}\sqrt{\frac{\varepsilon_m \varepsilon_d}{\varepsilon_m + \varepsilon_d}} \tag{2.1}$$

where λ is the wavelength in vacuum and ε_m and ε_d are the dielectric constants of the metal film and the dielectric medium, respectively. Excitation of SPW occurs only when the component of light wave vector that is parallel to the metal surface matches β of the surface plasmon [23]. Various devices such as prisms, fibers, waveguides and gratings have been investigated to enhance and couple the source light with surface plasmons. Among them, the prism coupler is the most frequently used method, and is often found in commercial SPR sensors. In a prism coupler, the incident light passes through a high refractive index prism and is totally reflected to the base of the prism, generating an evanescent wave penetrating into the metal film. A typical optical path of a SPR biosensor using a prism coupler is illustrated in Figure 2.2A. The evanescent wave excites surface plasmons and coupling occurs when the propagation constant of the two waves are equal as specified by the criterion:

$$\frac{2\pi}{\lambda} n_p \sin\theta = \beta_{sp} \tag{2.2}$$

where θ is the angle of incidence, n_p is the refractive index of the prism, and λ is the incident wavelength. By controlling the incident angle, one can adjust the propagation constant of the evanescent wave so as to match that of the surface plasmon, thus realizing resonance.

The propagation constant β_{sp} is sensitive to changes in the dielectric RI. When analyte attaches to the recognition molecule immobilized on the metal surface, an increase in local refractive index occurs, causing an increase in β_{sp}. The light characteristics change through the coupling condition to accommodate this increase. By measuring this change, biomolecular interactions can be measured directly. The output signal depends on the coupling method used. For a prism coupler, the angle of incidence yields the strongest coupling, and is used as sensor output. When surface-immobilized antibodies bind with target analytes, the change in RI can be detected as a shift in the resonance angle and provides a measure of analyte concentration as shown in Figure 2.2A. Continuous monitoring of resonance angle shift or reflectance change at a fixed angle enables determination of the association and dissociation kinetics between recognition molecule and analyte.

SPR provides label-free, continuous real-time measurement of biomolecular interactions. It has excellent repeatability and speed for affinity measurement. The SPR sensor surface is regenerable and can sense proteins at picomolar to nanomolar concentrations. These attractive characteristics enable SPR to be applied as a compelling analytical instrument for liquid phase analysis in a research environment. A variety of assays for detecting chemical and biological agents have been reported, including *E. coli* O157:H7, *Salmonella enteritidis* and *Cryptosporidium parvum*, etc. Several excellent reviews have been published recently on detailed working platforms and chemical/biological targets examined [24-26]. The drawback of a full-fledged SPR instrument is its cost and size. Considerable research is ongoing with the goal of developing low cost miniaturized and multi-channel SPR instruments.

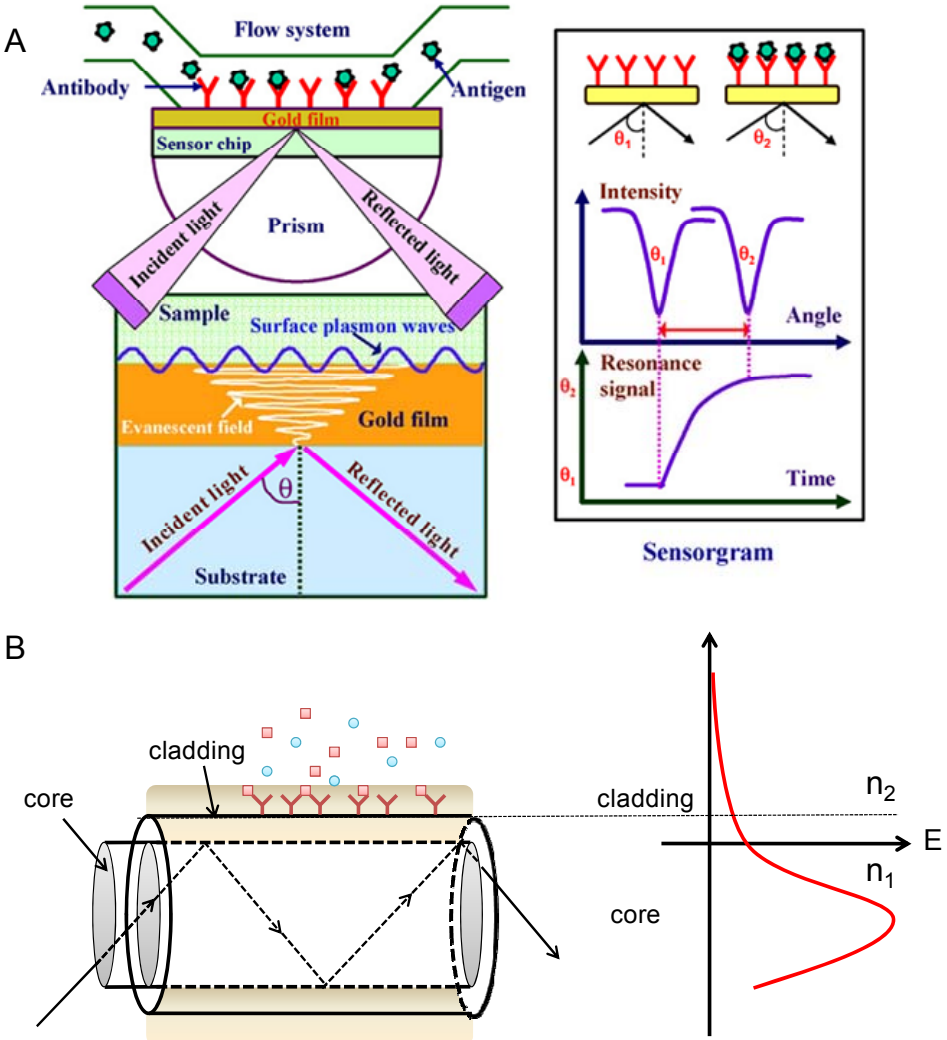

Figure 2-2. **(A)** Typical optical configuration of a surface plasmon resonance biosensor using a prism coupler. The sensor surface is coated with gold and immobilized with antibody specific to the analyte of interest. A liquid sample containing the target analyte flows across the sensor surface and binds to the antibody. Analyte binding causes a refractive index change that is transduced into resonant angle shifts from θ_1 to θ_2. The change is monitored non-invasively in real-time as a plot of resonance signal time profile. Reprinted with permission from Shankaran et al. (2007). **(B)** Schematic representation of a single mode optical fiber whose cladding has been removed to obtain access to the evanescent field. Propagation of light occurs by total internal reflection at the core-cladding interface. For evanescent wave fiber optic sensors, antibody is immobilized at the interface shown and analyte binding causes evanescent field changes resulting in optical throughput.

2.2.1.3 Fiber optic biosensors

Fiber optic biosensors use an inexpensive and commercially available optical fiber as a transduction element. These devices rely on the principle of total internal reflection (TIR) for light propagation. As shown in Figure 2.2B, the optical fiber is formed by a core with a refractive index, n_1, and a cladding with a lower refractive index, n_2. When source light strikes the core-cladding interface at an angle larger than the critical angle, θ_c ($\theta_c = \sin^{-1}\left(n_2 / n_1\right)$), it is totally internally reflected and thus propagates farther along the fiber.

Optical fiber biosensors may be divided into two broad groups based on the assay configurations: the optrode (optical + electrode) configuration and the evanescent wave configuration. Optrode configuration employs the light leaving the end of the fiber to generate a signal either at the distal end of the fiber or in the medium near the fiber end. Evanescent wave configuration relies on the electromagnetic component of the reflected light at the core-cladding interface for exciting the region at the surface, and thus reduces interference from the bulk solution.

Optrode sensors use glass or polymeric fibers with 50-500 μm diameters. Often dyes are coupled to the fiber end surface and the interaction of the analyte with the dye is converted into an optically detectable signal. Absorption, fluorescence and luminescence are the common optical phenomena that are monitored. Optrode biosensors can be connected to a fiber optic line for transmitting sensor signals over long distances, enabling remote applications.

When the incident light is totally internally reflected at the core-cladding interface in an optical fiber, its intensity does not abruptly decay to zero at the interface;

instead, an electromagnetic component of the light penetrates into the cladding over a distance of a small fraction of wavelength, which is called the evanescent wave (as shown in Figure 2.2B) [27]. The evanescent wave extends into the lower index medium and decays exponentially with distance. The penetration depth, d_p, defined as the distance at which the strength of the evanescent wave is *1/e* of its value at the surface, is typically about one hundred nanometers for wavelengths of 500 – 900 nm. This penetration depth is the main region of evanescent wave sensing. Hence, biological recognition molecules are immobilized on the surface of the fiber to ensure sensing is occurring within the penetration depth. Various designs and geometries of fibers, such as untapered and tapered fibers, have been investigated to accommodate specific sensing needs [28]. In addition, several fiber-based platforms have been examined, including fiber gratings, fiber-optic couplers, Fabry-Pertot cavity sensors and nanofibers. Fiber optic sensors can detect pathogens with 1 to 10^3 cells/mL sensitivity. Among these devices, fiber grating sensors are the most sensitive. A detailed review on fiber gratings was reported by Kersey et al. [29].

2.2.1.4 Interferometric biosensors

Interferometric biosensors use a variety of interferometric techniques in various configurations for measuring molecular binding events. Interferometry is an optical method that compares differences experienced by two light beams traveling along similar paths. It measures one of the three optical changes: wavelength (λ), path length (L), or speed ($v=c/n$, n is the refractive index) along the path of propagation. The change is reflected as a change in the phase (ϕ) of the light given by $\phi = 2\pi Ln / \lambda$. In biosensing

applications, biological interactions change the refractive index, which causes changes in properties of the propagating light. A reference beam and a sensing beam are combined to create an interference pattern of alternating dark and light fringes. The interference pattern shifts when the binding reaction occurs in the sensing channel and is measured as sensor output.

Various interferometers, such as Mach-Zehnder, Young, Hartman, Michelson, and backscattering have been reported [30]. Among them, the Mach-Zehnder interferometer has been most extensively investigated. It has two optical arms that split the source light equally into two arms. One arm is functionalized with biorecognition molecules and is exposed to the test sample while the other arm is protected from the sample using a thick cladding layer. At the output end the two light beams are mixed, and a photodetector detects the interference pattern. Instead of mixing the two light beams, a Young's interferometer keeps the light beams separated and a CCD camera captures the interference pattern. Interferometers are capable of detecting RI changes of 10^{-7}, which is estimated to correspond to $10^2 – 10^3$ whole cells, viruses or spores.

2.2.1.5 Other optical biosensors

Other optical biosensors, such as resonant mirrors [31], planar waveguides [32], reflectometric interference spectroscopy [33] and ring resonators [34] have been investigated for biosensing. Only limited biosensing investigations (e.g., pathogens detection) have been reported and therefore they are not discussed here. Excellent summary work has been done by Gorton [35] and Ligler and Rowe-Taitt [36].

2.2.1.6 Commercial optical biosensors

Selected commercially available optical biosensors and their suppliers are summarized in Table 2.1. SPR biosensors and fiber optic biosensors are the most popular ones. A miniaturized portable SPR, Spreeta™ is also available. Among the fiber optic biosensors, RAPTOR™ is a commercial product widely used for research purpose. Since optical biosensors development is an active research area, a large number of startup companies have begun developing prototypes and instruments for pathogen and toxin detection. Thus, Table 2.1 may not be a comprehensive list.

Table 2-1. Selected commercially available optical biosensors

Sensor type	Company	Products	Website
SPR	Biacore	BIAcore™ 1000, 2000, 3000, X, J, Q, S51, C models	www.biacore.com
	Biosensing Instrument	BI-2000, 2000G, 3000, 3000G, EC-DualFlow™	www.biosensingusa.com
	SENSIA	β-SPR	www.sensia.es
	IBIS	IBIS-iSPR	www.ibis-spr.nl
	ICx Nomadics	SensíQ®	www.discoversensiq.com
	Eco Chemie	Autolab Springle, Esprit	www.ecochemie.nl
	Texas Instruments	Spreeta™	www.ti.com
Optical fiber	Research International	RAPTOR™	www.resrchintl.com
	Illumina	BeadStation, iScan system	www.illumina.com
Interferometer	Farfield Group	AnaLight Bio200	www.farfield-group.com
	Fraunhofer IPM	IBS 201	www.ipm.fraunhofer.de
Fluorescence	Zeptosens	ZeptoREADER, ZeptoMARK chip	www.zeptosens.com
	Affymetrix	GeneChip® System	www.affymetrix.com

2.2.2 Electrochemical biosensors

Electrochemical biosensors are in essence electrochemical cells in which one of the electrodes (typically gold (Au)) is immobilized with a recognition molecule. When analytes bind, a change in electrical properties occurs depending on the measurement format used which provides the sensor signal. Compared with optical biosensors, turbid samples can be directly applied and pose little or no interference though sensitivity is slightly lower. Various electrical properties are measured for signal detection including voltage (potentiometric), current (amperometric), and conductivity (conductometric) [37-39].

2.2.2.1 Amperometric sensors

Typical amperometric biosensors measure electric current changes in the redox reaction associated with biosensing. A typical amperometric biosensor, as shown in Figure 2.3A, is the most common electrochemical sensor investigated. In this biosensor, an enzyme is immobilized at the surface of an amperometric electrode. The enzyme reacts with the applied substrate, producing an electrical current proportional to analyte concentration. The amperometric method is frequently used with a redox enzyme system that increases current signal proportional to analyte concentration. Due to the rich redox chemistry available, wide variety of systems can be utilized for sensor construction. Besides widely used for chemicals detection, amperometric sensors have been successfully used for detecting pathogens and toxins with various surface functionalization methods, including *E. coli* O157:H7 [40, 41], *Salmonella* [42] and Microcystin-LR (MC-LR) [43].

2.2.2.2 Potentiometric sensors

Potentiometric sensors measure the change in electric potential at the working electrode when target analyte binds to the biorecognition molecule immobilized on the measuring electrode. A typical potentiometric biosensor configuration is shown in Figure 2.3B. The sensor consists of an ion selective membrane covering the appropriate electrode and immobilized enzymes. The reaction catalyzed by the enzyme consumes or generates an ion and is detected by techniques such as ion-selective electrodes, ion selective field effect transistors (ISFETs), or chemical field effect transistors (ChemFETs) [44]. The sensing potential developed is governed by the Nernst equation, and thus the output is a logarithmic function of analyte concentration. Because of the logarithmic relationship, potentiometric sensors exhibit wide dynamic range and give sensitive response at low concentration. Potentiometric sensors have been used for detecting pathogens such as *E. coli* O157:H7 [45, 46] and *Legionella pneumophila* [47, 48].

2.2.2.3 Conductometric sensors

Conductometric sensors measure changes in the electrical impedance between two electrodes when a biomolecular reaction such as DNA hybridization or antibody-antigen binding occurs at the working electrode. A schematic conductometric biosensor is shown in Figure 2.3C. These sensors are attractive due to simplicity of design and ease of use. A specialized reference electrode is not needed. Conductometric sensors have been used to detect pathogens such as *E. coli* O157:H7 [49, 50].

With the development of nanotechnology, nanowires and carbon nanotubes in combination with field-effect transistor technology have drawn a lot of attention for

biosensing. Applications for detecting *E. coli* O157:H7 [51], DNA [52], RNA [53] and virus [54] have been recently reported.

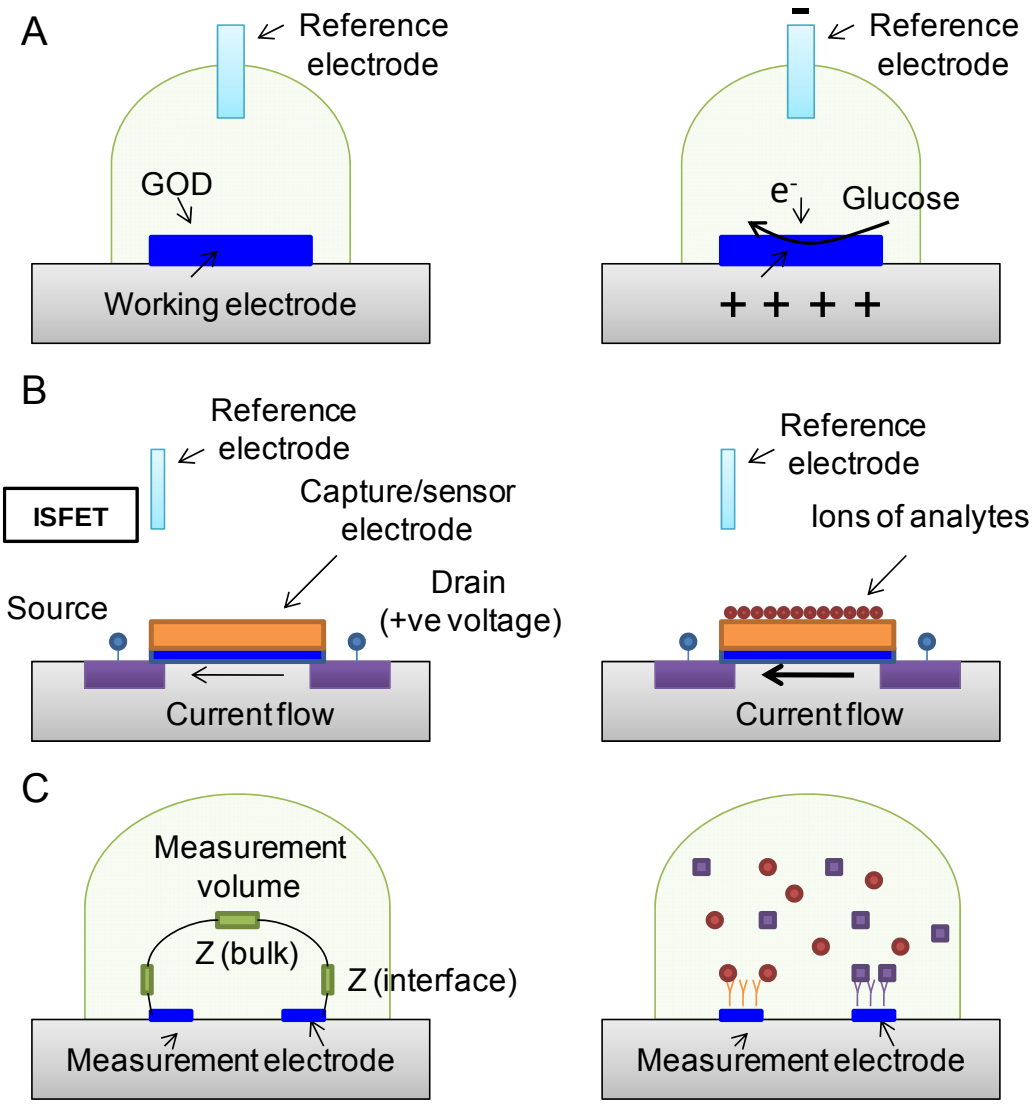

Figure 2-3. Schematic representation of electrochemical biosensors. **(A)** Amperometric sensors, **(B)** potentiometric sensors and **(C)** conductometric sensors. Adapted from Bashir (2004). In the above three sensors, binding of target analyte causes a change in current **(A)**, potential **(B)** or conductance or impedance **(C)**. Many arrangements of working, measuring and reference electrodes have been explored in the literature, and the above is a schematic representation of the transduction principle used.

2.2.2.4 Commercial electrochemical biosensors

Electrochemical biosensors were one of the earliest types of biosensors to be commercialized. The glucose biosensor, for example, is a successful commercial product with a large market volume. A group of suppliers share the glucose biosensor market. Selected commercially available electrochemical biosensors for pathogens detection and their suppliers are listed in Table 2.2. Companies such as Osmetech, CombiMatrix and AJ eBiochip market instruments for nucleic acids or protein microarrays based on electrochemical measurements. Applied BioPhysics markets instruments that use impedimetric measurements for investigating cell behavior. Although the use of these devices for pathogen detection is few, they have the measurement capability for detecting pathogens. Electrochemical sensors for chemical detection are not listed in the list.

Table 2-2. Selected commercially available electrochemical biosensors

Sensor type	Company	Products	Website
Amperometric	Osmetech	eSensor® XT-8, CFCD	www.osmetech.com
	CombiMatrix	ElectraSense™ Platform	www.combimatrix.com
	AJ eBiochip	eMicroLISA, eMicroLISA10	www.ebiochip.com
Impedimetric	Applied BioPhysics	ECIS Z, Zθ	www.biophysics.com

2.2.3 Electromechanical biosensors

Electromechanical biosensors are mass-change sensors that are attractive for pathogen detection as they are highly sensitive and do not require labeled reagents. Reported sensors in this category can be divided into two major groups: acoustic wave sensors and cantilever sensors. The former is made of quartz crystal that is electrically

stimulated and its resonant frequency changes when target analytes bind to its surface. Cantilever sensors reported in the literature either bend or resonate at a lower frequency as a result of analyte binding that induces surface stress or mass change. Electromechanical biosensors measure the mass of attached analytes directly. Since the extent of binding is proportional to concentration in the sample, the sensor response is directly proportional to analyte concentration.

2.2.3.1 Acoustic wave sensors

The functioning of acoustic wave devices is based on the propagation of bulk or surface launched acoustic waves in piezoelectric and other materials [55]. Most of the acoustic wave sensors require a piezoelectric material, such as quartz, for propagating acoustic waves. Application of an alternating electric field across a quartz crystal generates an oscillatory motion of the crystal which results in the generation of acoustic waves. The change in resonant frequency (Δf) of the crystal is used as the detection signal. Recently, other parameters (such as motional resistance, dissipation factor) have also been exploited when sensor is operating in liquid. Various modes of electromechanical coupling have been exploited to measure changes in resonant frequencies, including the thickness shear mode sensor (TSM), the surface acoustic wave sensor (SAW), the shear horizontal acoustic plate mode sensor (SH-APM), and the flexural plate wave sensor (FPW) [56]. Among these modes, TSM has been most frequently investigated for in-liquid applications and biological detections as liquid introduces less influence on sensor performance than others. Here we focus on TSM while other mechanisms are just briefly noted.

2.2.3.1.1. TSM sensors

TSM sensors, also called bulk acoustic wave (BAW) sensors or quartz crystal microbalance (QCM) sensors, have been widely investigated. Even though QCMs are less sensitive than FPW or SAW sensors, they are more robust, readily available and most importantly can be used with liquid samples. Although early work with QCM was in gas phase, applications to liquid samples enabled a series of investigations on biological samples [57]. Typically only one side of the crystal is exposed to liquid samples, but exposing both sides of the crystal to liquid was reported recently to enhance sensitivity [58, 59].

QCM consists of an AT-cut quartz crystal disc that exhibits piezoelectric behavior. Metal electrodes are deposited on opposite faces for applying alternating electric field, and the configuration is shown in Figure 2.4A. When an alternating electric field is applied, shear vibration orthogonal to the electric field is generated and propagation of a transverse shear wave occurs through the crystal in the thickness direction. It has been shown that the resonant frequency depends on the shear-wave velocity (v) and the quartz thickness (d_Q) and is given by [60]:

$$f = \frac{nv}{2d_Q} \tag{2.3}$$

An increase in mass bound to the quartz surface causes the crystal resonant frequency to decrease. Sauerbrey showed that there is a correlation between mass attached to the QCM and decrease in its resonant frequency, and is given by [61]:

$$\Delta f_m = -\frac{2f_0^2}{A\sqrt{\rho_q \mu_q}}\Delta m = -S_f \Delta m \tag{2.4}$$

where Δf is the measured resonant frequency decrease (Hz), f_0 is the intrinsic crystal resonant frequency, Δm is added mass (g), A is the crystal area, ρ_q is the density of quartz (2.65 g/cm^3), and μ_q is the shear modulus (2.95 × 10^{11} dyn/cm^2). S_f is the integral mass sensitivity, which depends on the square of the frequency and increases proportionally with crystal fundamental resonant frequency. One can quantify the mass attached to the surface at nanogram resolution. The Sauerbrey equation is valid for small changes in mass. It over-predicts the frequency shift when the added mass gives a frequency shift greater than about 2% of the unloaded resonant frequency. Another point to note is that the Sauerbrey model assumes that the added mass couples to the shear oscillatory motion of the crystal. When dealing with non-rigid films such as protein layers, this model may not provide an accurate value as such films would naturally deform. Additionally, the resonant frequency is affected not only by the mass loading but also by the viscous loading due to liquid. The frequency change of QCM due to fluid loading is expressed as [62]:

$$\Delta f_L = -f_0^{3/2} \frac{\sqrt{\rho_L \eta_L}}{\sqrt{\pi \rho_Q \mu_Q}} \tag{2.5}$$

where ρ_L is the fluid density and η_L is the fluid viscosity. When measuring the resonant frequency in liquid, one measures total frequency change $\Delta f = \Delta f_m + \Delta f_L$, and it is not possible to distinguish mass from liquid loading effect. To deconvolute these two contributions, electrical circuit models, such as the Butterworth-van Dyke (BVD) model, have been investigated. The BVD model combines a parallel and series resonance circuit. The motional branch consists of an inductor L_q, capacitor C_q and resistor R_q. The electrodes on both sides of the crystal plate provide an additional parallel capacitance C_0.

Motional resistance R_q contains intrinsic viscosities of the quartz and represents the energy dissipation component expressed as [63]:

$$R_q = \left(2\pi f \rho_L \eta_L\right)^{1/2} A / k^2 \tag{2.6}$$

where k is the electromechanical coupling factor. Mass and viscosity effects may be determined simultaneously by measuring the motional resistance and resonant frequency shift [64].

As pointed out earlier, when QCM is loaded with soft films, the Sauerbrey equation often fails to provide satisfactory prediction of mass uptake using frequency change values. By introducing a dissipation factor (D), the viscoelastic properties of the adsorbed mass and frequency shift can be distinguished [65-67]. The energy dissipation is a dimensionless value given by [66]:

$$D = \frac{1}{Q} = \frac{E_{dissipated}}{2\pi E_{stored}} \tag{2.7}$$

where Q is the quality value, E_{stored} is the energy stored in the oscillating system, and $E_{dissipated}$ is the energy dissipated during one period of oscillation. The dissipation factor can be directly measured using an impulse excitation technique [67]. QCM used in such a mode has become known as QCM-D, and is commercially available (Q-Sense, Goteborg, Sweden). Simultaneous measurement of both f and D allows calculation of the viscous and elastic components of the region immediately adjacent to the quartz crystal where analytes bind.

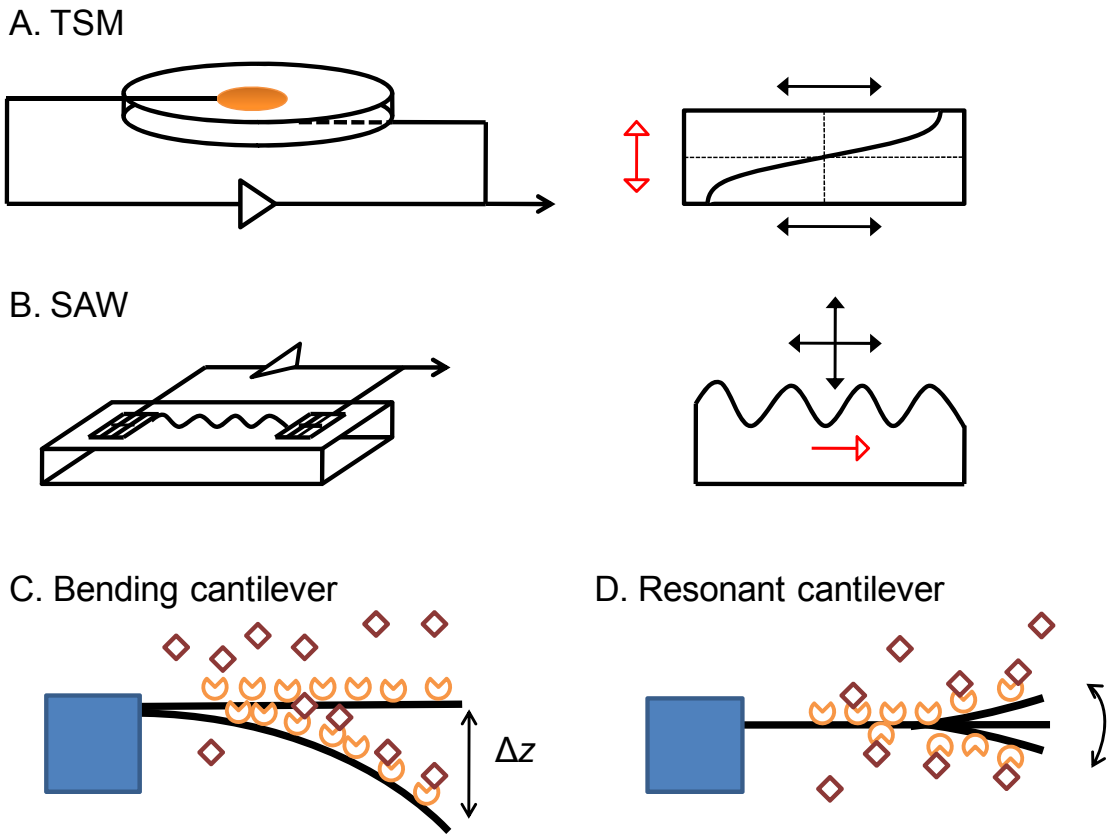

Figure 2-4. Illustration of **(A)** Thickness Shear Mode (TSM) resonator, **(B)** Surface Acoustic Wave (SAW) resonator, **(C)** Bending-mode and **(D)** Resonant-mode cantilever sensors. In TSM, the crystal deformation occurs through its thickness, while in SAW, acoustic waves generated on the crystal surface travel only on the surface to receiver electrodes. The direction of wave propagation is indicated by an open arrow and the particle displacement by a solid arrow. In bending mode, the cantilever deflects as surface stress changes, while in resonant mode resonant frequency decreases when target mass attaches.

2.2.3.1.2. SAW sensors

SAW sensors are comprised of two pairs of closely spaced interdigital electrodes separated by a region of piezoelectric substrate, commonly ST-cut quartz, and is shown in Figure 2.4B. An alternating electric field applied to the transmitter electrode pairs

produce periodic surface strain that launches a surface acoustic wave, whose frequency is given by $f = v_p / d$, where v_p is the propagation velocity and d is the distance between the interdigital electrodes. The interaction of the surface wave with attached analyte in the region between the two electrode arrays causes changes in the surface acoustic wave velocity and amplitude and is sensed by tracking frequency change. The influence of wave velocity change on the resonant frequency is expressed as [23]:

$$\frac{\Delta f}{f} = \frac{\Delta v}{v_p} = -c_f^{SAW} f \rho_s \tag{2.8}$$

where c_f^{SAW} denotes mass sensitivity and ρ_s is the surface mass density of the attached analyte layer. The application of SAW devices in liquid is significantly compromised due to high energy loss. Thus, in spite of higher sensitivity SAW sensors exhibit compared to QCM, they are not widely used for pathogen detection in liquid samples.

2.2.3.1.3. Other acoustic wave sensors

Other acoustic wave sensors, such as SH-APM sensors, FPW sensors and thin-rod acoustic wave sensors (TRAW) have been investigated for biosensing. However their application for pathogen detection in liquid sample are extremely few and are not discussed. A comprehensive book on the topic is available [23].

2.2.3.2. Cantilever sensors

Cantilever-based measurements were initially used in the context of atomic force microscopy (AFM) for surface characterization [68]. Over the past decade, they have

been adapted for detecting biomolecules and measuring biomolecular interactions. Cantilever sensors are operated in two modes: bending mode (or static mode), in which deflection is measured when analyte binds, and resonant mode (or dynamic mode), in which resonant frequency change is measured when analyte binds. Schematic representation of the two types of cantilevers is shown in Figure 2.4C and 2.4D. Various designs and geometries of cantilever sensors have been explored for sensitive detection, as shown in Figure 2.5. Details of these two types of cantilevers are further discussed.

2.2.3.2.1. Bending-mode cantilever sensors

Bending-mode cantilever sensors were the first to be applied for detection as their response measurement (deflection) instrumentation is the same as that used in AFM (see Figure 2.4C). The cantilevers convert the surface stress due to analyte binding into measurable deflection, which is given by [69]:

$$R = \frac{Et^2}{6\Delta\sigma(1-\upsilon)} \tag{2.9}$$

where R is the radius of cantilever curvature, E is the Young's modulus, t is the thickness, $\Delta\sigma$ is the differential surface stress across the cantilever surface, and υ is the Poisson's ratio. Decreasing radius of curvature will result in increased deflection at the free end of the cantilever. Tip displacement of a microcantilever of length l is given by:

$$\Delta z = \frac{3l^2(1-\upsilon)}{Et^2}\Delta\sigma \tag{2.10}$$

The above equation shows that deflection is directly proportional to the differential surface stress. Thus differential surface stress is calculated by measuring the

deflection. Deflection of a few tens of nanometers is measurable using various laser-based instrumentation systems. When optics are used to measure deflection, turbid liquid samples may present difficulties and impose a challenge for biological detection in complex matrix.

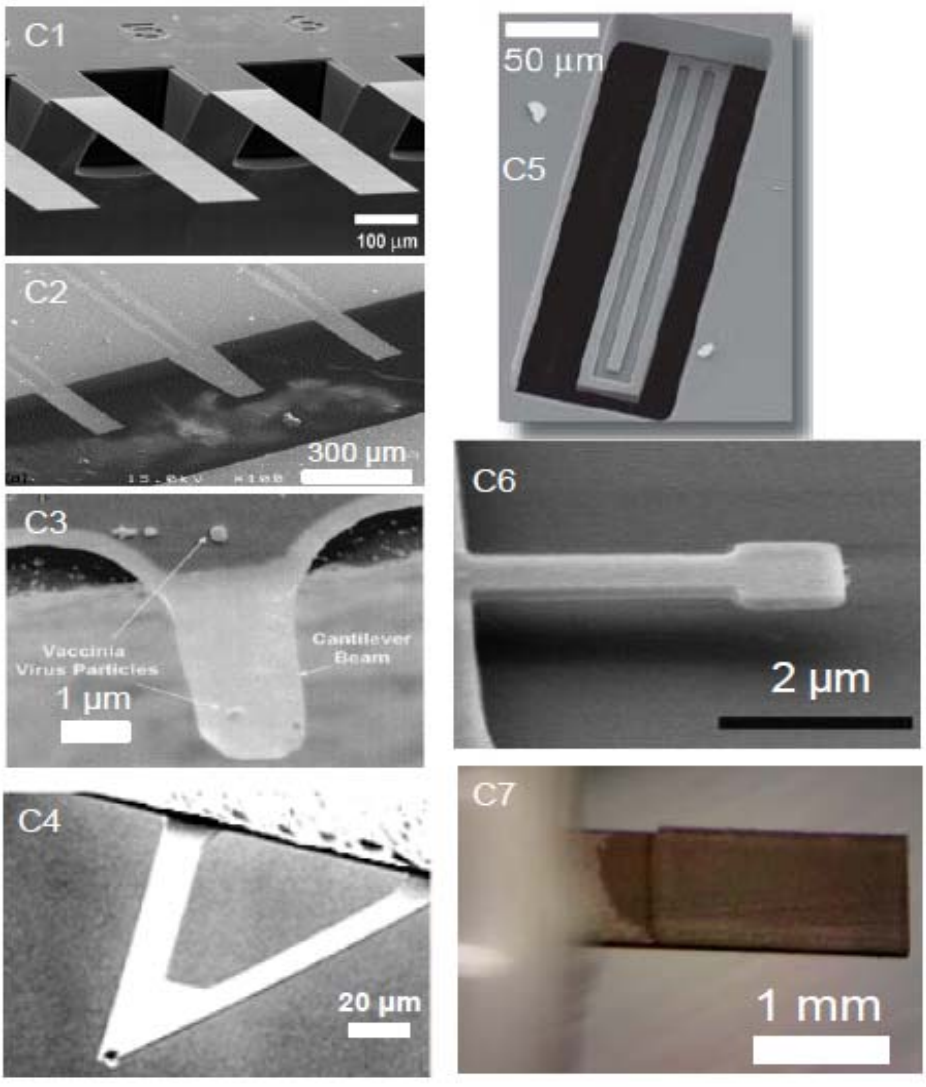

Figure 2-5. Various cantilever designs reported in literature. The operation frequencies of resonant-mode cantilevers are: f_0(C1) = 686 kHz (bending mode can also be used), f_0(C2) = 16 kHz, f_0(C3) = 1.27 MHz, f_0(C5) = 220 kHz, f_0(C6) = 13.3 MHz and f_0(C7) = 1 MHz. Reproduced with permission from Refs. [4, 8, 10, 70-72].

Various materials have been used in fabricating cantilevers including silicon, silicon nitride, SU-8 [73], polystyrene [74] and other polymer materials [75]. The benefit of using polymer is the advantage of tailorable mechanical and chemical properties. For example, the modulus of SU-8 is sixty times lower than silicon, and thus Δz would be significantly larger (see Eq. 2.10) for the same surface stress loaded.

In a typical assay, a microcantilever is modified on one surface with a receptor that exhibits selectivity to the analyte of interest. The opposite side is designed to be passive for the intended analyte. Hence, binding is targeted to occur on only one surface. Such a design can detect minute changes in surface stress. Since the surface stress produced is proportional to the extent of binding, the deflection is proportional to analyte concentration. Reference sensors that do not have surface functionalization are used to reduce background noise and to enhance reliable measurement [5, 76-78].

Using the bending mode, cantilever sensors have been widely investigated for a number of different applications such as detection of bacteria [79, 80], volatile organic compounds [81], vapor-phase analytes [77], DNA hybridization [4], biomarkers [6], and self-assembled monolayers [82]. However, the capture of larger analytes such as bacteria may not produce uniform surface stress change and hence only limited investigation on detection of microorganisms has been reported.

2.2.3.2.2. Resonant-mode cantilever sensors

Resonant-mode cantilever sensors measure the resonant frequency change due to mass change which occurs as a result of analyte binding (Figure 2.4D). The *n*th resonant mode frequency of a uniform cross-section cantilever is:

$$f_n = \frac{1}{2\pi}\sqrt{\frac{k}{m_{e,n}}} \tag{2.11}$$

where k is the effective spring constant, and is given as $k = 3EI_z/L^3$ where E is the effective Young's modulus, I_z is the moment of inertia and L is the cantilever length. $m_{e,n} = 3m/\lambda_n^4$ is the equivalent mass of the cantilever sensor at the nth resonant mode, m is the mass of the sensor and λ_n is the nth eigenvalue of the associated dynamic equation. As the mode number increases, the effective mass decreases. The relationship between frequency change and mass change is given by [83]:

$$\Delta m = \frac{k}{4\pi^2}\left(\frac{1}{f_m^2} - \frac{1}{f_0^2}\right) \tag{2.12}$$

where f_0 and f_m are the resonant frequency before and after mass loading.

The quality value of a cantilever sensor is characterized by the peak shape of the resonance response. Mathematically, the nth mode quality value, Q_n, is defined as the ratio of the resonant frequency of the nth mode, f_n, to the width at the half-height of the peak, and is expressed as $Q_n = f_n / w$, where w is the width at the half-height of the peak. The Q-value depends on physical properties of the cantilever and sample fluid. A high Q-value is desirable since it provides good frequency resolution. Cantilever sensors of nanoscale dimensions have Q-values as high as $10^3 \sim 10^5$ and have mass-change sensitivity in the order of attograms (10^{-18} g) to femtograms (10^{-15} g) in a vacuum environment [72, 84-86]. In gas phases, these sensors exhibit damped response or lower Q-values, resulting in lower frequency resolution. In liquid environments, Q-value diminishes substantially and they are rendered unusable [87]. Even though amplification methods to enhance Q-value have been attempted [88-90], no successful biosensing

experiments in liquids using such techniques have appeared. On the other hand, larger cantilever sensors maintain reasonable *Q*-values in liquids and have been demonstrated for successful biosensing experiments [91, 92]. Composite cantilevers with a width of 1 mm and length of 2.5 – 3.5 mm containing a self-actuating piezoelectric material and exhibiting *Q*-value in the range of 20 – 60 in liquid have been demonstrated for pathogen detection using a flow configuration. Since the Reynolds number (*Re*) of such type of cantilever sensors are very high (10^6), viscous damping effect of liquid to its operation is negligible. This is its unique feature that distinguishes itself from other nanocantilevers or microcantilevers. Such sensors exhibit mass-change sensitivity at femtogram levels and have been successfully applied for liter-sized liquid samples [93]. Another approach to reduce damping was exploited by fabricating microfluidic channels embedded within the cantilever and was successfully demonstrated for detection at femtogram resolution [8].

Resonant-mode cantilever biosensors were shown to be sensitive devices for detecting pathogens and toxins in liquid samples, and included *E. coli* O157:H7 [94], *Bacillus anthracis [9]*, *Salmonella typhimurium* [95], *Cryptosporidium parvum* [96], staphylococcal enterotoxin B [97] and others. Growth of benign *E. coli* cells on the cantilever surface has also been reported [98, 99].

2.2.3.3. Commercial electromechanical biosensors

Acoustic wave biosensors such as QCM and SAW are commercially available. A short list of suppliers is given in Table 2.3. The most successful platform is QCM, which is available from a large number of manufacturers and has been extensively investigated

in academia as well as in industry for thin film deposition thickness monitoring. SAW sensors are available and are primarily used for chemical detection in gas phase.

Cantilever technology has given birth to a number of startup companies but only a few have products available commercially. Various microcantilever and nanocantilever arrays are available that operate primarily in bending mode. Only recently have resonant-mode cantilever sensors entered the commercial market.

Table 2-3. Selected commercially available electrochemical biosensors

Sensor type	Company	Products	Website
QCM	Q-Sense	QCM-D, EQCM	www.q-sense.com
	Inficon	Maxtek RQCM	www.inficon.com
	QCM Research	CQCM, TQCM, Passive QCM	www.qcmresearch.com
	Masscal	Masscal G1	www.masscal.com
	Initium	Affinix® Q series	www.initium2000.com
	SRS	QCM-100, 200, EQCM	www.thinksrs.com
SAW	Nanofilm	S-sens® K5 biosensor	www.nanofilm.de
	Microsensor Systems	HAZMATCAD™, CW Sentry™ 3G, SAW MiniCAD mk II	www.microsensorsystems.com
Cantilever	Concentris	Cantisens® CSR-801, CSR-801G, Cantilever Arrays	www.concentris.ch
	Cantion	CantiChip 8, CantiLabPro, CantiLab3D, CantiSpot,	www.cantion.com
	NANOSENSOR	Silicon AFM sensor	www.nanosensors.com
	Leversense	PEMC sensor	www.leversense.com

2.2.4. Lateral flow assays (LFAs)

A lateral flow assay strip is a simple, small, and inexpensive sensor for detecting pathogens and toxins. It consists of a sample pad, a conjugate pad, a test zone, a control

zone and an absorbent pad, as illustrated in Figure 2.5. Various combinations of chemistries can be used to design assays. Antibodies and nucleic acids are the common recognition molecules used. Recognition molecules are immobilized on the strip surface and dried. Liquid sample (10 – 100 µL) is applied at the sample pad and the contents migrate to the conjugate zone by capillary action. Binding of the analyte and the reporter occurs, and the combined entity migrates further to the test and control zone. A response at the control zone confirms that proper transport conditions are present.

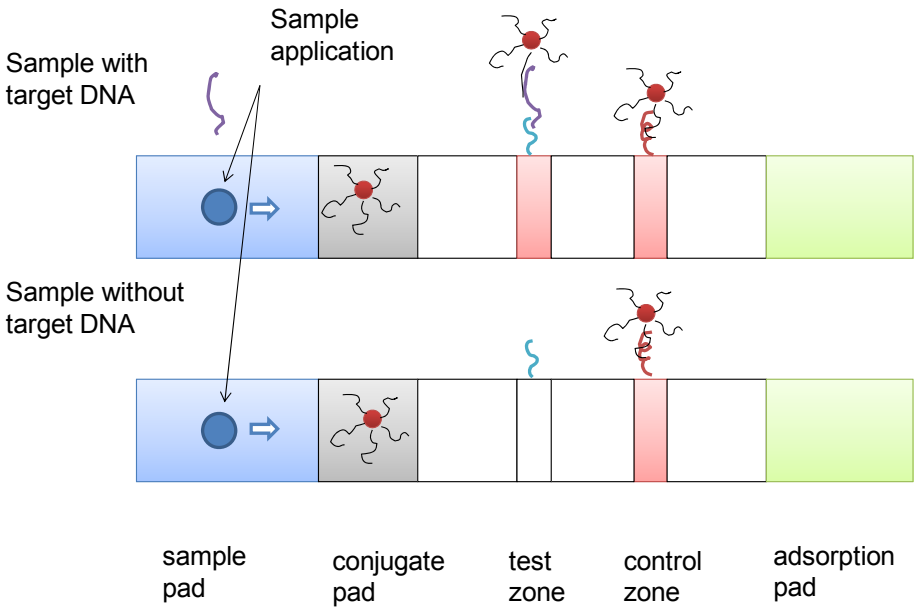

Figure 2-6. Illustration of a typical lateral flow assay. Liquid sample (10 – 100 µL) is applied to the sample pad. The sample migrates by capillary action through the conjugate pad which contains gold nanoparticles that have DNA probe strands attached. The presence of target hybridizes with the probe in the test zone and shows color changes. In the control zone, DNA strands on gold nanoparticles hybridize with immobilized complementary strands. A control response is used to ensure that response is due to proper sample transport.

By visual inspection at the test and control zone, one can qualitatively obtain information on the presence of target analyte. Using a strip reader for signal strength analysis, the concentration of the analyte can be measured. LFAs have been successfully

used for qualitative and quantitative measurement of a number of biological analytes, such as pathogens, toxins and drugs. The main advantages of LFAs are rapidity (5 – 20 minutes), low cost, and long term stability. However, the sensitivity of LFAs is relatively poor using antibody-based methods, at ~10^6 cells/mL [100, 101]. For nucleic acid based methods, when including an amplification scheme such as the PCR or nucleic acid sequence-based amplification (NASBA), the sensitivity can be as low as 40 CFU/mL for viable *E. coli* [102] and 1 – 10 oocysts for viable *Cryptosporidium parvum* [103, 104]. Lateral flow array sensors were used to demonstrate the detection of marker RNA from as few as two *Bacillus anthracis* spores after amplification [105].

2.3. Recognition chemistry

Recognition chemistry is an extremely important part of a biosensor as it endows the biosensor with its desired selectivity property. Since the biological recognition molecules are immobilized on the sensor surface, the following two characteristics are required for proper functioning of the biosensor: (1) the immobilized biomolecules should be presented in high density and in active form; (2) the activity and selectivity of the biomolecules should remain intact after immobilization. Commonly used biorecognition molecules including antibodies, DNAs, aptamers and enzyme. Currently, a great deal of effort of spent on developing novel recognition chemistry with the expectation that newly developed molecules will have higher affinity to the target of interest as well as form a steady layer for long-term storage of functionalized biosensors. In this section effective immobilization methods for the main classes of recognition molecules will be discussed.

2.3.1. Antibody immobilization

Antibody-based detection currently is one of the most common methods for pathogenic bacteria detection. Polyclonal and monoclonal antibodies have been widely used both in practical and research settings. Monoclonal antibodies (mAb) that are produced in hybridoma are far more specific to the analyte of interest. On the other hand, polyclonal antibodies (pAb) are produced in animals, and thus may vary from batch to batch in binding affinity and selectivity. Thus monoclonal antibody normally is preferred when constructing a highly specific biosensor. Various strategies have been reported for forming dense antibody layers on the sensor surface. Several reviews were recently published [106, 107] .

2.3.1.1. Physical adsorption

Physical adsorption of antibody to the sensor surface can be achieved via electrostatic and hydrophobic interactions. The method is simple and rapid, but is thought to be less reliable. Antibodies can also be entrapped in materials such as conducting polymers, polyacrylamide, polyvinyl alcohol, epoxy, or sol-gels for biosensing purpose. Entrapment gives better control of protein loading and stability, but loss of activity is a concern.

2.3.1.2. Covalent attachment on glass surface

Silanization is a widely used method for silica surface functionalization [108, 109]. Organosilanes contain a silicon atom tetrahedrally bound to three similar

functional groups, and the fourth is the functional group of interest used in the immobilization reaction. Three major silane compounds used in practice are 3-mercaptopropyltrimethoxysilane (thiol functional group), 3-aminopropyl-triethoxysilane (APTES; amine functional group), and 3-glycidoxypropyl-trimethoxysilane (epoxide functional group) [110]. The hydroxyl group on the glass is converted to one of the functional groups depending on the silane used. By activating the amine or carboxyl group on an antibody, one can immobilize antibody to the sensor surface.

2.3.1.3. Avidin-biotin

Avidin-biotin chemistry can be utilized for antibody immobilization onto sensor surfaces. The sensor surface is first functionalized with a layer of (strept)avidin on gold surface and then biotinylated antibody is immobilized via the high affinity bond between avidin and biotin [111]. A variety of modifications using avidin-biotin chemistry have been examined and are reviewed for antibody immobilization [112].

2.3.1.4. Immobilization on gold surfaces

Self-assembled monolayers (SAMs) are formed by the chemisorption of thiol compounds (R-SH) onto a gold surface forming Au-SR bonds [113]. Compounds such as 3-mercaptopropionic acid (3-MPA) and 11-mercaptoundecanoic acid (11-MUA) are bifunctional and have a thiol and a carboxyl end group. They form a monolayer on Au

surfaces via the thiol group while the exposed carboxyl group is available for reaction with amine groups on the antibody.

Antibody immobilization can also be carried out via Protein G. The Fc region of IgG antibody binds to Protein G leaving the binding region, Fab, exposed for antigen binding. Immobilization using Protein G offers the best opportunity for orienting antibody on the sensor surface. Enhancement of Protein G binding to gold surfaces can be accomplished by introducing thiol groups using 2-iminothiolane [114, 115]. An alternative approach is to immobilize Protein G or A on self-assembled monolayers (SAM) formed with 3-MPA or 11-MUA [116, 117]. Another approach is to immobilize cysteamine on gold surfaces via their thiol group, followed by reaction with glutaraldehyde. Glutaraldehyde is bifunctional and can introduce an exposed reactive aldehyde group that is available for immobilizing antibody.

2.3.1.5. Antibody fragments

Immobilization of only the antigen-binding portion of the antibody is known to increase surface recognition sites within the same area and improve their orientation. The Fab' fragment contains a free thiol group as well as an antigen-binding site, and can directly chemisorb onto gold. The IgG antibody can be cleaved using pepsin and 2-mercaptoethylamine to obtain the corresponding Fab' fragments [118, 119].

2.3.2 Nucleic acid immobilization

DNA-based biosensors have gained a great deal of interest recently because DNA recognition probes are easily synthesized and are more stable in storage, even more so

than antibodies. Further, thermal melting of the DNA duplex makes the regeneration of sensor surfaces feasible and practical. There are four classes of probes designed for nucleic acids immobilization. These are: (i) linear oligonucleotide probes, (ii) hairpin oligonucleotide probes, (iii) peptide nucleic acids (PNAs), and (iv) locked nucleic acids (LNAs). Detailed descriptions of these probes were recently reviewed by Lucarelli et al. [120]. Among them, linear oligonucleotide probes have been extensively reported. Various techniques have been developed to immobilize the probes on the sensor surface while preserving the hybridization property. The most frequently used techniques are described further.

2.3.2.1. Covalent attachment via functional groups

Covalent attachment utilizes the reaction between two different functional groups to attach probes to the sensor surface. Molecules with various different functional groups (e.g., -OH, -NH_2, -COOH and -CHO) have been employed for surface functionalization. In many cases, the sensor surface is first functionalized with thiolic acids and then the terminal carboxylic group of the monolayer is activated with 1-ethyl-3-[3-dimethylaminopropyl]-carbodiimide hydrochloride (EDC)/*N*-hydroxysulfosuccinimide (sulfo-NHS) and then reaction with amine-terminated oligonucleotide probe is carried out.

2.3.2.2. Thiolated probes

Since gold-coating of sensors can be readily carried out in a research laboratory, a popular approach has been to use thiolated DNA probe which takes advantage of the

strong thiolate bond. Two different strategies can be used. One is the formation of a SAM of a reactive thiol followed by carbodiimide coupling (described earlier) of amino- or carboxyl-terminated oligonucleotides. The other is the direct chemisorption of thiolated oligonucleotides (15 to 25-mer) on the gold surface. For the second method, a second thiol (e.g., mercaptohexanol, MCH) is used to maximize hybridization efficiency by orienting the probe in an upright position [121]. Another attractive feature of the latter is the stability of the thiolate bonds facilitating month-long storage.

2.3.2.3. Affinity immobilization

The high affinity of biotin-avidin is often used for DNA immobilization [122]. One popular protocol is the binding of avidin to carboxylic acid modified gold surfaces followed by attachment of biotinylated DNA [123]. Other combinations of biotin-avidin chemistries have been investigated such as biotin/streptavidin/biotin-probe which takes advantage of multivalent streptavidin as a bridge molecule [124]. A study comparing the hybridization strength of the covalently bonded avidin via activated carboxyl groups with electrostatically absorbed avidin on polyelectrolyte films showed that both provide high hybridization efficiency [125].

2.3.3. Other biorecognition molecules

DNA and antibody are the most common sensing molecules for biological detections as they bear excellent specificity to the target of interest. Other biorecognition molecules useful in constructing a biosensor are aptamers, bacteriophages and enzymes. They are briefly discussed in this session.

2.3.3.1. Aptamers

Aptamers are single stranded DNA or RNA ligands designed to bind biological targets with similar or superior specificity than antibodies. They are selected from a large library of molecules containing randomly created sequences. A massive amount of aptamers which have specific affinity to biological targets have been developed by *in vitro* selection or as in SELEX (systematic evolution of ligands by exponential enrichment) protocol, and these include, but are not limited to, cells and bacteria [126, 127], nucleotides [128], RNA [129], antibodies [130], viral proteins [131], amino acids [132], and metal ions [133, 134]. Starting from an aptamer library, specific aptamers can be isolated that bind with high affinity to any analyte of interest. Since they are nucleotide sequences, immobilization of aptamers on the sensor surface could use any of these methods and have, for example, been used in DNA immobilization as reviewed in Balamurugan et al. [135].

Compared to antibodies, aptamers have a number of advantages making them quite attractive as substitutes for antibodies [136]. Since aptamers are developed *in vitro*, they can be designed to bind any target of choice and the binding affinity of aptamers can be much higher than those of antibodies. Aptamers can be cost competitive as they are produced *in vitro* and production can be easily scaled up. Since aptamers are smaller (3 – 30 kDa) than antibodies (150 kDa), larger numbers of binding sites are available for an assay on the same sensing area and are more stable than antibodies. Long term storage of aptamers functionalized biosensor is also superior than antibody functionalized ones. Due to the above desirable characteristics, currently there is an increasing trend in the development of aptamers for sensing purposes.

2.3.3.2 Bacteriophages

Bacteriophages, or phages for short, are small viruses that can be genetically engineered for recognizing and binding to receptor molecules on the bacterial cell envelope. They have been used as substitutes for antibodies owing to their robustness for binding and storage. Direct adsorption has been used for immobilizing phages on gold surfaces, and good surface coverage has been reported [137]. Avidin-biotin chemistry has been investigated via biotin-modified bacteriophages [138]. Formation of covalent bonds between phage amine groups and carboxyl groups on the sensor surface have also been used for immobilization [139]. Since phages generally have a protein coat, any method that has been successfully used for antibodies can be used for immobilizing phages.

2.3.3.3 Enzymes

Enzymes are widely employed as labels in pathogen detection (ELISA, for example), and used directly as sensing molecules on electrodes. Normally, enzyme-based biosensors are a combination of an electrochemical probe (amperometric, potentiometric or conductometric) with a layer of immobilized enzyme. To fulfill the requirements for a biosensor, the enzyme should have a high degree of specificity and a high level of catalytic efficiency. Enzymes are immobilized on the sensor surface mainly through physical adsorption (i.e., entrapment in polymeric membranes), or chemical immobilization. They have been mainly used as recognition molecules for the detection of small molecules. Their application for electrochemical detection of environmental toxins such as the marine toxin okadaic acid [140], microcystin [141], anatoxin-a [142], cholera toxin [143] and ricin [144] have been reported.

2.4. Conclusions

Biosensors have been shown to detect a large pool of biologics in a laboratory setting. Commercialization is an essential step for the highly sensitive devices to become available for the specialists who monitor food, water, and biomanufacturing qualities. A commercial biosensor should exhibit robust mechanical properties, highly sensitive detection and provide reproducible detection responses. It is especially important that their false positive and false negative rates be near zero. Normally for a platform to be robust and marketable, requirement of highly false positive free is a necessity (<1%). The developments that have occurred in the biosensor field over the last 5 – 10 years, has spawned several startup companies that are beginning to make commercial instruments. A few companies have commercial biosensors on the market, such as the fiber-optic sensor platform. It is anticipated that newer biosensor-based instruments will become available in the future. The incentive for commercialization is the broad field of applications for biosensors. Besides the applications in detecting pathogens and other biological contaminants mentioned in this chapter, biosensors have also been applied widely in other fields, namely for detecting chemicals, biomarkers, drugs, bioreactor monitoring, and fundamental studies of molecular interactions.

Currently there is a great need for developing biosensors for rapid and reliable analysis of water quality and bioprocess monitoring and this is reflected directly in the rapid increase in the number of research reports on biosensors. Portable, inexpensive, automated systems or simple strip assays are of great interest as they have the potential to reduce waterborne disease occurrence and alleviate human suffering. The outlook for using simpler biosensors to replace laboratory-based traditional immunoassays is very

promising. However, challenges remain for robust biosensor application because their performance is just beginning to approach the accuracy and reproducibility of traditional analytical and immunoassay methods.

CHAPTER 3 : A NOVEL METHOD FOR MONITORING MASS-CHANGE RESPONSE OF PEMC SENSORS

3.1. Introduction

Cantilever biosensors have received extensive attention in recent years due to their high sensitivity for detecting a wide range of analytes [145-148]. They can be divided into two types; namely, bending-mode and resonant-mode cantilever sensors. Bending-mode sensors deflect in proportion to surface stress caused by surface binding. Examples are antigen binding to antibody, DNA hybridization to surface-immobilized complementary strand, and others. Resonant-mode sensors exhibit resonant frequency decrease as a result of mass-change due to analyte binding. Both types of cantilever sensors provide highly sensitive and label-free detection.

Resonating cantilever sensors that have high *Q*-value (ratio of resonant frequency to the width at half the peak height, $>10^4$) can be monitored using electronic oscillator circuit for measuring resonant frequency [10, 72]. On the other hand, when they exhibit modest *Q*-values of 20 to 100, the design of such oscillator circuits and their implementation become difficult to achieve. Therefore, one measures resonant frequency by sweeping excitation frequency in the relevant frequency region, followed by measuring the resulting response and then determining the frequency at which resonance occurs. This is repeatedly carried out during a detection process. This approach, while quite accurate and effective, requires a complex measurement and data management system. For example, one needs to provide a means to step excite frequency at a desirable resolution in a systematic manner, followed by determining the location of resonance, and then revise sweep band based on the location of resonant frequency. In addition, at

each excitation frequency the sensor response must be obtained after it reaches steady state. In situations where the sensor is immersed in liquid sample, the wait time to reach steady state is relatively long and the frequency sweep must accommodate not only the dynamics of the sensor, but also the fluid environment in which the sensor operates. That makes the measurement noisy, lengthy and the process complex. In this chapter, the suitability of measuring total impedance ($|Z(f)|$) at a fixed frequency near the initial resonant frequency (f_R) is examined. The results suggest that the impedance approach is an equally effective alternate method for monitoring resonant cantilever response. The significant advantage is that the sensor is excited at a *fixed frequency* resulting in a much shorter wait time and a simpler measurement system. Our hypothesis is that total impedance change is equivalent to resonant frequency change in a sensing experiment.

Previous investigations with QCM have developed equivalent electric circuits such as Butterworth-Van Dyke (BVD) model [149, 150] and observed that motional resistance and other circuit parameters are useful for characterizing QCM response to surface attachment of proteins and bacteria [151-153]. Similarly removal of surface layers from QCM can also be measured by tracking equivalent circuit parameters of electrochemical processes [154, 155]. Resistance and inductance of equivalent circuits increase as cells adhere to QCM [156, 157]. All of the above researches used equivalent circuit parameters *at resonance* as an indicator of detection. That is, the method required characterizing the QCM response over reasonable frequency width that included the resonant frequency. In our study, impedance magnitude of a piezoelectric resonating cantilever sensor is monitored *not at resonant frequency*, but at a *fixed frequency* near the initial resonant frequency. This alternate approach lends itself to a simplified

implementation for either a single PEMC sensor or a bank of multiple PEMC sensors. Because of its relative simplicity, the method would be suitable for high-throughput systems where multiple sensors are used simultaneously.

In this chapter, we show experimentally that total impedance change at a fixed frequency directly relates to resonant frequency shifts of PEMC sensor. This is so because of two properties; (1) *Q*-value of PEMC sensors is in the range of 30 to 60. And, (2) in a typical biosensing experiment, the change in resonant frequency is less than 5 kHz. We demonstrate the application of impedance measurement approach by two types of experiments. In the first one, mass-change response due to density is systematically evaluated. In the second, samples containing *E. coli* O157:H7 cells are exposed to antibody-functionalized PEMC sensor and the resulting response of impedance is shown to be the detection response.

Response of PEMC sensors to density change in a continuous temperature-controlled flow system was reported recently [158]. We examine similar density change experiments here by measuring the change of impedance for validating the proposed approach. The Reynolds number (*Re*) of a PEMC is in the order of 10^6, and thus all measurements are in the inertia-dominated region, so that the frequency response is mainly due to mass-change caused by density change [159]. Aqueous solutions of sodium chloride (NaCl), 1-propanol and glycerol are fluids of known density, and we use them in the density experiments. Density calculations are shown in Table 3.1.

We also examine the case of *E. coli* O157:H7 detection. *E. coli* O157:H7 was chosen as a model pathogen due to our previous experience with it and the availability of calibrated samples [160, 161], and its current day importance [39].

Table 3-1. Density of NaCl, glycerol and 1-propanol solutions at various mass fractions.

NaCl		**Glycerol**		**1-propanol**	
Mass fraction (X)	ρ_X (g/mL)	Mass fraction (X)	ρ_X (g/mL)	Mass fraction (X)	ρ_X (g/mL)
0.00000	0.99850	0.00000	0.99830	0.00000	0.9972
0.00010	0.99857	0.00026	0.99836	0.00050	0.99713
0.00050	0.99885	0.00182	0.99871	0.00100	0.99706
0.00100	0.99920	0.01068	1.00071	0.01003	0.99576
0.00501	1.00200	0.02757	1.00456	0.05013	0.99008
0.01001	1.00551	0.08046	1.01686	0.10025	0.98314
0.05007	1.03403	0.13451	1.02984	0.14069	0.97766
0.10013	1.07075			0.20045	0.96976
0.15019	1.10866				
$\rho_X = 0.9985 + 0.6976X + 0.2387X^2$		$\rho_X = 0.9983 + 0.225X + 0.0705X^2$		$\rho_X = 0.9972 - 0.1437X + 0.034X^2$	

Density correlations are based on Ref. [162].

3.2. Theory and model

3.2.1 Response to density change

A PEMC sensor is a two layer composite structure of non-uniform thickness consisting of a piezoelectric material (lead zirconate titanate, PZT) layer and a glass layer. The PZT layer acts both as actuating and sensing element, while glass layer provides a surface for antibody or nucleic acid immobilization. The principles of the PEMC sensor was described earlier [2], and its sensitivity characterization was also reported [163].

The resonant frequency of a uniform cross section cantilever in an inviscid fluid is given by [159, 164] :

$$\frac{f_{R_{fluid}}}{f_{R_{vac}}} = \left(1 + \frac{\pi \rho b}{4 \rho_c h}\right)^{-1/2} \tag{3.1}$$

where $f_{R_{fluid}}$ and $f_{R_{vac}}$ are the resonant frequencies in fluid and vacuum respectively, ρ_c is the density of the cantilever, b and h are the width and thickness of the cantilever and ρ is the density of the surrounding fluid. The implied assumptions in Eq. (3.1) are: (1) uniform cross section, (2) cantilever length is much longer than its thickness, and (3) amplitude of vibration is much smaller than any sensor length scale. For the case of PEMC sensor, using approximations it was shown that the ratio of resonant frequency in aqueous solutions of various densities to that in water is given by [158]:

$$\frac{f_{Rw}}{f_{Rx}} = \frac{\sqrt{1 + \gamma \rho_x}}{\sqrt{1 + \gamma \rho_w}} \tag{3.2}$$

where γ is a sensor parameter that accounts for non-uniform thickness of PEMC sensors. The terms f_{Rw} and f_{Rx} refer to resonant frequencies in water and in solution of solute mass fraction X, respectively. Typical value of γ reported was ~2 [158]. Eq. (3.2) suggests that as liquid density increases, the resonant frequency of PEMC sensor decreases, and vice versa. Experimentally the validity of this relationship has been demonstrated using density changes of solutions of NaCl, 1-propanol and glycerol. This frequency and density relationship is also used as the guidance for experiments design in the following chapters as complex matrixes (normally have higher density than buffer) are widely used in the study to test the robustness and sensitivity of the PEMC sensor in real world samples.

3.2.2 Total impedance relations changes near f_R

Typical PEMC sensor frequency response near resonance is shown in Figure 3.1. The phase angle represents the vectorial difference between excitation voltage and the resulting current signal measured at steady state by an impedance analyzer. The total impedance of the sensor is also shown as a function of the excitation frequency. The sensor exhibits resonance near 912 kHz with a *Q*-value of 38. The impedance rises linearly from 250 Ω at 900 kHz to 700 Ω at 925 kHz. One notes that impedance is a linear function of frequency in the region described by, $(f_R - \alpha) \leq f \leq (f_R + \alpha)$, where α is ~12 kHz. In a typical detection experiment, the change in resonant frequency associated with detection is usually a few kHz. For example, binding of antigens such as *E. coli* O157:H7 at 100 cells/mL causes a frequency decrease of ~1 kHz [97, 160], while Staphylococcus enterotoxin B (SEB) at 100 fg showed a decrease of ~250 Hz [97]. Thus resonant frequency movement is well within the frequency bound between $(f_R - \alpha)$ and $(f_R + \alpha)$. In the neighborhood of f_R, impedance at frequency f can be approximated as:

$$|Z(f)| = |Z(f_R)| + \left.\frac{\partial |Z|}{\partial f}\right|_{f=f_R} (f - f_R) \tag{3.3}$$

where the expression $\left.\frac{\partial |Z|}{\partial f}\right|_{f=f_R}$ gives the slope-dependence of impedance near f_R, and f is an arbitrary frequency near resonant frequency. When a change in fluid density or binding of the target analyte causes small changes in resonant frequency, the impedance spectrum in the $(f_R - \alpha) \leq f \leq (f_R + \alpha)$ region will move in a parallel fashion as illustrated in Figure 3.1. Therefore, we propose that the measurement of the impedance change at a fixed frequency is a useful method for monitoring sensor response.

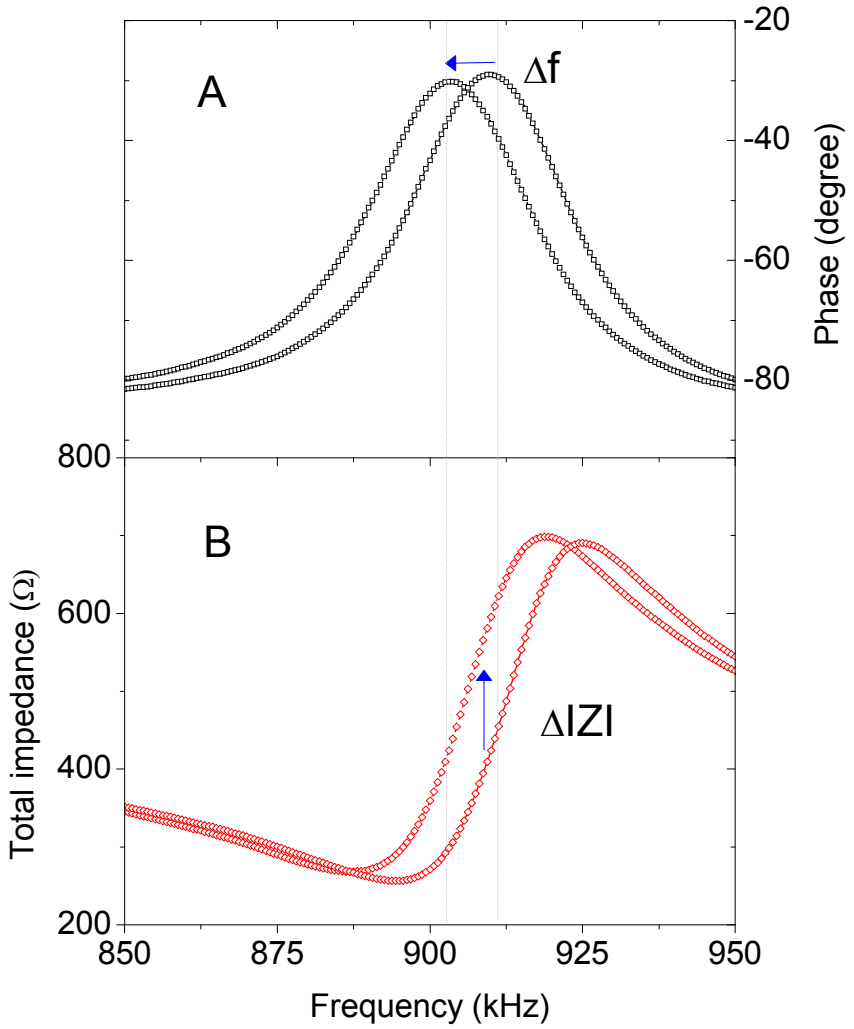

Figure 3-1. Illustration of a typical PEMC sensor frequency response near resonance. **(A)** Phase angle spectrum (□), **(B)** Impedance spectrum (◊). By monitoring at a fixed frequency, the impedance change reflects mass change.

Combining Eq. (3.2) and (3.3), and defining $|Z(f_{nr})|$ as impedance measured at a fixed non-resonant monitoring frequency (f_{nr}), one can express $|Z(f_{nr})|$ as a function of fluid density as:

$$\frac{f_{Rw}}{f_{Rx}}=\frac{\left.\frac{\partial|Z|}{\partial f}\right|_{f=f_{Rx}}\left(\left|Z\left(f_R\right)\right|_w+\left.\frac{\partial|Z|}{\partial f}\right|_{f=f_{Rw}}\cdot f_{nr}-\left|Z(f_{nr})\right|_w\right)}{\left.\frac{\partial|Z|}{\partial f}\right|_{f=f_{Rw}}\left(\left|Z\left(f_R\right)\right|_x+\left.\frac{\partial|Z|}{\partial f}\right|_{f=f_{Rx}}\cdot f_{nr}-\left|Z(f_{nr})\right|_x\right)}=\frac{\sqrt{1+\gamma\rho_x}}{\sqrt{1+\gamma\rho_w}} \tag{3.4}$$

where $\left.\frac{\partial|Z|}{\partial f}\right|_{f=f_{Rx}}$, $\left.\frac{\partial|Z|}{\partial f}\right|_{f=f_{Rw}}$, $\left|Z\left(f_R\right)\right|_w$, $\left|Z\left(f_R\right)\right|_x$, f_{nr} are all constant values in the $(f_R-\alpha)$ $\le f\le(f_R+\alpha)$ region. Simplifying Eq. (3.4) by introducing $A_x=\left.\frac{\partial|Z|}{\partial f}\right|_{f=f_{Rx}}$, $A_w=\left.\frac{\partial|Z|}{\partial f}\right|_{f=f_{Rw}}$, $B_x=\left|Z\left(f_{Rx}\right)\right|+\left.\frac{\partial|Z|}{\partial f}\right|_{f=f_{Rx}}\cdot f_{nr}$, $B_w=\left|Z\left(f_{Rw}\right)\right|+\left.\frac{\partial|Z|}{\partial f}\right|_{f=f_{Rw}}\cdot f_{nr}$, one gets

$$\frac{f_{Rw}}{f_{Rx}}=\frac{A_x\left(B_w-\left|Z(f_{nr})\right|_w\right)}{A_w\left(B_x-\left|Z(f_{nr})\right|_x\right)}=\frac{\sqrt{1+\gamma\rho_x}}{\sqrt{1+\gamma\rho_w}} \tag{3.5}$$

Note that f_R decreases and $\left|Z(f_{nr})\right|$ increases when density increases in Eq. (3.5), and vice versa. However, the above relationship holds true only in the $(f_R-\alpha)\le f\le(f_R+\alpha)$ region. We will test Eq. (3.5) with density change experiments.

3.3. Experiments

3.3.1 Reagents

All chemicals for density experiments were purchased from Sigma-Aldrich. Aqueous solutions of NaCl, glycerol (99%) and 1-propanol (99%) were prepared in de-ionized (DI) water (18 MΩ, Milli-Q system, Millipore) at various mass fractions. The density values are from [158]. Phosphate buffered saline (PBS, 10 mM, pH 7.4) were prepared in DI water. Protein G was purchased from Pierce (Rockford, IL). Aliquots of 20 μg/mL Protein G solutions were prepared in PBS and stored at -20℃. Goat polyclonal

anti-*E. coli* O157:H7 antibody and *E. coli* O157:H7 positive controls were purchased from KPL (Kirkegaard & Perry Laboratories, Gaithersburg, MD). Aliquots of 20 μg/mL antibody solutions were prepared in PBS and stored at -20℃; various concentrations of *E. coli* O157:H7 positive controls were prepared in PBS and stored at 4℃.

3.3.2 PEMC sensor fabrication

Details of PEMC fabrication can be found in earlier publications [2]. Briefly, the sensor consists of two layers: a PZT layer (Piezo Systems,Woburn, MA) and a glass layer (SPI, West Chester, PA), bonded by a non-conductive adhesive. The dimensions of the PZT and glass were 2.7 × 1 × 0.127 mm, and 2 × 1 × 0.160 mm ($l \times w \times t$), respectively. The PZT end was anchored at one end and glass layer was attached at the free-end. Wires were soldered to electrodes of PZT layer and epoxy fixed in 6 mm glass tubing, and subsequently the sensor was coated with 10 μm parylene C as per vendor supplied protocol in a parylene coating machine (PDS 2010 LABCOTER® 2, SCS). The parylene coating provides resistance to water and chemicals since all measurements were made in liquids.

3.3.3 Experimental setup and methods

The experimental setup consisted of an impedance analyzer (Agilent 4294A) and a custom-fabricated apparatus, details of which are in [165]. The flow cell with 120 μL holding volume was maintained at 25.0 ± 0.1℃ in an incubator (Quincy Lab, 10-140E) to ensure constant temperature. Prior to an experiment, sensor surface was cleaned with 100% ethanol followed by copious amount of DI water. The entire flow system was

rinsed with ethanol, followed by DI water. Total impedance change during an experiment was measured by impedance analyzer with a LabVIEW® program that records impedance and phase angle. In a typical experiment, the excitation voltage was 100 mV and monitoring frequency was set at ~1 kHz of resonance.

For density experiments, both batch and flow methods were used. In batch mode, the sensor was immersed completely in test liquid and the resonant frequency was monitored until steady state was reached. In flow mode, PEMC sensor was installed in a flow cell [165] and DI water flow was set at a flow rate of 0.6 mL/min. After impedance value at the chosen frequency value reached steady value, test solutions were switched into flow system, DI water was turned off at the same time. The impedance value was monitored until steady state was reached.

E. coli O157:H7 detection experiments were done in the flow apparatus at 25.0℃, and all measurements were carried out similar to the density experiments in flow mode, except that flow rate was 0.8 mL/min. For these experiments, 2 mm^2 PEMC sensor tip surface was freshly sputter-coated with 100 nm gold in a Desk IV sputtering system (Denton Vacuum, Moorestown, NJ). After stabilization in PBS flow, 1 mL Protein G (20 μg/mL) was introduced and the flow was set in recirculation mode. Once immobilization was complete indicated by impedance reaching a stable value, the flow was changed to PBS to rinse the flow circuit. Subsequently 1 mL anti-*E. coli* O157:H7 (20 μg/mL) was introduced in a manner similar to Protein G introduction. Binding of anti-*E. coli* O157:H7 was monitored by impedance response and after steady state was reached, the flow circuit was flushed with PBS and 1 mL *E. coli* O157:H7 (1,000 cells/mL) was introduced and set to recirculation mode.

3.4. Results and discussion

3.4.1 Typical total impedance spectrum of PEMC sensor

Fabricated sensors showed high-mode resonance near 900 kHz with *Q*-value in the range of 35 – 60. The phase angle and impedance spectra of a typical PEMC sensor in air and DI water are given in Figure 3.2. When the surrounding medium of the sensor was changed from air to DI water, the resonant frequency decreased by ~60 kHz, and the *Q*-value decreased from 43 to 33, and are similar to previous results [3]. As shown in Figure 3.2, when excitation frequency was increased, the impedance value decreased and reached a minimum and then increased in a near linear fashion to a maximum, followed by a further decrease. The maximum phase angle occurs midway between the minimum and maximum impedance values. Similar impedance profiles of resonators such as QCM have been reported [153, 156, 157, 166]. However, QCM is a shear-mode resonator while PEMC is a bending resonator. The later is a relatively new sensor whose high-mode resonant frequency is significantly more sensitive than QCM and was reported only recently. We have characterized over 200 sensors with same geometric design and seven representative ones and their impedance properties are summarized in Table 3.2. Similar spectral properties have been observed universally. The magnitude of the parameter α depends on *Q*-value. When Q is in the range of 35~60, α is 8~12 kHz. It is important to note that in typical sensing experiments with PEMC sensors, the resonant frequency response is in the order of 0.1 to 5 kHz [97, 167]. Therefore, it is reasonable to suggest that impedance varies linearly with frequency over the frequency range of interest in a typical sensing experiment.

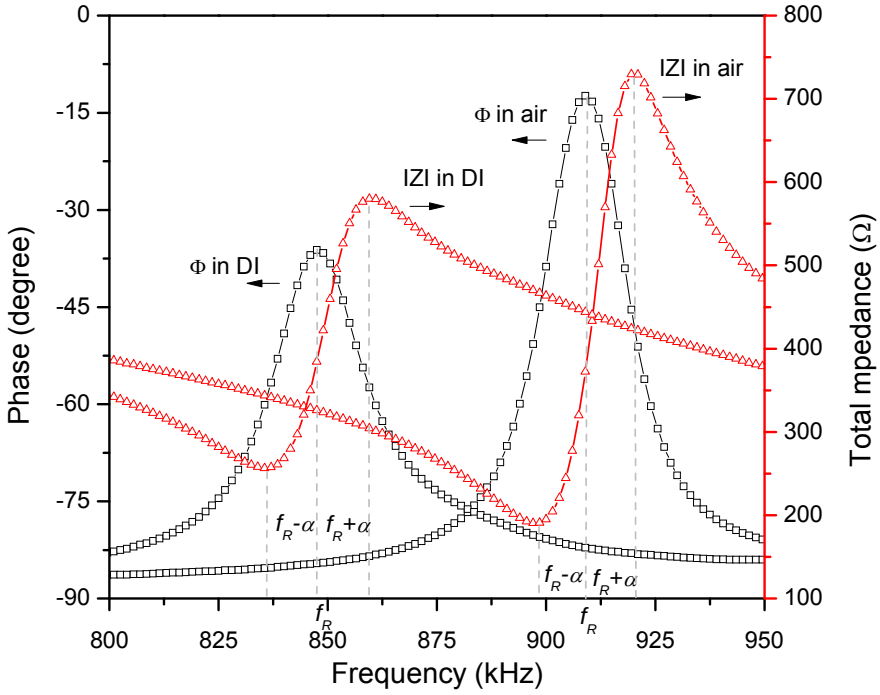

Figure 3-2. Typical PEMC spectra of phase angle (□) and total impedance (Δ) as a function of excitation frequency in air and in DI water. Resonant frequency decreased from 909 kHz to 848 kHz, and phase angle of the resonance peak decreased from -12.4° to -36.2°, respectively.

3.4.2 Response of PEMC sensor to density change

Having shown that impedance profile of PEMC sensor is a near-linear function of frequency near resonant frequency, we next compare the performance of the two approaches with sensor responses to density change. Diluted aqueous solutions of NaCl, glycerol and 1-propanol solutions are suitable density-test solution for introducing both increase and decrease density changes [158]. The resonant frequency and total impedance responses of PEMC sensor (f_R=858 kHz, Q=35) in liquids of various densities are shown in Figure 3.3. Initially the sensor was allowed to reach steady state in NaCl-solution (X=0.0301, ρ=1.0197 g/mL). Subsequently, the steady values in glycerol solution

(X=0.0107, ρ=1.0007 g/mL) and 1-propanol solution (X=0.0100, ρ=0.9958 g/mL) were recorded. Resonance frequency increased from 855.125 kHz to 858.500 kHz (Δf=3,375 Hz), and then to 860.375 kHz (Δf=1,875 Hz) in the three solutions noted. Phase angle increased from -31.34° to -29.36°, then to -28.98°, respectively. That is, as density decreased from 1.0197 g/mL to 1.0007 g/mL, and then to 0.9958 g/mL, both resonant frequency and the phase angle increased. As shown in Figure 3.3, for the three changes the impedance spectrum moved in the same direction as resonant frequency, an expected result.

Table 3-2. Impedance characteristics of PEMC sensors.

Sensor No.	f_R **(kHz)**	Q**-value**	α **(kHz)**	$\lvert Z \rvert$ **vs.** f **in** $(f_R - \alpha) \le f \le (f_R + \alpha)$	R^2
Sensor 1	925.50	40 ± 1	10.50	$\lvert Z \rvert = 31.761f - 28954$	0.974
Sensor 2	909.00	43 ± 1	11.50	$\lvert Z \rvert = 29.004f - 25948$	0.962
Sensor 3	912.00	38 ± 1	11.75	$\lvert Z \rvert = 23.956f - 21436$	0.961
Sensor 4	876.00	42 ± 1	10.50	$\lvert Z \rvert = 37.132f - 32080$	0.960
Sensor 5	877.00	35 ± 1	12.00	$\lvert Z \rvert = 22.312f - 19111$	0.984
Sensor 6	910.00	45 ± 1	10.00	$\lvert Z \rvert = 34.955f - 31431$	0.977
Sensor 7	911.00	60 ± 1	8.00	$\lvert Z \rvert = 16.157f - 14373$	0.983

A significant observation is the total impedance spectra for the three cases are nearly parallel to each other in the range of 850 – 865 kHz. Note that the total impedance in higher density solution is always larger than it is in lower density liquids; and, the larger the resonant frequency change is, the higher the impedance response magnitude is. The similarity of response to density confirms the usefulness of method proposed.

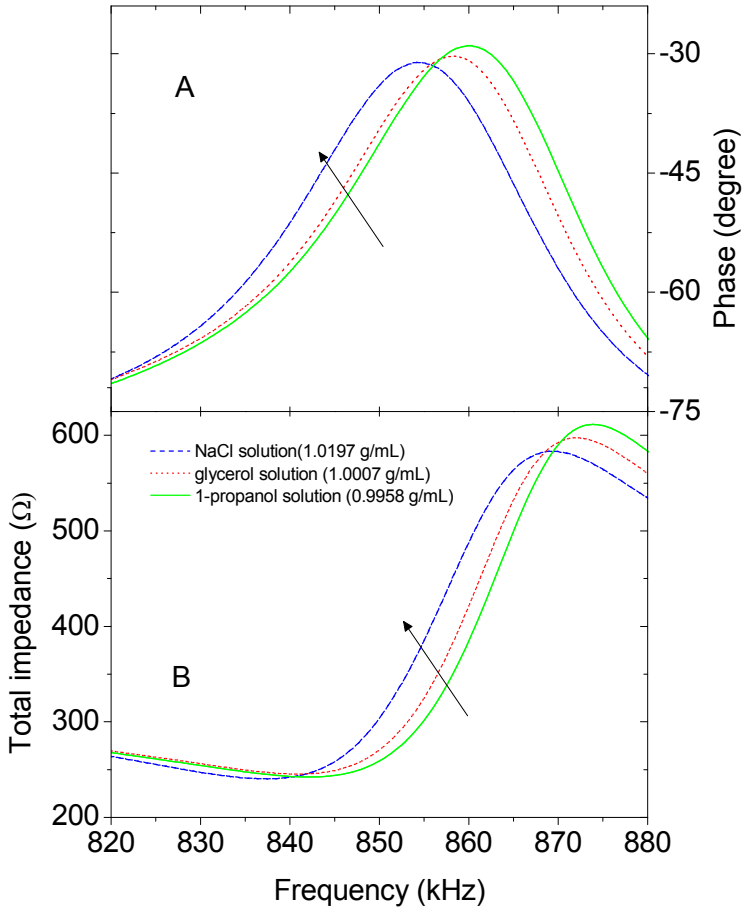

Figure 3-3. Resonant frequency **(A)** and total impedance **(B)** response of a PEMC sensor subjected to density change. Dashed lines are for NaCl-solution (X=0.0301, ρ=1.0197 g/mL). Dotted lines are the spectra in glycerol solution (X=0.0107, ρ=1.0007 g/mL). Solid lines are the spectra in 1-propanol solution (X=0.0100, ρ=0.9958 g/mL). Note the impedance profile moves to right in a lower density solution.

The measurement of total impedance change at a fixed frequency gives data directly related to density change of liquids, or effective added mass response. Since the sensor is used for obtaining mass-change response, we suggest monitoring impedance ($|Z|$) at a fixed frequency, instead of the more laborious method of monitoring resonant frequency. If it is verified by experiments, potentially the impedance method can be

applied for resonating sensors that have modest *Q*-values and for low cost high-throughput screening.

3.4.3 Choice of monitoring frequency

The choice of frequency for monitoring total impedance response to density change or biological sensing experiments is important as it directly affects sensitivity that can be achieved. We examine the sensor response at various frequencies near f_R for a given imposed change. NaCl-solution (X=0.0100, ρ=1.0055 g/mL) and 1-propanol solution (X=0.0100, ρ=0.9958 g/mL) were used as test solutions, and responses were determined with respect to DI water. Total impedance responses obtained at various frequencies are shown in Figure 3.4 for NaCl-solution and 1-propanol solution. In all cases, on both sides of resonant frequency, impedance increased when changing from DI water to NaCl solution, and is consistent with Eq. (3.5). The location where maximum impedance change occurred was at f=859 kHz, which is ~1 kHz higher than the resonant frequency (f_R=858 kHz). For NaCl-solution, decrease of the response magnitude occurred as monitoring frequency was either increased or decreased away from the resonant frequency. Beyond the region of +15 ~ -13 kHz from resonant frequency, the impedance value decreased instead of an increase. For 1-propanol solution, the impedance response was exactly in the opposite direction from that for NaCl solution, since 1-propanol solution is less dense than DI water. The features of the impedance response were similar between NaCl and 1-propanol solutions except that they are in the opposite direction.

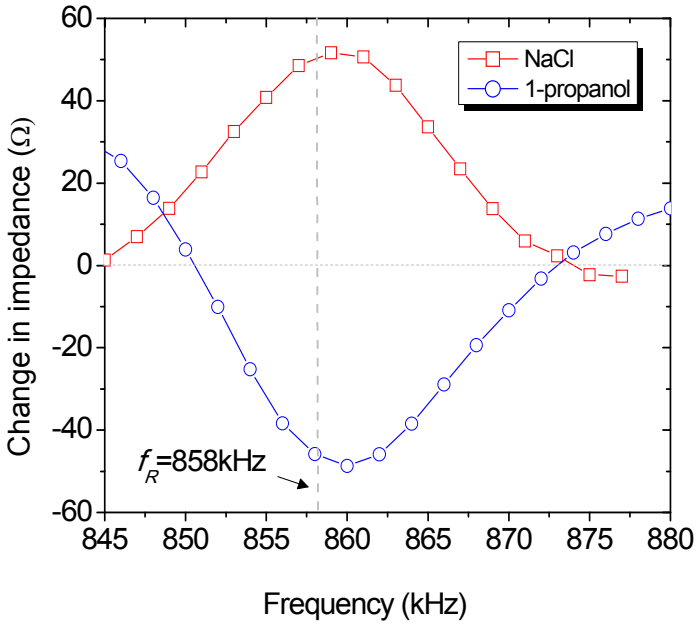

Figure 3-4. Total impedance responses to density changes at various monitoring frequencies near resonant frequency (± 20 kHz). Responses by changing from DI water to NaCl solution (X=0.0100, ρ=1.0055 g/mL) (□) and 1-propanol solution (X=0.0100, ρ=0.9958 g/mL) (○) were symmetric to each other.

Results in Figure 3.4 indicate that impedance change is higher in the region close to resonant frequency. Selection of monitoring frequency closer to resonant frequency will yield the largest overall response for a given imposed change, while a choice closer to the base of the resonant peak will yield a very small overall response. The choice should also take into account the overall expected resonant frequency shift in a sensing experiment. We conclude therefore, monitoring frequency within ± 2 kHz of the resonant frequency is suitable for total impedance change measurement. In this study we used the frequency at $f = f_R + 1$ kHz as it gave nearly the maximum response for the imposed density changes.

3.4.4 Comparison of impedance response with resonant frequency response

In order to examine the validity of the impedance monitoring approach to the established method of resonant frequency monitoring, a wide range of aqueous solutions of NaCl, glycerol and 1-propanol of various mass fraction were prepared and both resonant frequency and total impedance changes were measured following changes from DI water to various density solutions ranging from 0.9698 to 1.1087 g/mL. The density of DI water is 0.9985 g/mL (X=0), and density values of various solutions are from reference [158]. Obtained total impedance and resonant frequency changes to change of densities of all three solutions are summarized in Table 3.3.

Table 3-3. Impedance and resonant frequency response to change of density in three solutions: NaCl, 1-propanol and glycerol.

NaCl Density (g/mL)	**$\Delta\|Z\|$ (Ω)**	**Δf (kHz)**	**1-propanol Density (g/mL)**	**$\Delta\|Z\|$ (Ω)**	**Δf (kHz)**	**Glycerol Density (g/mL)**	**$\Delta\|Z\|$ (Ω)**	**Δf (kHz)**
0.9985	0	0	0.9985	0	0	0.9985	0	0
0.99857	5.01	-0.38	0.99843	1.793	0.88	0.99856	9.85	-0.75
0.99885	15.19	-0.56	0.99836	-6.897	1.63	0.99891	20.33	-1.25
0.9992	27.18	-1.31	0.99706	-11.16	2.00	1.00091	51.4	-3.25
1.002	44.31	-2.06	0.99139	-31.233	2.94	1.00475	59.02	-5.00
1.00551	48.57	-2.25	0.98445	-76.227	6.88	1.01706	48.53	-5.50
1.03403	63.47	-3.00	0.97898	-92.308	8.38			
1.07075	79.47	-5.25	0.97109	-90.076	10.06			
1.10866	76.85	-6.75						

As shown in Eq. (3.5), total impedance response is in the opposite direction with resonant frequency response, i.e., when density increases, total impedance increases and resonant frequency decreases, and vice versa. To illustrate the relationship between total

impedance response and resonant frequency response, total impedance change due to density change at f=859 kHz is plotted as a function of resonant frequency change under the same conditions in Figure 3.5. One notes that when liquid density was increased (or decreased), total impedance at f=859 kHz increased (or decreased), and for the same conditions the resonant frequency decreased (or increased). The higher the density difference was, the larger was the resonant frequency and total impedance change. This applies to all three test solutions. From experimental results shown, one sees that density difference as low as 0.0001 g/mL is easily measurable using impedance or resonant frequency measurements. The response of total impedance at f=859 kHz and resonant frequency gave excellent correlation ($\Delta|Z| = -11.295\Delta f$, R^2=0.9242), which confirms the proposed approach in Section 3.4.2.

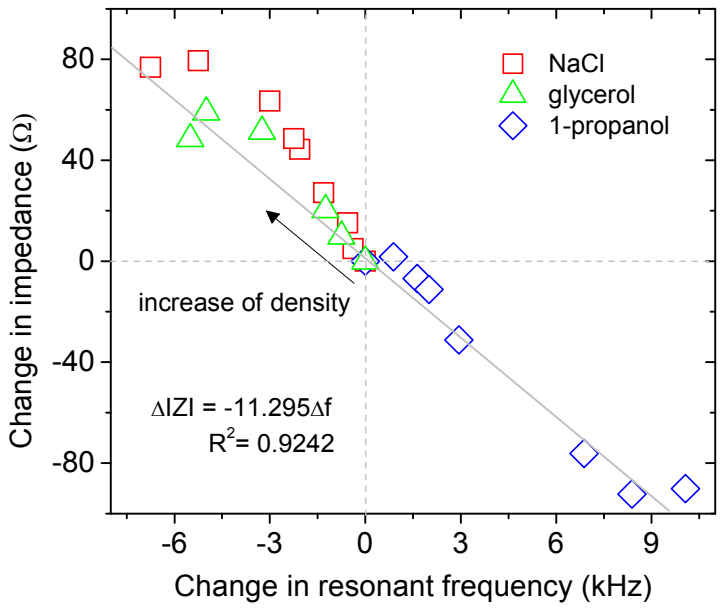

Figure 3-5. Resonant frequency (Δf) and total impedance ($\Delta|Z|$) response to density changes from 0.9698 g/mL to 1.1087 g/mL.

3.4.5 Response of PEMC sensor to density changes in a flow apparatus

Continuous flow apparatus give us real-time measuring ability of sensor response as it is subjected to density change. Examples of total impedance response of PEMC sensor to density changes from DI water to NaCl solutions and from DI water to 1-propanol solutions in the flow experiments are shown in Figure 3.6. The flow rate was 0.6 mL/min and the test solutions were not re-circulated to avoid cross contamination. Figure 3.6A shows a typical total impedance response from DI water (X=0, ρ=0.9985 g/mL) to NaCl-solution (X=0.05, ρ=1.03403 g/mL) at monitoring frequency of f=859 kHz. After PMEC sensor was stabilized in flowing DI water, NaCl-solution was introduced into the flow loop while shutting off the in-flowing DI water. The total volume of flow loop was ~4 mL, and a 15 minute run ensured the entire system was filled with the NaCl-solution. Once the flow loop was filled with the introduced NaCl-solution, a new stable value was reached and showed a total impedance increase of 24.34 Ω. After stabilization for 5 min, DI water was re-introduced to replace NaCl-solution, and the total impedance returned to the original value.

Figure 3.6B shows a typical density change response conducted with 1-propanol solutions at two concentrations. The experimental conditions are the same as in Figure 3.6A. After sensor stabilized, 1-propanol solution (X=0.005, ρ=0.9978 g/mL) was introduced and the impedance change was recorded. The impedance decreased sharply by 2.59 Ω and reached a steady state value in ~3 min. Repeat of DI water to same density 1-propanol solution change gave an identical response. For the third cycle, a higher mass fraction of 1-propanol (X=0.05, ρ=0.9914 g/mL) was used, and a 17.10 Ω decrease was observed. Since the 1-propanol solution is lighter than DI water, the decrease in total

impedance is expected. The noise level of the impedance measurement in flow system was ±0.1 Ω as shown in the inserted graph in Figure 3.6A. Compared with the response magnitude obtained for density changes, the signal to noise ratio is quite high (S/N=12.5 to 120) in these sensing experiments.

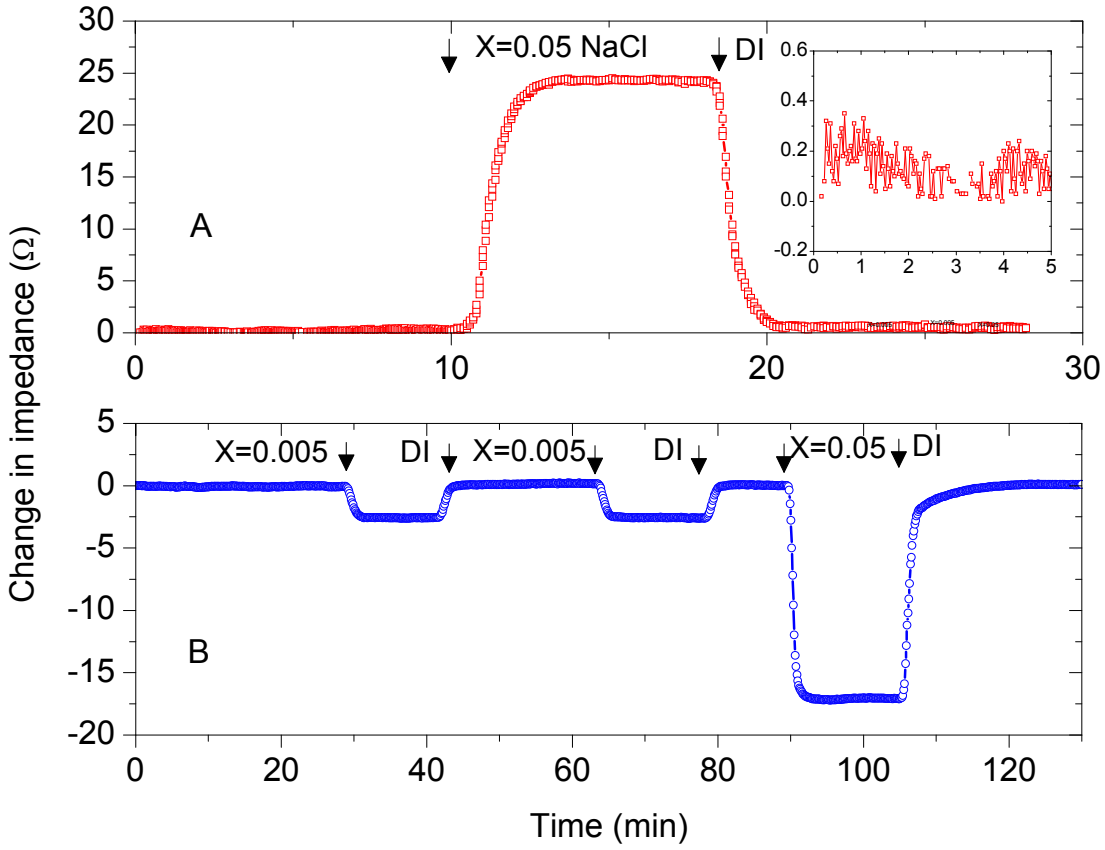

Figure 3-6. Typical total impedance response of PEMC sensor to density change. **(A)** Impedance response to NaCl solution (X=0.05, ρ=1.0340 g/mL) in flow system (0.6 mL/min). Initially the sensor was stabilized in DI water for ~10 min, and then flow was switched to NaCl solution that gave a impedance increase of 24.34 Ω. When the flow was switched back to DI water, the impedance returned to the original value. Inset graph shows impedance noise level was ±0.10 Ω. **(B)** Impedance response to 1-propanol solution (X=0.005, ρ=0.9978 g/mL; X=0.05, ρ=0.9914 g/mL) in flow (0.6 mL/min). After the sensor stabilized in DI water, two concentrations of 1-propanol solution were introduced sequentially and multiple times. A decrease of 2.59 Ω was seen for X=0.005 and a decrease of 17.10 Ω was observed for X=0.05, respectively.

The results of density flow experiments show impedance measurement is a comparable alternate approach to monitoring resonant frequency. Compared with resonant frequency monitoring as well as impedance monitoring at resonance (note: this impedance monitoring tracks the change of total impedance at phase angle resonance), impedance monitoring has higher signal-to-noise ratio, which is another advantage of this method [168].

3.4.6 Detection of E. coli O157:H7 using impedance measurement

To further test the impedance approach as a practical method in biosensing experiments, we conducted pathogen detection experiments. In previous work we showed that PEMC sensor can detect the pathogen *E. coli* O157:H7 with immobilized anti-*E. coli* O157:H7 on the sensor. The resonant frequency was monitored and detection of as few as 10 cells/mL was shown to be feasible [160]. Here we examine the use of impedance method for *E. coli* O157:H7 detection. A typical result, given in Figure 3.7, was conducted in the flow apparatus at 0.8 mL/min and 25.0 ℃. After the sensor stabilized in PBS, 1 mL of 20 μg/mL Protein G solution was introduced in re-circulation mode. A near-exponential increase of 5.66 Ω was observed as Protein G bound to Au<111> sites on the sensor surface in 40 min. Followed by PBS rinse, 1 mL of 20 μg/mL antibody was injected and resulted in a further 12.51 Ω near-exponential increase of impedance. At t = 215 min 1,000 *E. coli* O157:H7 cells were introduced into the flow loop, and the sample was allowed to re-circulate. A 6.63 Ω increase in impedance was observed due to the binding of *E. coli* O157:H7 cells to the sensor surface. The noise level was low (±0.20 Ω) and signal to noise ratio was greater than 30. The increase of impedance as the

cells attached is in the same direction as was the response to density increase and is the expected result. Control experiments with sensors that did not have gold coating showed no response (±0.5 Ω) to Protein G, antibody or *E. coli* O157:H7 cells, thus confirming that the increase of impedance was indeed due to the pathogen binding. Note that at the Protein G concentration used the density may at most have increased by 0.00002 g/mL which is far too small a change to cause a density-induced response. Hence the response of 5.66 Ω is entirely due to chemisorptions of Protein G. The binding rate constant k was calculated as 0.053 ± 0.002 min^{-1}, and is in the same range reported earlier [169]. The above results show that the impedance measurement of PEMC sensor response is a practical alternate method for monitoring pathogen detection.

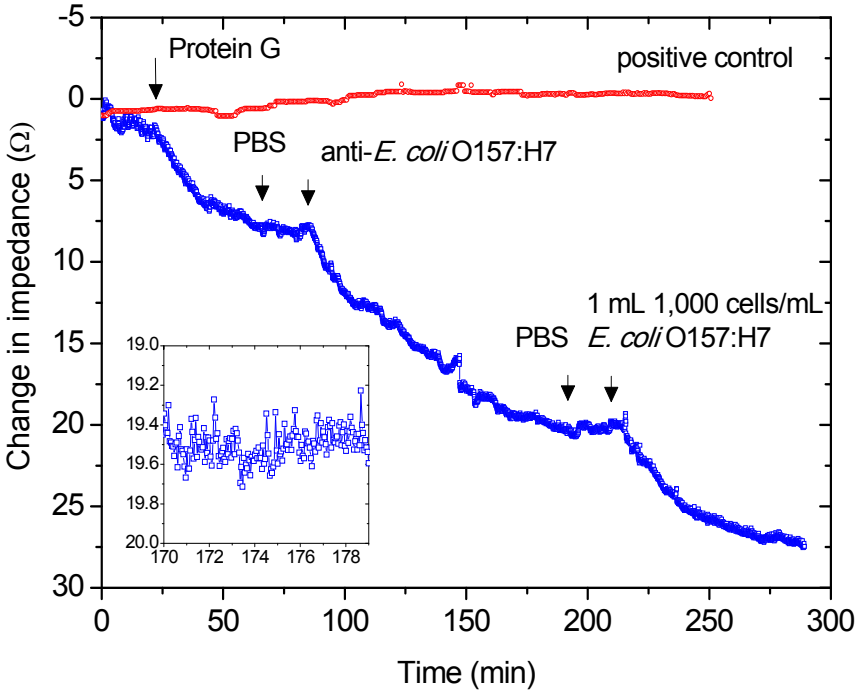

Figure 3-7. Detection of *E. coli* O157:H7 using total impedance. Experiment was done at a flow rate of 0.8 mL/min at 25.0°C. Square (□) is the detection experiment. Positive control (○) shows no response. In the positive control the pathogen was in the sample, but the sensor was not immobilized with antibody. Inset graph shows detection noise level was ±0.20 Ω.

3.4.7 Limitation of impedance measurement for density experiments

While the impedance response approach promises to simplify measurement, it does have limitations when measuring large mass-changes. Earlier in Figure 3.5 the impedance responses to density changes from the three solutions were shown to correlate directly to density of samples. However, when change in density was large the correlation became poor and we discuss this aspect of the method limitation further.

We use density change experiments to illustrate the limitation of the impedance approach. Total impedance values at f=859 kHz in various solutions were measured and impedance changes to various density changes are plotted in Figure 3.8A. One notes that total impedance increased for small changes of ~1% in density and it is nearly linear. At higher density changes for glycerol solution (X=0.0275, ρ=1.0048 g/mL), impedance change saturated at 59.02 Ω, and at an even higher density (X=0.0803, ρ=1.0171 g/mL) a small decrease to 48.53 Ω was observed. For NaCl solution, when X=0.1, ρ=1.0708 g/mL, total impedance change was the highest of 79.74 Ω, and at a higher density (X=0.15, ρ= 1.1087 g/mL), the impedance change decreased to 76.85 Ω. For 1-propanol, total impedance decreased with the decrease of density (mass fraction increase). It also decreased initially linearly and then reached a minimum. At X=0.15, ρ=0.9788 g/mL, impedance change was at a minimum, -92.31 Ω. At lower density (X=0.20, ρ=0.9711 g/mL) impedance change magnitude increased to -90.08 Ω.

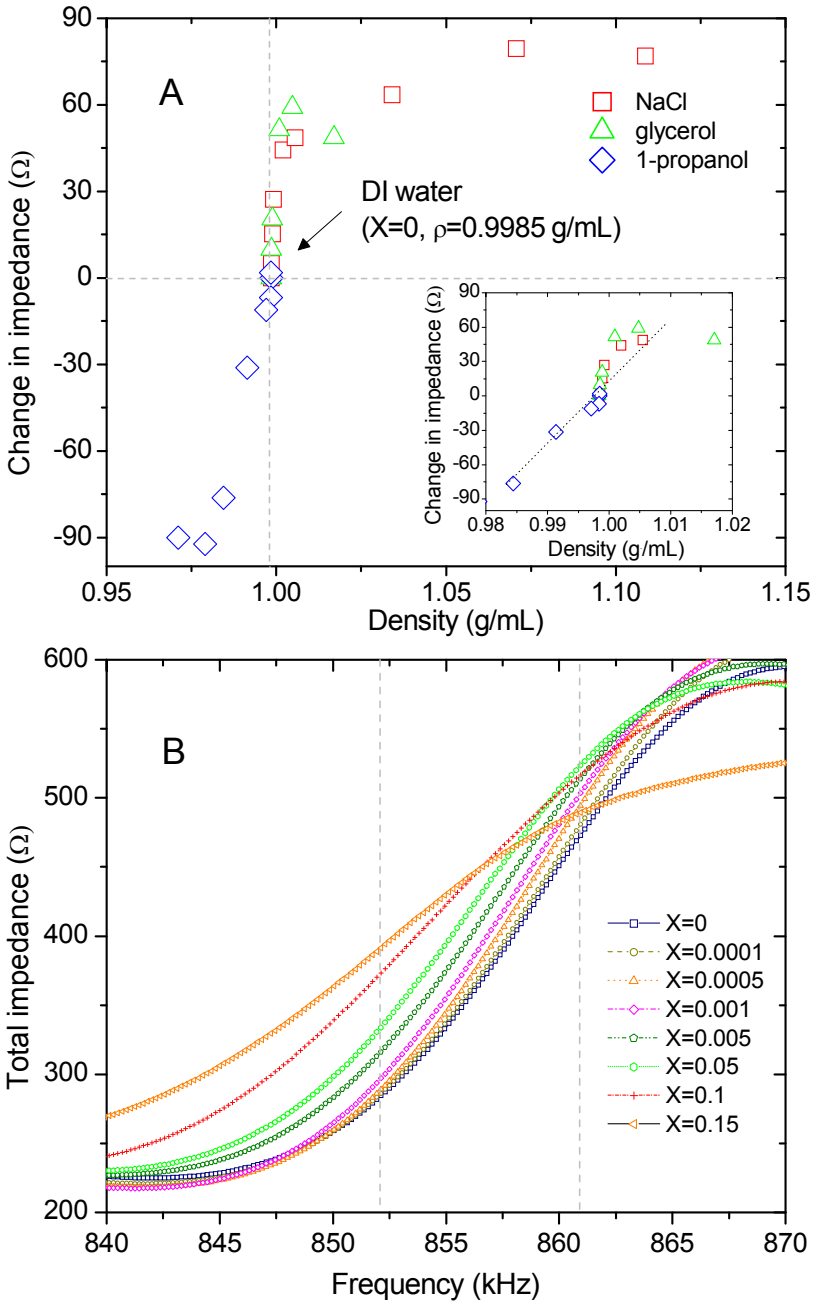

Figure 3-8. (A) Total impedance change of PEMC sensor to NaCl (□), 1-propanol (◊) and glycerol (Δ) solutions with density range from 0.95 g/mL to 1.15 g/mL. The responses were obtained by comparing the impedance difference between various solutions and DI water. Inset shows the response in a narrow density range from 0.98 g/mL to 1.02 g/mL. **(B)** Effects of solute concentrations on impedance profile. NaCl solutions with various mass fractions (X=0~0.15) were used. The parallel impedance profile observed at small density changes give rise to intersecting profiles at larger density changes.

To examine the reason for the above inverse changes, the impedance profiles near resonant frequency (±40 kHz) were characterized. Figure 3.8B shows a typical total impedance spectra corresponding to NaCl solutions in density range from (X=0, ρ=0.9983 g/mL) to (X=0.15, ρ=1.1087 g/mL). From 0.9983 g/mL to 1.0340 g/mL, the impedance spectrum shifted to the left in a near-parallel fashion in the frequency range of 852-861 kHz. At higher densities (X=0.1, ρ=1.0708 g/mL) and (X=0.15, ρ=1.1087 g/mL), the spectral shape flattened due to large added-mass effects resulting in intersecting impedance profiles. In essence, the phase angle decreased quite considerably. Similar transitions were observed for glycerol solutions (data not shown). For 1-propanol solution the impedance decreased with increase in concentration, and an increase in Q-value occurred (data not shown). It is clear that when density change is small impedance approach provides a simple and reliable method.

3.5. Conclusions

We showed impedance response as equivalent to PEMC sensor resonant frequency response. Experimentally it was found that monitoring frequency for impedance change should be located within ±2 kHz of resonant frequency. We verified the proposed approach using density change (both increase and decrease) experiments and antibody-based *E. coli* O157:H7 detection experiments. The impedance approach is limited to responses where only small changes in Q-value occur, which is typical of biosensing applications using PEMC sensors.

CHAPTER 4 : DETECTION OF *CRYPOSPORIDUM PARVUM* IN PBS AND 25% MILK AT 5 OOCYSTS/ML

4.1. Introduction

Cryptosporidium parvum is an important parasitic protozoan responsible for numerous waterborne and foodborne outbreaks of diarrheal disease, causing a majority of gastrointestinal parasitic infections globally [170]. It causes cryptosporidiosis that is potentially lethal for immunocompromised or immunosuppressed segment of the population. In United States alone, an estimated 300,000 cases of cryptosporidiosis occur each year causing 66 deaths [171]. Median infective dose is estimated as 87 oocysts for the Iowa calf isolates [172]. Oocysts have been found in surface water samples with concentrations ranging from 0.1 to 10,000 oocysts per 100 L [173, 174]. Therefore, there is a great need for developing highly sensitive and reliable method for detecting ultralow concentration of *Cryptosporidium* in source and finished water.

EPA established Method 1623 for simultaneous detection of *Cryptosporidium* spp. and *Giardia* spp. The method involves multiple steps of filtration, immunomagnetic separation, and a detection method based on immunofluorescence assay, with confirmation through vital dye staining (4,6-diamidino-phenylindole, DAPI) and differential interference contrast microscopy [175]. The EPA method is tedious and requires specially trained personnel for conducting the assay. Nucleic acids based methods [176, 177] and immuoassays based methods [178, 179] are also routinely used for *C. parvum* identification. Although these techniques are quite sensitive, they are time-consuming, laboratory-based and require trained personnel. More importantly, many of the finished water operators are not staffed with specialists and thus collected samples are

sent to central or commercial labs and turnaround time for results can be as long as 4 to 7 days. Thus rapid sensing sensors would be of great benefit.

PEMC sensor has been used for the detection of a variety of pathogens and toxins due to its high mass-change sensitivity. Similar to SPR and QCM, PEMC has the advantage of label-free, real-time detection in a flow setup. Mass change sensitivity at levels of femtogram (10^{-15} g) was reported in flow conditions and in complex media [97]. Recently, we reported using an IgM antibody for detecting *C. parvum* in buffer that showed limit of detection as 100 oocysts/mL [96]. Since that study, several new antibody types have appeared in the market. Therefore, the purpose of this study is to investigate the use of IgG antibody for *C. parvum* detection and challenge the PEMC sensor at lower *C. parvum* concentrations and develop an improved method for low concentration detection via secondary antibody binding. We examine sensor response in complex medium to show the feasibility of using it in practical matrixes. Milk medium was chosen as a surrogate for complex medium as it contains proteins, lipids, carbohydrates and salts. We believe similar sensitivity of detection could be obtained in other complex media such as contaminated source water.

4.2. Overview of biosensors for *C. parvum* detection

Recently, several reports on detecting *Cryptosporidium* using biosensors have appeared and they are summarized in Table 4.1. SPR sensors using direct binding assays have yielded detection sensitivity of 10^6 oocysts/mL *C. parvum* in buffer background [180]. In an effort to improve sensitivity, the same authors in a later study reported a

competitive binding assay that yielded detection sensitivity of 10^2 oocysts/mL [181]. Detection sensitivity did not deteriorate when natural water samples were analyzed.

Table 4-1. Overview of biosensors for *C. parvum* detection

Biosensor type	**Matrix**	**LOD**	**Estimated time of analysis**	**Ref.**
SPR	Buffer Buffer	10^6 oocysts/mL 10^2 oocysts/mL	2 h	[180]
SPR direct	Buffer, natural water	10^2 oocysts/mL	2 h	[181]
QCM-D	Clean matrix	10^5oocysts/mL	5 min	[182]
PEMC	PBS PBS, milk	10^2 oocysts/mL 5 oocysts/mL	1 h 1 h	[96] [183]
NASBA + ECL	Buffer Environmental samples	5 viable oocysts 10 viable oocysts	2 h	[184]
IMS + NASBA + LFA	Environmental samples	1 oocyst/5 mL	4.5 h	[104]
RT-PCR + LFA	Reagent water Raw water samples	20 oocysts/mL 1 oocyst/L	3 h	[185]
LFA	Environmental samples	10 oocysts	30 min	[103]
Chronopotentiometric	Drinking water, river water	ng/mL DNA target	15 min	[186]
Fluorescence microfluidic	Buffer	1 oocyst	5 min	[187]

Abbreviations: SPR: surface plasmon resonance; QCM-D: quartz crystal microbalance with dissipation monitoring; NASBA: nucleic acid sequence based amplification; ECL: Electrochemiluminescence; IMS: immunomagnetic separation; RT-PCR: reverse transcription polymerase chain reaction; LFA: lateral flow assay.

QCM-D was used for the detection of viable *C. parvum* in water matrixes of varying complexity, where both frequency and dissipation factors were measured [182]. In a clean matrix, a good log-log response was observed for the concentration range of 3×10^5 to 10^7 oocysts/mL. However, the presence of contaminating latex microspheres,

Enterococcus faecalis, or *E. coli* led to a considerable decrease in biosensor response, suggesting a loss in sensitivity.

Detection of *C. parvum* using DNA/RNA based methods were investigated using an electrochemical hybridization biosensor by detecting 38-mer DNA (from 18S rRNA) fragments unique to *Cryptosporidium*. The 38-mer DNA probe was immobilized on the carbon-paste transducer and a highly sensitive chronopotentiometric transduction mode was used for monitoring hybridization [186]. This biosensor showed detection sensitivity at ng/mL levels within a very short time period.

In an attempt to measure viable oocysts, Baeumner et al. [184] measured the heat shock response via mRNA associated with the *hsp70* gene using NASBA amplification. Amplified mRNA was quantified with an ECL sensor system. The results suggest detecting 5 viable oocysts in buffer solution as well as less than 10 oocysts in a 10 mL environmental sample are feasible. Recently, the same research group used the same mRNA-based detection technique combined with lateral flow assay and showed feasibility of single oocyst detection in 10 μL sample, verified by flow cytometry [104]. A handheld single use lateral flow strip assay has also been reported for measuring the amplicons generated by the NASBA technique [103].

4.3. PEMC physics

A detailed description of PEMC physics was reported earlier [12]. Briefly, the *n*th mode resonant frequency of a cantilever in air is expressed as:

$$f_n = k_n \sqrt{\frac{K}{M_e}} \tag{4.1}$$

where k_n = 0.1568, 0.9827, 2.7517 and 5.3923 corresponding to the first four eigenvalues for a rectangular cantilever [188]. K is the effective spring constant of the composite structure and is a function of thickness, width, length and the Young's modulus of the cantilever material. M_e is the effective mass of the cantilever in air.

When the sensor is immersed in liquid, the fluid adjacent to the cantilever's surface becomes part of the oscillating mass. Therefore, the resonant frequency response ($f_n^{'}$) to the added mass of liquid can be written as:

$$f_n^{'} = k_n \sqrt{\frac{K}{M_e + m_{ae}}} \tag{4.2}$$

where the term m_{ae} is the effective mass of added oscillating liquid. One has to keep in mind that m_{ae} varies when liquid property varies, and will be shown in the results section. Upon the attachment of target analyte to the sensor surface, the equivalent mass (Δm) of the analyte modified Eq. (4.2) to:

$$f_n^{''} = k_n \sqrt{\frac{K}{M_e + m_{ae} + \Delta m}} \tag{4.3}$$

where $f_n^{''}$ is the resonant frequency after analyte binding. By comparing the resonant frequency pre- and post-experiment, one can qualitatively and quantitatively measure the target of interest directly in liquid. In a typical sensing experiment, we measure $f_n^{''}$ as a function of time and using the difference in resonant frequency change, ($f_n^{''} - f_n^{'}$), to concentration of the analyte.

4.4. Experimental

4.4.1. Materials and reagents

Protein G was purchased from Pierce (Rockford, IL). Goat polyclonal IgG Anti-*C. parvum* was purchased from Abcam (Cambridge, MA). Mouse monoclonal IgM anti-*Cryptosporidium* and inactivated *C. parvum* oocysts (5×10^6 oocysts/8 mL) were purchased from Waterborne, Inc. (New Orleans, LA). Phosphate buffered saline (PBS, 10 mM, pH 7.4) and other common chemicals were purchased from Sigma-Aldrich (St. Louis, MO). Whole milk was purchased locally. Aliquots of Protein G (20 μg/mL) and antibody solutions (20 μg/mL for IgG and 10 μg/mL for IgM) were prepared in PBS and stored at -20 ℃. Various concentrations of *C. parvum* were prepared by diluting from a stock calibrated sample in PBS and stored at 4 ℃. Stock sample was determined with flow cytometry with 1% error. Experimentally, glass slides deposited with 15 μL samples were examined under microscope and accuracy of each diluted concentration was found to be within 10 – 15%.

4.4.2. Sensor fabrication and experimental procedures

Fabrication details are described in the previous chapter. Briefly, a PEMC sensor consists of two layers: a PZT layer (Piezo Systems, Woburn, MA) and a quartz layer (SPI, West Chester, PA), bonded by a non-conductive adhesive. The dimensions of the PZT and glass were 2.8 × 1 × 0.127 mm, and 2 × 1 × 0.160 mm ($l \times w \times t$), respectively. 30 gauge wires were soldered to electrodes of PZT layer and the sensor was epoxy anchored in 6 mm glass tubing. Prior to a detection experiment, 2 mm^2 sensor tip surface was freshly sputter-coated with 100 nm gold layer. Sensor was incubated in 1 mL Protein G

(20 μg/mL) for 2 h, then rinsed with DI water and installed in a home-made flow cell. Detection experiments were done in the flow apparatus (as shown in Figure 4.1) at 1.0 mL/min at 32.0 ± 0.1 ℃. *C. parvum* immobilization process is depicted in Figure 4.2. Five reservoirs were used for injection of various reagents such as antibody, antigen and release buffer. During the course of experiments, only one valve of the reservoir was open and reagent in the reservoir was transported to the flow cell for reaction on the sensor surface by the peristaltic pump. Upon stabilization in PBS, 1 mL IgG anti-*C. parvum* (20 μg/mL) was introduced and the flow was set in recirculation mode for 1 h for antibody immobilization. For detection experiments in PBS, the flow system was filled with PBS and *C. parvum* samples containing various concentrations were switched into the flow loop.

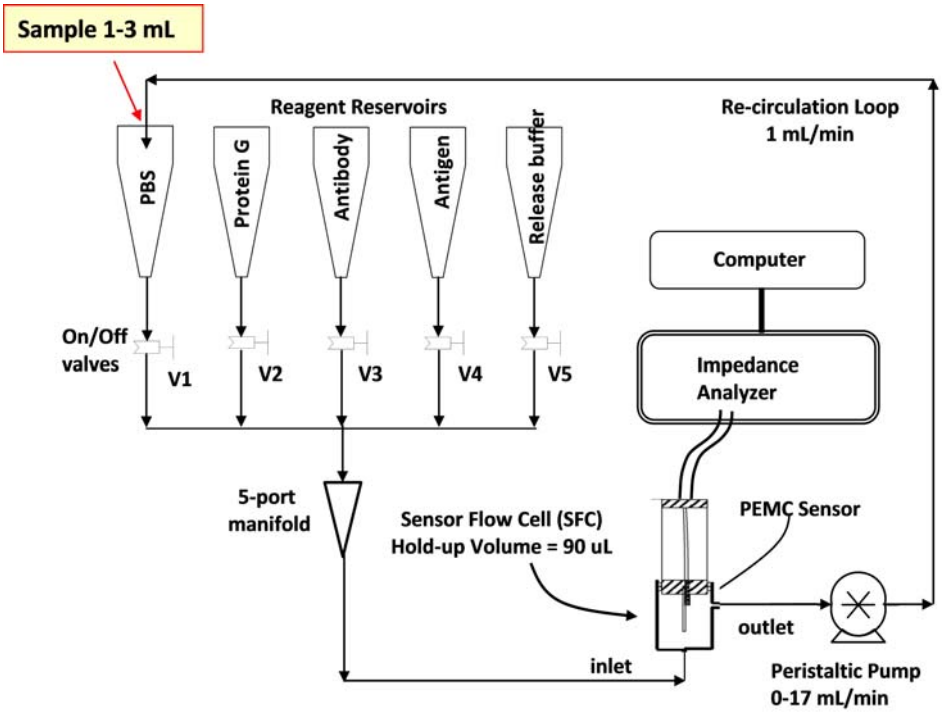

Figure 4-1. Flow configuration for *C. parvum* detection. Flow rate of the system was controlled by a peristaltic pump in the range of 0-17 mL/min.

For detection in milk, sensor was pre-stabilized in PBS, and then 1 mL whole milk was introduced into the flow system set in recirculation mode. Since the total volume of flow system was ~4 mL, recirculation of 1 mL milk gave ~25% milk content in PBS. In that milk background, detection experiments were carried out. *C. parvum* samples were also prepared in milk/PBS (1:3) solution to ensure the background is the same as that in the flow loop. For detection confirmation, 1 mL of 10 µg/mL IgM was introduced into the flow circuit set in a recirculation mode after the flow loop was rinsed with PBS. Additional confirmation of attachment was obtained by releasing the bound *C. parvum* by low pH glycine buffer. Glycine release buffer was prepared with 100 mM glycine in PBS with 1% v/v ethylene glycol and adjusted with 1 M hydrochloric acid. All release experiments were carried out in once-through flow mode.

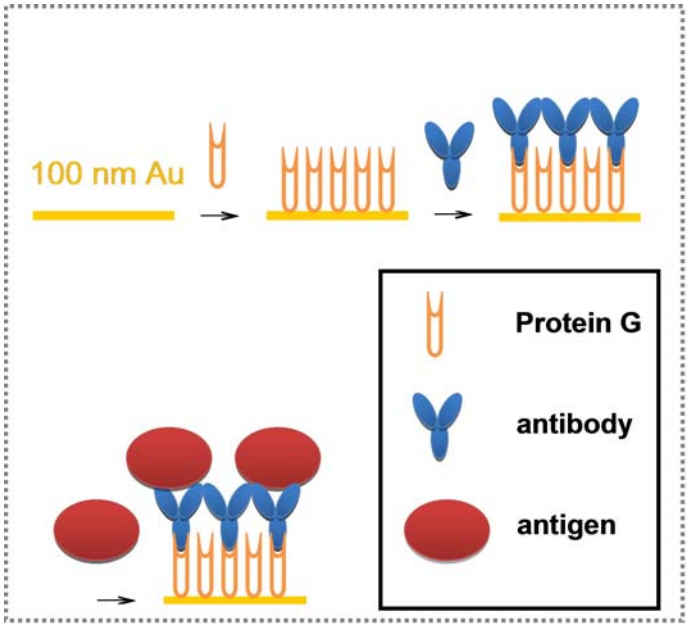

Figure 4-2. Schematic immobilization process for *C. parvum* attachment to the sensor surface via Protein G. Sensor surface is coated with 100 nm gold, then exposed to Protein G for 2 h. IgG anti-*C. parvum* is captured by Protein G to form an antibody layer on the sensor surface. *C. parvum* is captured through antibody-antigen reaction.

4.5. Results and discussion

4.5.1. Sensor characteristics

A set of PEMC sensors (n=15) with similar spectral properties was used in this study. All sensors exhibited a resonant mode in 920 ~ 950 kHz region and showed similar air to water frequency shift (70.50 ± 4.50 kHz) which we recognize as a measure of similar sensitivity. In the detection experiments we characterized the sensitivity values directly from frequency response to oocysts attachment, which also gave relatively small variations. Figure 4.3A shows a microscopic picture of PEMC sensor with a 2.8 mm PZT length, where quartz was attached to the end of PZT layer. Figure 4.3B shows the resonance spectra in air and when the sensor was fully immersed in DI water. Sensor exhibited resonant frequency at 940.75 kHz in air and 865.25 kHz in DI water, which gave a Δf = 75.50 kHz shift due to the difference in density of the surrounding medium. The decrease of resonant frequency is explained by Eq. (4.2), in which the effective cantilever mass in Eq. (4.1) is modified by adding the oscillating liquid mass present immediately adjacent to the cantilever surface. Quality value of the sensor decreased from 35 in air to 30 in liquid, which is only a ~14% decrease. Unlike nanocantilever sensors [189, 190] or microcantilevers [9], PEMC sensors do not suffer from liquid damping because of high Reynolds number (Re~10^6), and hence the resonant frequency is relatively easy to measure. This feature enables the conduct of continuous flow experiments where one changes the flowing sample and monitors the resulting resonant frequency response. Since the measurement is made *in situ* without removing the sensor from its housing, changes in resonant frequency can be totally attributed to the detection response.

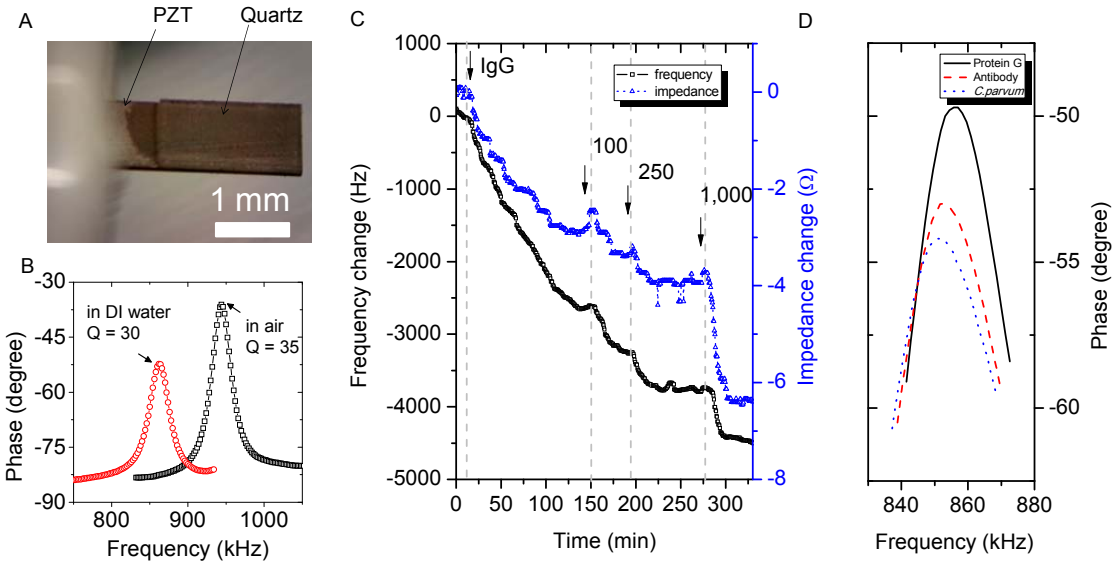

Figure 4-3. **(A).** A microscopic picture of PEMC sensor. The width of the sensor is 1.0 mm; overall length is 2.8 mm and the quartz length is 2.0 mm. **(B).** Spectra of the sensor on high mode in the 750 – 1050 kHz region in air and in DI water. Resonant frequency is 940.75 kHz (Q=35) in air and 865.25 kHz in DI water (Q=30), respectively. No significant damping of resonance peak occurs because the sensor functions in the inertia dominated regime. **(C).** Typical responses of resonant frequency and total impedance at resonance to antibody reaction and subsequent binding of oocysts (100, 250 and 1,000 oocysts, respectively). A 20 min PBS rinsing step was used between each oocysts sample injection and is not labeled in the graph for clarity. **(D).** The shapes of resonant peak during the detection correspond to t=0 min (Protein G immobilized), 150 min (IgG antibody immobilized) and 320 min (*C. parvum* oocysts attached).

A typical response of PEMC sensor to antibody and a sample containing *C. parvum* oocysts is shown in Figure 4.3C. In this experiment, we used Protein G as the linking agent and goat polyclonal IgG as the capture antibody. Antibody immobilization via Protein G allows the binding region (Fab) of IgG to be exposed to sample since Protein G binds to the Fc region. Antibody introduction caused a resonant frequency decrease of 2,552 Hz. After a PBS rinsing step, samples containing 100, 250 and 1,000 oocysts were added to the flow loop sequentially and between each addition PBS was used to rinse the system. Resonant frequency response of 642, 479 and 756 Hz were

observed for each of the additions, respectively. The response to antibody was higher than for the target oocysts which are much heavier than the antibody molecules. Such a response has been observed previously and the sensor response is higher for the same mass if it is directly attached to its surface [2]. In Figure 4.3D, the phase angle characteristics after each addition of Protein G, IgG antibody and *C. parvum* oocysts are shown. The peaks correspond to the resonant frequency changes following each binding step. The decrease suggests an increase of the sensor mass due to analyte attachment. Another feature we present for the first time here is that the impedance value at resonance also showed a parallel decrease for each of the binding steps and corresponded to the dynamics of resonant frequency. For antibody immobilization, the impedance change was -2.91 ± 0.06 Ω and the measured value stabilized well in PBS. Although the impedance change was small, the S/N ratio was high (~48) and thus it provides a useful measure. Impedance change for the various oocysts concentrations were -0.48, -0.57 and -2.45 Ω, respectively. As can be seen in Figure 4.3C, changes in impedance were parallel to resonant frequency changes, and we believe they could potentially be used for monitoring sensor response. However, in this study we monitored the resonant frequency change for detection purposes.

4.5.2. Detection in PBS and in milk

To test and compare the performance of PEMC sensor in matrixes that contain contaminants, detection experiments in PBS and in milk medium were carried out using the same sensor used in Section 4.5.1. Typical responses in PBS and in milk are shown in Figure 4.4. Sensor was installed in the flow cell and flow rate used was 1 mL/min after

functionalizing with IgG anti-*C. parvum*. Various concentrations of *C. parvum* oocysts were introduced into the flow loop and the flow was set in recirculation mode. Resonant frequency responses to sequential additions of 50, 250 and 10,000 oocysts in PBS were 150 Hz, 535 Hz and 1,525 Hz, respectively, and is shown in Figure 4.4A. Sensor showed a rapid resonant frequency decrease in the first ~15 min followed by a slower response reaching steady state in ~30 min. The total frequency response for the cumulative addition of 10,300 *C. parvum* oocysts was 2,210 Hz. Positive controls that expose the same concentrations of oocysts to blank sensor showed no response and exhibited a noise level of ±10 to ±15 Hz, suggesting no binding occurred. Negative control with IgG immobilized also showed no response to buffer.

For detection experiments in milk, the sensor was stabilized in PBS at 1 mL/min, and then 1 mL whole milk was introduced and the flow was set in recirculation. As shown in Figure 4.4B, the resonant frequency decreased by ~380 Hz after a few cycles of mixing due to the density difference between milk and PBS (relationship shown in Chapter 3). Its important to recognize that for a given excitation level (100 mV), the volume of surrounding liquid that oscillates with the cantilever is relatively constant for PBS or milk, because viscosities of the two fluids are similar. When a density change occurs, the oscillating fluid mass increases causing resonant frequency decrease.

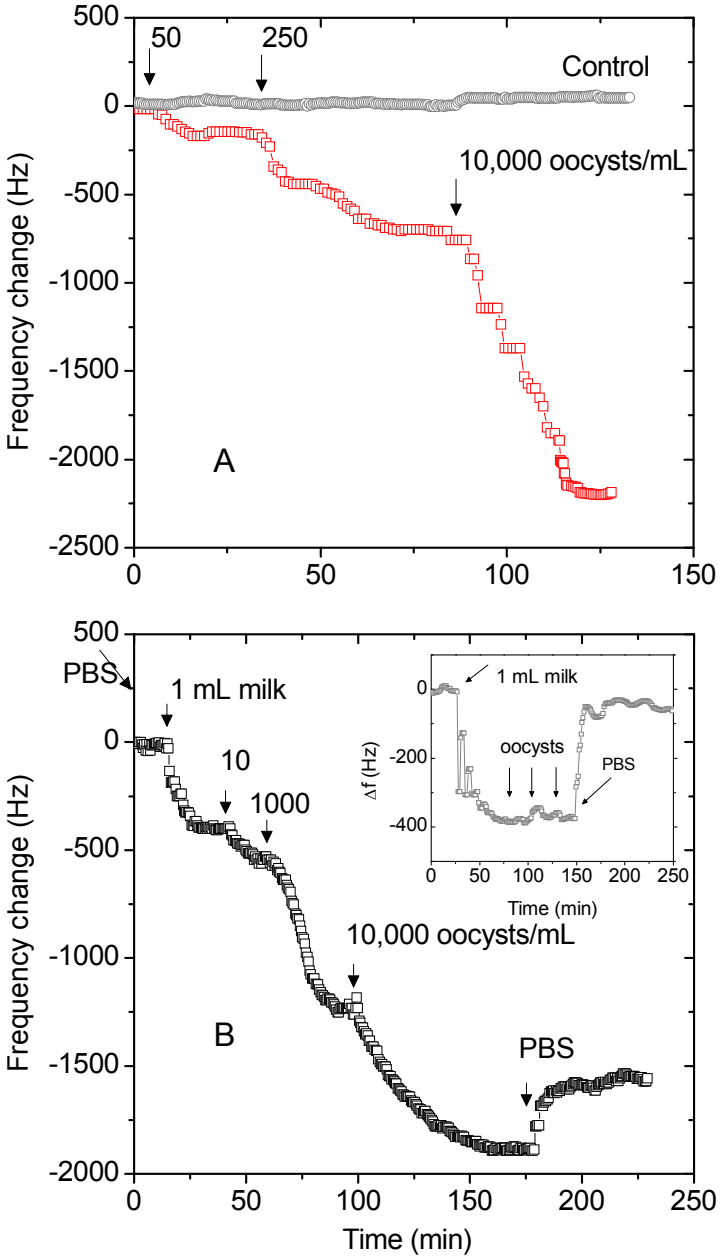

Figure 4-4. Sequential detection of *C. parvum* in PBS **(A)** and in 25% milk medium **(B)**, respectively. For detection in PBS, 1 mL 50, 250 and 10,000 oocysts/mL samples were injected into the flow loop sequentially. For detection in milk, 1 mL 10, 1,000 and 10,000 oocysts/mL samples were injected sequentially. Inset in **(B)** shows a positive control (bare sensor exposed to oocysts at same concentrations) that shows density response. No response was observed for injections of oocysts in both control experiments.

Given this background, detection of *C. parvum* oocysts at various concentrations were measured. Frequency responses for sequential additions of 10, 1,000 and 10,000 oocysts in 25% milk medium were 145 Hz, 680 Hz and 650 Hz, respectively. One notes in Figure 4.4B, the response was rapid upon sample introduction, followed by a slower change. For addition of 10,000 oocysts, the response reached a steady state after 50 min, which is much longer than in PBS. The total frequency response for the cumulative *C. parvum* exposure (11,010 oocysts) was 1,745 Hz. After reaching a new steady state, PBS rinse caused a recovery of ~360 Hz, which was approximately the initial density response. The nearly full recovery suggests that no permanent non-specific attachment of milk components occurred on the sensor surface. The control experiment (see inset in Figure 4.4B) conducted separately confirmed that the initial density response was reversible. Additionally, unfunctionalized sensor showed no response to various concentrations (10 to 10,000 oocysts/mL) of oocysts injections. By comparing the total resonant frequency changes in PBS and in milk, one notices the response in milk was lower than in PBS. Additionally, the binding in milk also took a longer time, which we attribute to milk constituents impeding or hindering the binding process. A quantitative comparison of kinetics and sensor response is discussed further.

4.5.3. Confirmation of detection using a second antibody

One way of confirming that the detection response was due to *C. parvum* oocysts binding, was to determine whether a second antibody that recognizes *C. parvum* will attach to the already bound oocysts on sensor surface. We used two antibodies from different sources. Goat polyclonal IgG antibody specific to *C. parvum* has become

available very recently. To our knowledge, no IgG-based sensor response for *C. parvum* detection has been reported. Monoclonal IgM antibody (Waterborne, Inc) was approved for use in the EPA Method 1623 and it shows good binding affinity to oocysts of *Cryptosporidium* species [175]. We used goat IgG as capture antibody and IgM as a second antibody for confirming the detection response. This approach of using capture and a secondary antibody is called a sandwich assay in traditional immunological methods. We use the same strategy here, except that the secondary antibody is not labeled and we use the sensor response as the "label" reaction.

A typical second antibody binding response is shown in Figure 4.5A. After sensor stabilized in milk medium, 1 mL 1,000 oocysts/mL *C. parvum* prepared in 25% milk was introduced into the flow loop and was set in recirculation mode. A 540 Hz resonant frequency decrease was observed in ~52 min. After a PBS rinse, 1 mL 10 μg/mL IgM was introduced and the flow was set in recirculation mode; a further decrease of 470 Hz occurred in ~60 min. The decrease due to IgM binding suggests that initial response observed was indeed due to *C. parvum* oocysts binding to the sensor. Figure 4.5B shows the resonant frequency responses to 10 μg/mL IgM antibody after exposing the IgG immobilized sensor to 50, 250 and 1,000 oocysts. The various responses have been time-shifted for ease of comparison. Resonant frequency decreases after IgM introduction were 93, 358 and 470 Hz, respectively. The control experiment with IgM injection to IgG immobilized sensor showed no binding as indicated by a response of ~20 Hz, which is within the noise level. The second antibody response magnitude is proportional to the number of oocysts introduced prior the IgM binding step, which suggest the usefulness of second antibody binding response for very low concentration measurement. Furthermore,

second antibody binding serves not only as an amplification method for extremely low concentration detection, but also to confirm detection thus reducing or eliminating false signals.

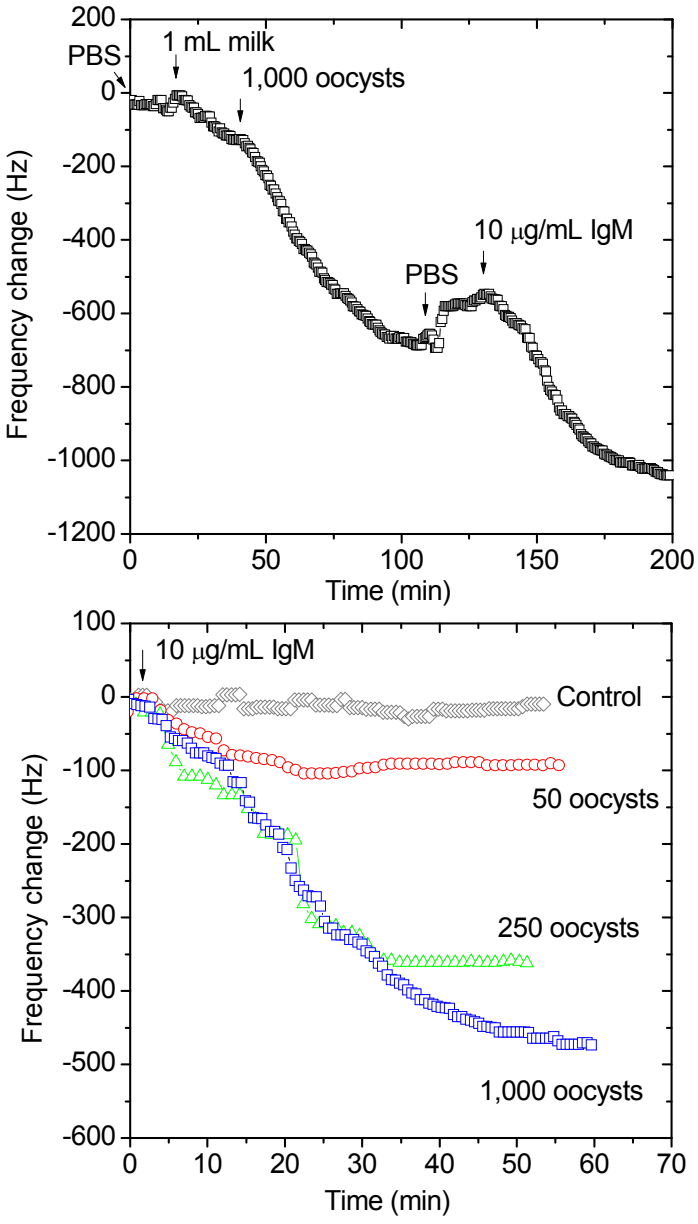

Figure 4-5. Confirmation of *C. parvum* detection using a second IgM antibody.

4.5.4. Release using low pH buffer

Another method for confirming that the sensor response is due to oocysts attachment is to release the attached oocysts by a low pH buffer and determine if resonant frequency recovers to pre-attachment value. This approach may also be useful for regenerating the sensor surface for reuse. There have been a number of reports that showed antigen release and sensor regeneration can be achieved using low pH buffer. In Figure 4.6, we show two examples of releasing bound oocysts after detection in PBS and in milk. As shown in Figure 4.6A, resonant frequency decreased by 1,610 Hz for 1,000 oocysts in PBS. After releasing with glycine buffer, resonant frequency recovered 1,400 Hz within 35 min. Upon switching back to PBS, no further change in resonant frequency occurred. The difference between the decrease and recovery was ~210 Hz, which is small (13%) compared to the sensor response. The difference may be attributed to unreleased oocysts. Figure 4.6B shows a similar experiment done with the same *C. parvum* concentration in 25% milk medium. Recirculation of 1,000 oocysts caused 890 Hz decrease in resonant frequency. Glycine release buffer caused a recovery of 820 Hz in 30 min, which constitutes a 92% release. A number of other release experiments (data not shown) showed release ranging from 75 to 95% (n=15).

4.5.5. Quantitative analysis of sensor response

Comparing the detection and release responses in Figure 4.6, one notes that the frequency response for the same number of oocysts (1,000 oocysts) in PBS was ~1.5 times greater than the response obtained in milk. The binding kinetics in Figure 4.6 can be analyzed using Langmuir kinetic model [191]:

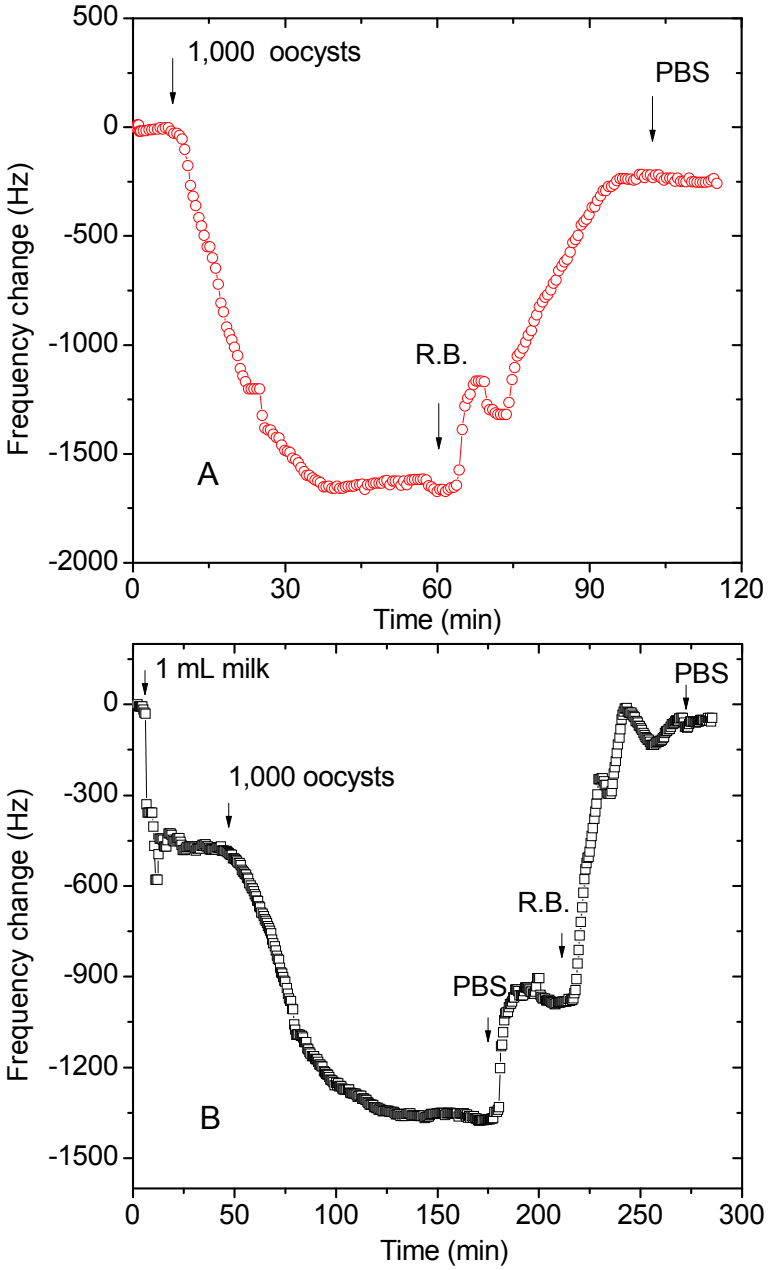

Figure 4-6. Release of bound oocysts using glycine release buffer after detection of 1,000 oocysts in PBS **(A)** and in milk medium **(B)**, respectively.

$$\ln\left(\frac{\Delta f_{\infty}-\Delta f}{\Delta f_{\infty}}\right)=-k_{obs}\tau \qquad (4.4)$$

where Δf is the change in resonant frequency at time τ, Δf_∞ is the total steady state frequency change, and k_{obs} is the observed binding rate constant. Binding rate constant was obtained by fitting a straight line to the data obtained during the first 10 min of the sensor response and was found to be 0.0873 min^{-1} in PBS and 0.041 min^{-1} in milk medium, respectively (Figure 4.7). The reason for slower binding rate in milk could be due to the presence of various proteins, lipids, dissolved salts and particles in milk. Complex medium impede both the accessibility of antibody binding site and the transport of oocysts to the sensor surface. It is possible that surface antigens on *C. parvum* may weakly bind to milk component, which rendering them unable to bind to surface antibody. Similar decreased response magnitude and binding rate constant have been observed in other biosensor systems [182, 192].

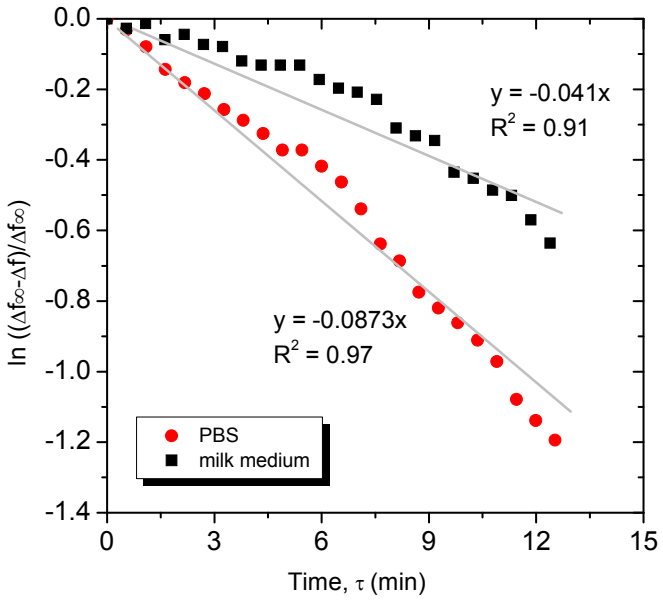

Figure 4-7. Kinetic analysis of detection of 1,000 oocysts in PBS and in 25% milk medium. Initial binding constants were 0.0873 and 0.041 min^{-1} for oocysts attachment in PBS and in milk medium, respectively.

It is useful to quantitatively compare the sensor response to oocysts concentration since that relationship can provide a calibration for analyzing unknown samples. Sensor response to *C. parvum* oocysts in PBS and milk medium is collectively presented in a semi-logarithmic graph in Figure 4.8. Similar correlations have been reported for *Bacillus anthracis* spores measured with a low-order resonance mode (~60 kHz) and staphylococcal enterotoxin B with high-order resonance mode (~940 kHz). The experimental data obtained in this study correlated reasonably well with the following equation:

$$(-\Delta f) = A\log(C) + B \tag{4.5}$$

where A and B are sensor constants and depend on cantilever geometry, antibody-antigen binding constant, and antibody surface concentration. The term $(-\Delta f)$ is the steady-state resonant frequency response and C is the concentration of oocysts added to the flow loop.

Fitting the experimental data (n= 3 to 5 for each concentration) to Eq. (4.5), one gets $(-\Delta f) = 1206.9 \log (C_{crypto}) + 2105.9$ for PBS samples, and $(-\Delta f) = 594.8 \log (C_{crypto}) + 1005.9$ for milk samples. In Figure 4.9 we present results obtained using various different sensors (n=15) that had similar sensitivity. Considering sensitivity variability due to manual fabrication, the response to various concentrations gave a good correlation (R^2 = 0.93 for PBS, and 0.91 for milk medium). Note that the parameters A and B are ~50% lower in milk than in PBS. The lower value of the constants A and B is due to a decrease in resonant frequency response. We found the sensor frequency response magnitude was ~45% lower in milk than in PBS for the same *C. parvum* concentration.

However, the response of PEMC sensor for 5 oocysts in milk still gave a response. Among the six attempts of detecting 5 oocyst, four gave positive detection

response. The sensor responses were 140, 50, 90 and 98 Hz, which gave an average of 95 ± 37 Hz (n=4) with a signal to noise ratio > 4 since the noise level of most of the detection was ~15 – 20 Hz. Three repeated detection experiment results are shown in Figure 4.8. As one notes, sensor positive responses to the concentration of 5 oocysts/mL were quite rapid, within 2 – 3 min.

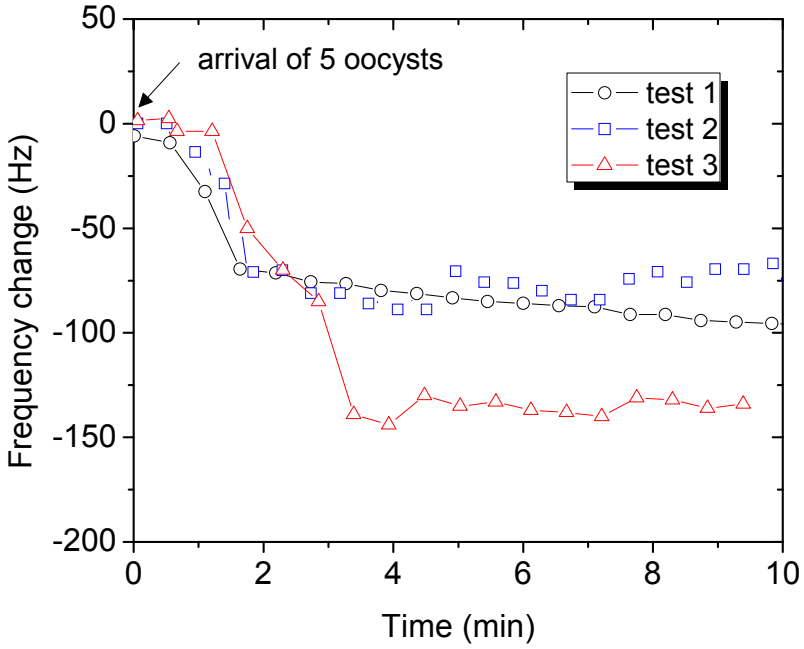

Figure 4-8. Three separate detection experiments with *C. parvum* concentration at 5 oocysts/mL.

We thus estimate the limit of detection as 5 oocysts/mL. Since flow loop is ~4 mL, the actual concentration that can be detected is 1.25 oocysts/mL. Experimentally, we made many attempts for detecting samples containing 1 oocyst with the flow in recirculation. The results were not sufficiently reproducible and the experiments were abandoned.

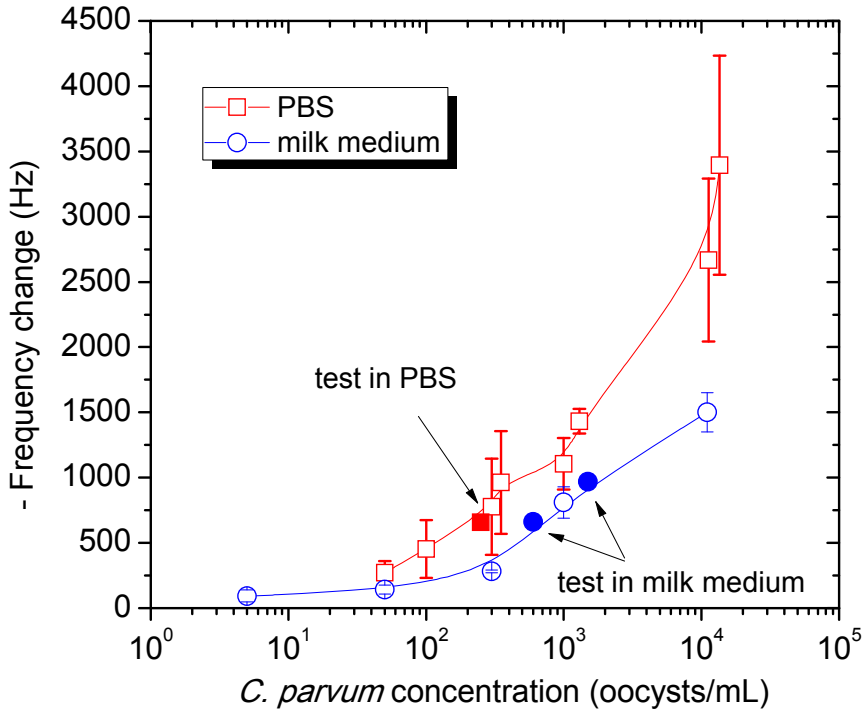

Figure 4-9. Resonant frequency responses to various concentrations of *C. parvum* oocysts in PBS and in milk medium. (n=3 to 5). Responses in milk medium (○) and in PBS (□) show good semi-log correlation with the number of oocysts. Filled circle (●) are the responses of test solution (600 oocysts/mL and 1,500 oocysts/mL) in milk and filled square (■) is response of test solution (250 oocysts/mL) in PBS.

To further test the reliability of the quantification relationship derived (Eq. 4.5), three test samples containing known number of *C. parvum* oocysts were introduced into the flow loop separately in either PBS or milk as background. The data from these three test samples are plotted as filled data points in Figure 4.9. The frequency shifts were well within the expected responses.

4.6. Conclusions

In this chapter, we showed that the detection of *C. parvum* in PBS or milk background is feasible at as low a concentration as 5 oocysts/mL in a flow apparatus. The selectivity of PEMC sensor was not compromised in milk matrix even though the frequency response magnitude decreased (~45%) and binding kinetics was slower. The second antibody binding method provided confirmation of sensor detection response. The sensor showed a semi-log relationship between resonant frequency change and *C. parvum* oocysts concentration with a dynamic range of 50 – 10^4 oocysts/mL. Since the sensor "collects" the target oocysts and the response is proportional to the number of the collected oocysts (which is demonstrated by examination of sensor surface under scanning electron microscope), one can flow a larger sample volume, such as 100 mL, and detection of 5 oocysts in the 100 mL sample would be feasible. Achievement of such detection sensitivity would reduce the volume of source water that is to be sampled.

CHAPTER 5 : RAPID AND SENSITIVE DETECTION OF *GIARDIA LAMBLIA* IN FINISHED AND SOURCE WATER AT 10 CYSTS/ML

5.1. Introduction

Giardia lamblia is a flagellated enteric protozoan parasite and a causative agent of human giardiasis [193]. Giardiasis causes acute or chronic diarrhea, asymptomatic illness and severe mal-absorption resulting in weight loss, and is frequently implicated in waterborne outbreaks. Infection occurs by ingestion of *G. lamblia* cysts present in contaminated water and food, or by fecal-oral route [194]. Together with *Cryptosporidium*, *Giardia* has been classified as one of the important pathogens in the WHO Neglected Disease Initiative [195]. Since ingestion of as few as ten cysts may cause giardiasis, there is a great need for sensitive method for detecting and monitoring *G. lamblia* in source and finished drinking water samples.

As introduced in Chapter 4, EPA has established Method 1623 for simultaneous detection of *Cryptosporidium* and *Giardia*. However, the evaluation is a long process. To reduce time of analysis, alternate methods, PCR and ELISA, have been investigated [196-199]. Although PCR is extremely sensitive (1 – 10 cysts), it requires a pre-concentration step following the filtration step. ELISA, on the other hand, exhibits poor sensitivity – 10^4 to 10^5 cysts. Although several advanced methods have been investigated for *G. lamblia* detection, they are either tedious or exhibit poor sensitivity [187, 200, 201]. On the other hand, cantilever biosensors have exhibited high sensitivity and selectivity for pathogen detection [93, 202]. Since they are responsive to mass-change at femtogram levels in liquid, we examine the applicability for detecting *Giardia* cysts. Unlike bacterial

pathogens the cysts are large, and no antibody-based biosensor method has been reported for *G. lamblia* detection. This we believe is in part due to their size as it is considerably larger (~8 – 13 μm) than bacterial pathogens (~1 μm). While QCM and similar resonators have been found to exhibit sensitivity at nanogram levels for molecules, they exhibit poor detection limit *Cryptosporidium parvum* (10^5 oocysts/mL) which is larger (~3 – 5 μm) than a bacterium, but smaller than *Giardia* [182]. In Chapter 4 we have shown that PEMC sensor was sensitive to detect *C. parvum* at as low as 5 oocysts/mL in buffer and 25% milk matrix.

In this chapter, we examine if antibody-immobilized PEMC sensors exhibit detection sensitivity at a much lower concentration of *G. lamblia* cysts in more practical water matrixes of tap water and river water. We also show successful detection of cysts in one liter samples and at a flow rate of 5.0 mL/min. The latter is significant as most biosensor assays are carried out at low flow rates. For example, SPR and QCM typically operate at 10 – 200 μL/min; and for most of microcantilever and nanocantilever, they simply could not work in a liquid environment due to the enormous viscous damping effect. Studies on high flow rate detection with biosensors are few. In one study with 55 MHz QCM for protein detection flow rate was found to give a larger overall sensor response [59]. Higher flow rate sensing is advantageous because a larger sample volume can be analyzed without a pre-concentration step.

5.2. Overview of biosensors for *G. lamblia* detection

Immunoassays and direct fluorescent kits are commercially available for *G. lamblia* detection [203-205]. However, more rapid and sensitive methods are needed for

environmental monitoring. Li et al. [201] used the catalytic growth of gold nanoparticles for detecting *G. lamblia* cysts. In that immunoassay, cysts were captured by antibody functionalized gold nanoparticles (Au-NPs) and then separated by centrifugation. The quantitative detectable color development was derived from the catalytic growth of Au-NPs and was measured by a common UV-Vis spectrophotometer. All the immunoassays were completed in a homogenous liquid phase and a detection limit of ~ 10^3 cysts/mL was achieved.

A filter-based microfluidic device was described for *G. lamblia* and *C. parvum* detection [187]. Parasites were injected into a coin-sized device consisting of filter weirs (~1 μm gap) where fluorescent-labeled antibodies were available for binding. Single oocysts or cysts could be observed microscopically within 5 minutes after injecting the sample.

Table 5-1. Overview of biosensors for *G. lamblia* detection

Biosensor type	**Matrix**	**LOD**	**Estimated time of analysis**	**Ref.**
AuNP + absorbance	Growth solution	10^3 cysts/mL	~2 h	[201]
Fluorescence microfluidic	Buffer	1 cyst	5 min	[187]
PEMC sensor	Buffer, Tap and river water	10 cysts/mL	1 h	[206]

Abbreviations: AuNP: gold nanoparticle.

5.3. Experimental

5.3.1. PEMC sensor

PEMC sensor is a cantilever sensor that measures mass change by change in resonant frequency, which is composed of a PZT layer and a glass layer. A detailed

description of cantilever physics and operation principles can be found in Chapter 4. For cantilever biosensors that operate in resonant (dynamic) mode, resonant frequency decrease is caused by binding of cysts to antibody immobilized cantilever surface.

5.3.2. Experimental details

Materials and reagents

Cysteamine, glutaraldehyde (25 wt% in H_2O) and PBS (10 mM, pH 7.4) were purchased from Sigma-Aldrich (St. Louis, MO). Anti-*G. lamblia* (murine monoclonal IgG) and inactivated *G. lamblia* cysts were purchased from Waterborne, Inc. (New Orleans, LA). Aliquots of antibody solution (10 μg/mL) were prepared in. *G. lamblia* samples were prepared by diluting stock sample in PBS and stored at 4 ℃ until use. Tap water was obtained locally. River surface water was collected from Schuylkill River near 30th and Market St. in Philadelphia, PA and stored at 4 ℃ until use. Water samples were replaced every two weeks. Both water samples were used without purification or treatment. Water samples spiked with cysts (10 – 10,000 cyst/mL) were prepared freshly prior to an experiment. Stock sample was determined with flow cytometry with 1% error. Experimentally, glass slides deposited with 15 μL samples were examined under microscope and accuracy of each diluted concentration was found to be within 10 – 15%.

Sensor fabrication and experimental procedures

Sensor fabrication details could be found in Chapter 3. Briefly, a PEMC sensor consists of two layers: a PZT layer (Piezo Systems, Woburn, MA) and a quartz layer (SPI, West Chester, PA), bonded by a non-conductive adhesive. The PZT and glass were 2.7 ×

1.0 × 0.127 mm and 2.0 × 1.0 × 0.160 mm ($l \times w \times t$), respectively. Wires (30 gauge) were soldered to electrodes of PZT layer and anchored in 6 mm glass tubing. The sensor was spin-coated with polyurethane (Wasser, Auburn, MA) for electrical insulation.

Prior to a detection experiment, 2 mm^2 sensor tip surface was freshly sputter-coated with 100 nm gold and incubated in 2 mM cysteamine overnight followed by incubation in 2.5% glutaraldehyde in DI water for 1 h. After rinsing with DI water, it was installed in a home-made flow cell (as depicted in Figure 4.1). The hold-up volume of the flow cell was 90 μL and the volume of the entire flow loop was ~4 mL. In a detection experiment, resonant frequency change was monitored by an impedance analyzer (HP 4192A) and real-time data was acquired by a LabVIEW® program. Detection experiments were carried out at 30.0 ± 0.1 °C, with various flow rates facilitated by either a Fisher mini-pump or a Masterflex® C/L® pump. After resonant frequency of the sensor stabilized for at least 20 min, 1 mL antibody solution (10 μg/mL) was introduced into the flow loop at 0.8 mL/min. The antibody solution was re-circulated for 60 min, and the flow loop was rinsed with PBS for 20 min. As the PBS rinsing was taking place, flow rate was adjusted to various desired values (0.8 – 5.0 mL/min). After the sensor reached a new steady state, various *G. lamblia* cysts samples were introduced into the flow loop, and the flow was set in recirculation mode.

Some sensors were examined in an environmental scanning electron microscopy (ESEM, FEI XL30) after detection experiments. In such cases, the sensor was removed from the flow cell, rinsed with DI water, dried in air, and then sputtered with a thin layer of platinum prior to examination in the ESEM.

5.4. Results and discussion

5.4.1. Sensor characteristics

A set of PEMC sensors (m=10) with similar spectral property was used in the detection experiments. All sensors were fabricated with exposed dimensions of 2.0 × 1.0 mm glass layer and 2.7 × 1.0 mm (l × w) PZT layer. They exhibited a dominant resonant mode in the 920 ~ 950 kHz frequency range. All sensors showed similar frequency shift for air to water transition of 64.50 ± 5.50 kHz, and we interpret this response as an approximate measure of sensitivity to mass-change.

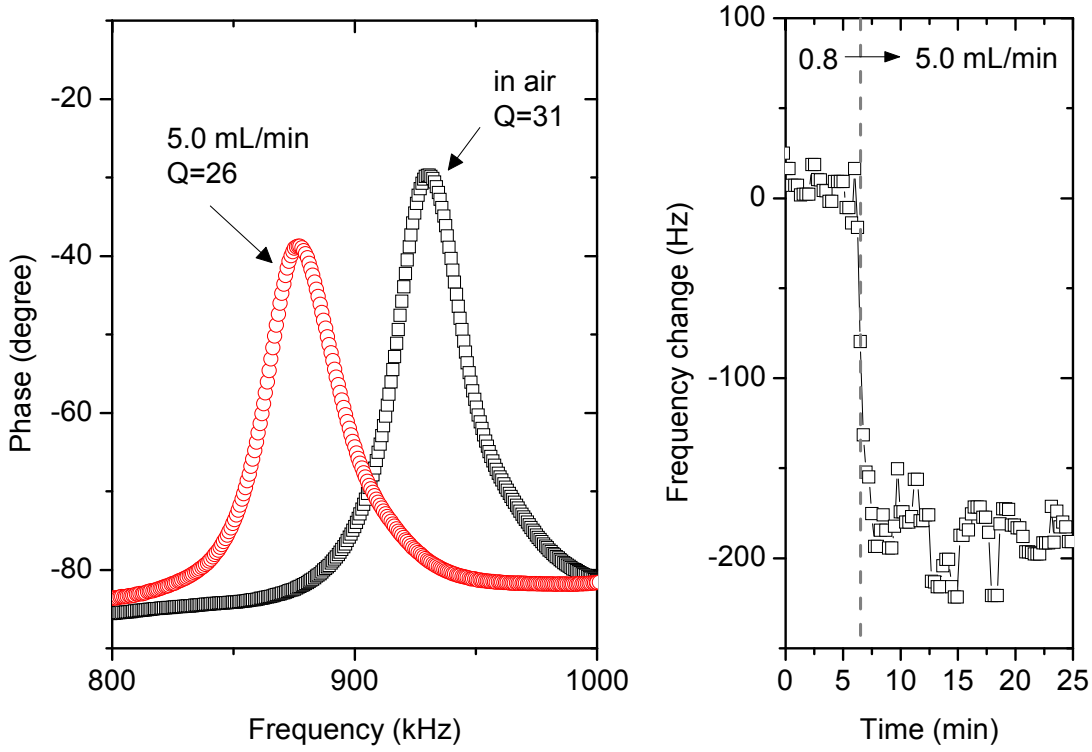

Figure 5-1. **(A)** Sensor spectra in air and in flow cell at 5.0 mL/min. The *Q*-value of the sensor decreased from 31 in air to 26 in DI water, but was sufficiently high for measuring resonant frequency within ± 25 Hz. **(B)** Noise level of resonant frequency increased from ± 10 Hz to ± 38 Hz when flow was adjusted from 0.8 mL/min to 5.0 mL/min.

The frequency spectra of a typical PEMC sensor in air and in flow cell at 5.0 mL/min are given in Figure 5.1. Sensor exhibits resonant frequency at 930.75 kHz in air and 869.25 kHz in liquid, which gives a Δf = 61.50 kHz. Q-value of the sensor, an indicator of peak sharpness, decreased from 31 in air to 26 in liquid, which is a modest decrease of ~16 %. The robustness of Q-value in liquid renders PEMC sensor as a useful device for direct in-liquid application and measurement.

Since we want to examine flow rate effects on sensor response to cyst binding, we first investigated the effects of flow rate on sensor resonant frequency dynamics. In this case, an unfunctionalized sensor was installed in the flow apparatus and the flow rate was changed from 0.8 mL/min to 5.0 mL/min. At this flow rate the average velocity of the fluid in the flow cell was 0.46 cm/s and the flow was laminar at a Reynolds number of 22. The resonant frequency decreased by ~200 Hz in an almost step-like manner and then stabilized rapidly at the new higher flow rate of 5.0 mL/min (see Figure 5.1). The noise level of measured sensor resonant frequency increased from ±10 Hz to ±38 Hz corresponding to the flow rate increase. This noise level increase was attributed to the change of the flow field introduced disturbance. The Q-value did not change (<2%) when flow rate was changed from 0.8 to 5.0 mL/min. The data in Figure 5.1 show that continuous monitoring of resonant frequency at 5.0 mL/min in the flow cell is feasible. Stability of sensor resonant frequency at such a high flow velocity indicates the robustness of the sensor and is an attractive characteristic of PEMC sensor.

5.4.2. Sequential detection using PEMC sensor

Sequential detection experiments were first carried out to examine antibody binding affinity and detection sensitivity for *G. lamblia* cysts. Repeat experiments were carried out with different sensors for testing antibody attachment to the cysteamine + glutaraldehyde functionalized sensor surface at a flow rate of 0.8 mL/min. Figure 5.2 shows the frequency responses for 11 separate antibody immobilization experiments on different sensors. For each experiment, a fresh prepared sensor was used. As one notes, the average response for antibody immobilization was 589 ± 98 Hz, only one sensor showed relatively higher antibody response (839 Hz). Considering the normal noise level of sensor operation in liquid is 18 ± 3 Hz, response got from antibody shows a relatively repeatable sensor response. Repeatable antibody response also verifies the similarity of sensitivity among different sensors used for experiments.

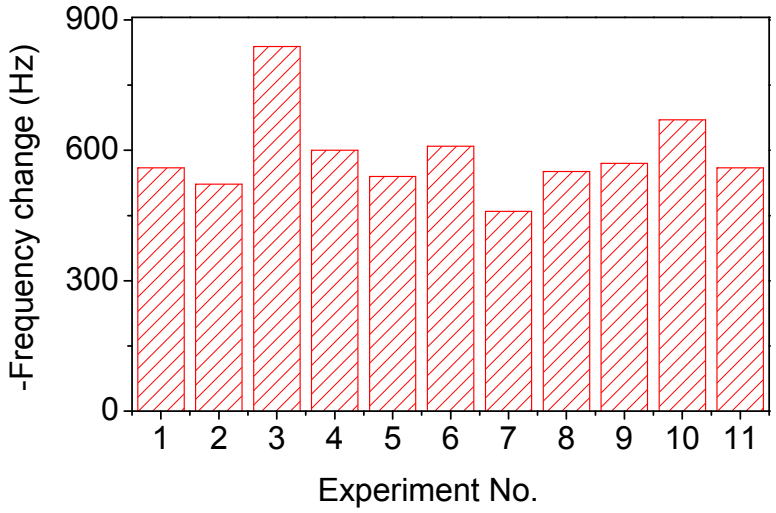

Figure 5-2. Sensor response to 10 µg/mL anti-*G. lamblia* with cysteamine and glutaraldehyde functionalized surface. Repeatable resonant frequency response was obtained.

After confirming the antibody response, *G. lamblia* detection experiments were carried out. In Figure 5.3, we show a sequential detection experiment conducted at 0.8 mL/min. Sensor functionalization was carried out by incubating a gold-coated sensor in cysteamine and glutaraldehyde, and then exposing to antibody in the flow loop set in recirculation mode. As can be seen in Figure 5.3, the resonant frequency showed a gradual decrease of 575 ± 5 Hz as antibody immobilization occurred via the surface aldehyde group. After steady state was reached indicating completion of antibody immobilization, various concentrations of *G. lamblia* from 10 to 10,000 cysts/mL were injected into the flow loop set in recirculation mode. Recirculation was found to be necessary as a 1 mL sample at 0.8 mL/min did not allow sufficient time for binding. After each injection sufficient time was allowed for binding reaction to occur and was assessed by the sensor resonant frequency reaching steady state. Frequency responses to sequential addition of increasing number of cysts – 10, 100, 1,000 and 10,000 gave frequency shifts of 67, 650, 490 and 360 Hz, respectively. Addition of a further 10,000 cysts sample gave a modest frequency decrease of 120 Hz, and the low response may suggest limitation of available antibody sites on the sensor. The functionalized sensor surface area was 2 mm^2, and if it was covered entirely with cysts (~12 μm in length and ~6 μm in width, obtained from ESEM micrograph, see Figure 5.5), the sensor could accommodate a maximum of ~30,000 cysts. The actual number captured by a sensor is likely to be a fraction of this value due to steric effects and non-uniform surface antibody distribution. Therefore a low response for 10,000 cysts after an exposure to 1,110 cysts could be attributed to availability of binding sites.

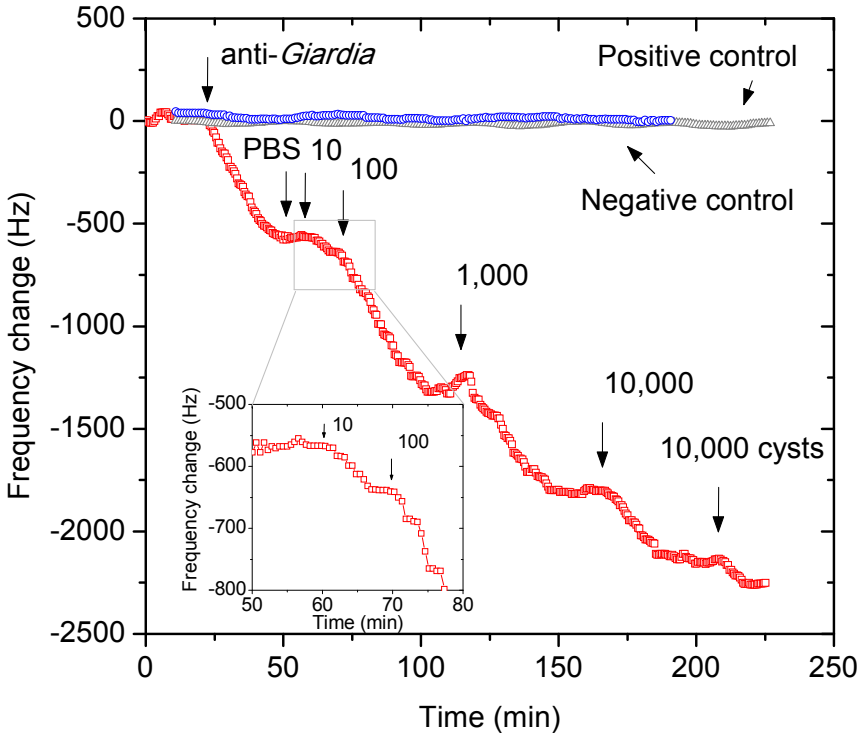

Figure 5-3. Sequential detection of *G. lamblia* cysts in PBS at 0.8 mL/min. After sensor was prepared with an exposed aldehyde group, it was installed in the flow cell with PBS as running buffer. Anti-*Giardia* (10 µg/mL) was injected in recirculation mode for antibody reaction to surface aldehyde group. As reaction occurred, resonant frequency decreased and reached a steady state. After a PBS rinse step, sequential cysts addition to the flow loop was made allowing for the sensor to reach steady state following each addition. Inset shows an expanded response for a 10 cysts sample.

The infectious dose of *G. lamblia* cysts has been reported to be as low as 10 to 25 cysts [207], which means for a biosensor to be of practical use, the limit of detection should be less than 10 cysts. Experiments at 0.8 mL/min showed the potential for detecting 10 cysts. The response was 81 ± 19 Hz (n=5). Compared with the average noise level (18 ± 3 Hz) at 0.8 mL/min, the response to 10 cysts detection was at a signal-to-noise ratio (S/N) of 4.5. Even though positive response to 10 cysts was obtained, the S/N ratio was modest for confident screening of samples. To improve the performance of

PEMC sensor for low concentration detection, we investigated sample flow rate effects on the total sensor response. Our underlying hypothesis was the sensor response was limited by cyst transport rate to sensor surface. It is important to remember that we rely on fluid flow to transport cysts to the vicinity of sensor surface. The immobilized antibody does not attract the cysts. To examine the validity of flow-field hypothesis, a series of experiments were carried out at a higher flow rate of 2.4 mL/min which is three times the flow rate used in Figure 5.3. The sensor responses obtained to separate exposures of low concentration samples 10 – 500 cysts given in Figure 5.4 validates the flow-field hypothesis. Positive control response with an unfunctionalized sensor exposed to 500 cysts in recirculation showed a small response of 10 ± 6 Hz, which is quantitatively at the noise level. As shown in Figure 5.4A, for 10, 50 and 500 cysts, the frequency decreases were 190, 450 and 790 Hz, respectively. Responses that were significantly larger than the noise level were observed in the first 5 min. Step-wise response was not commonly observed. The S/N ratio for 10 cysts detection was greater than 10, which was an improvement over sensor response at 0.8 mL/min. Repeat experiments (n=4) for detecting 10 – 500 cysts samples were carried out and the average response to each concentration is shown in Figure 5.4B. One notes the sensitivity of the same sensor can be enhanced by flow rate resulting in improved S/N, and therefore a lower limit of detection. S/N ratio is a very important parameter for evaluating the performance and establishing the detection limit of a biosensor. Normally higher S/N ratio is desired as it can guarantee the reliability of results.

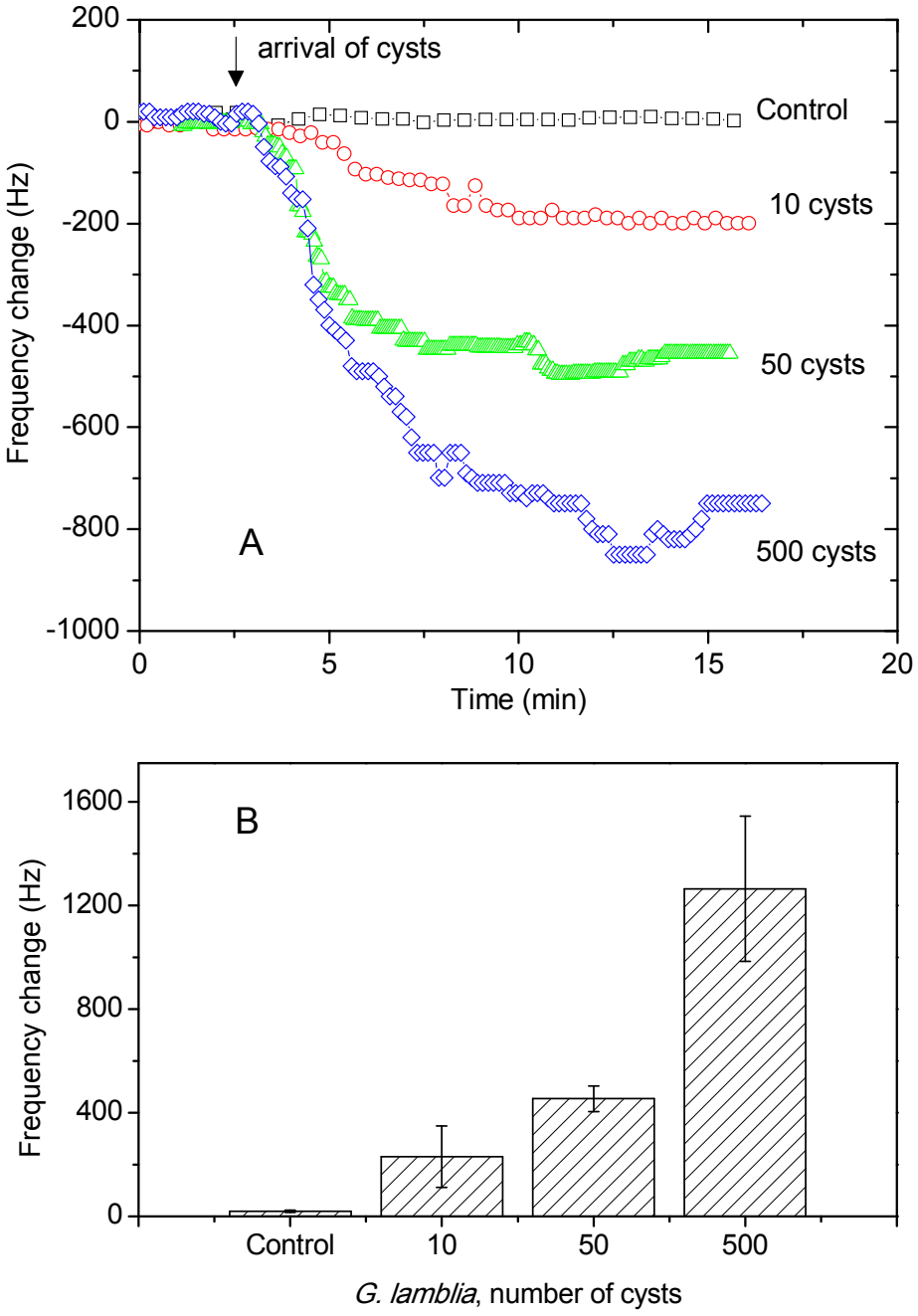

Figure 5-4. **(A)** Response of the sensor to addition of 1 mL sample containing 10, 50 and 500 cysts/mL *G. lamblia* samples to the flow loop set in recirculation mode at 2.4 mL/min. **(B)** Average frequency responses (n=4) to various concentrations at 2.4 mL/min. Negative control experiments showed responses of 20 ± 5 Hz (n=4).

To confirm that the PEMC sensor response was indeed due to *G. lamblia* binding to the sensor surface, the sensor surface was examined in ESEM after detection experiment. Figure 5.5 shows typical ESEM images of sensor surface taken after the detection experiment in which a cumulative exposure to 11,110 cysts had occurred. Attached cysts were evenly distributed through the 2 mm^2 sensor area. Figure 5.5B shows 1/250th of that area, and the captured cysts number on the sensor was ~1,000, which is less than one tenth of the total cysts exposed to the sensor. In effect, capture efficiency was ~10% and the captured cysts covered ~5% of the sensor area.

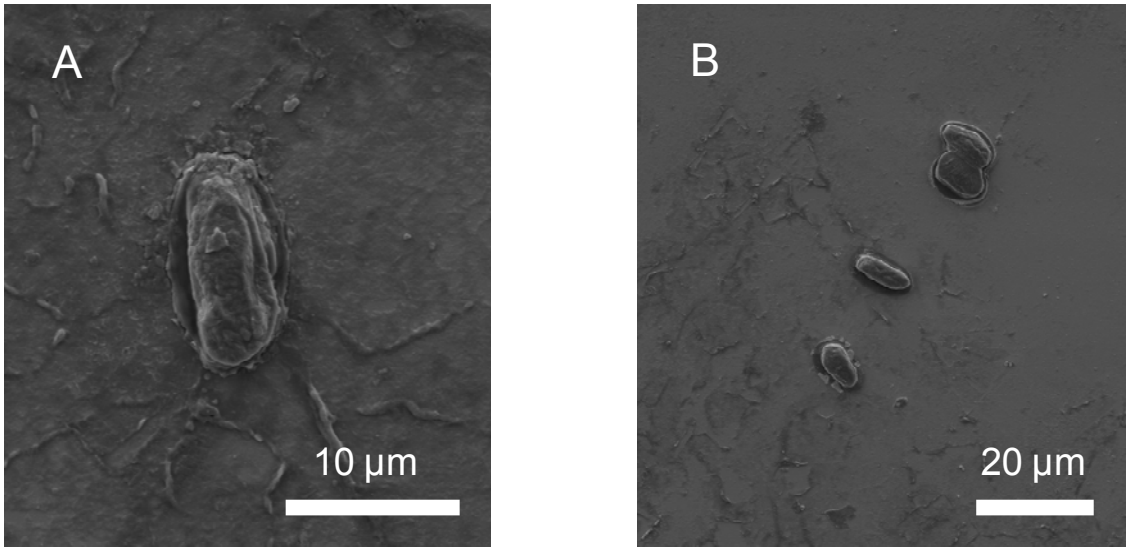

Figure 5-5. ESEM pictures of *G. lamblia* attached to the sensor surface. **(A)** 3,000× magnification **(B)** 1,000× magnification.

5.4.3. Effect of flow rate on sensor response and quantification

Comparing the results in Figure 5.3 and 5.4, one notes the sensor response for the same *G. lamblia* concentration depended on the flow rate used. We examined systematically the effects of flow rate by conducting detection experiments in the range

of 0.5 to 5.0 mL/min and cysts concentrations 10 to 10,000 cysts/mL. Figure 5.6 shows the sensor responses to two different *G. lamblia* concentrations: 500 and 10,000 cysts/mL at flow rates of 0.8, 1.5 and 2.4 mL/min. Samples containing 500 cysts gave progressively higher responses of 470, 640 and 790 Hz as the flow rate was increased. Similar experiments with 10,000 cysts gave responses of 1,210, 1,470 and 2,820 Hz, respectively. At both concentrations, the magnitude of response to the same number of cysts increased as the flow rate was increased from 0.8 to 1.5, and then to 2.4 mL/min. Reports on using flow rate as a means to improve biosensor response are few. The most likely reason is most biosensor platforms exhibit high measurement noise at high flow rates due to the limitation of sensor flow cell design used. Examples are QCM and SPR which are typically conducted in a flow format at less than 0.1 mL/min. As shown in Figure 5.1, the PEMC resonant peak shape remained intact and relatively noise-free at 5.0 mL/min and the noise level for resonant frequency measurement was ±38 Hz. We found PEMC sensor to be usable at an even higher flow rate of 17.0 mL/min, but at a higher measurement noise. Experimentally we found 5.0 mL/min as an intermediate value at which continuous monitoring of resonant frequency gave response at reasonable S/N.

As noted earlier, a group of PEMC sensors with nearly identical geometry was used in the present study. For a biosensor to be useful in practical applications, one important consideration is repeatability of detection responses using different sensors but of same design. We examined the response of a set of different sensors to the same *G. lamblia* concentration at the same assay condition.

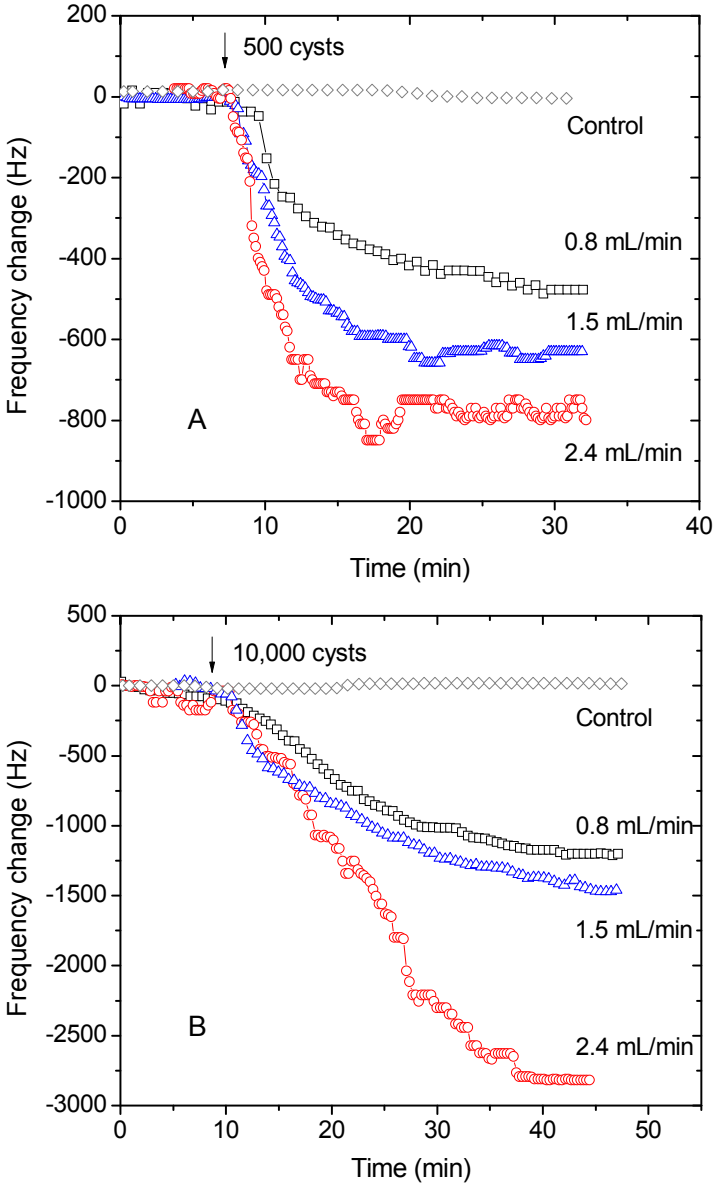

Figure 5-6. Responses of PEMC sensor to **(A)** 500 cysts and **(B)** 10,000 cysts at the three flow rates: 0.8, 1.5 and 2.4 mL/min. Higher flow rate resulted in higher magnitude of sensor response. Since the sensor measures the binding reaction, the increased response is due to a higher transport rate of cysts to sensor surface. Responses to the positive controls (bare sensor) were in the noise level.

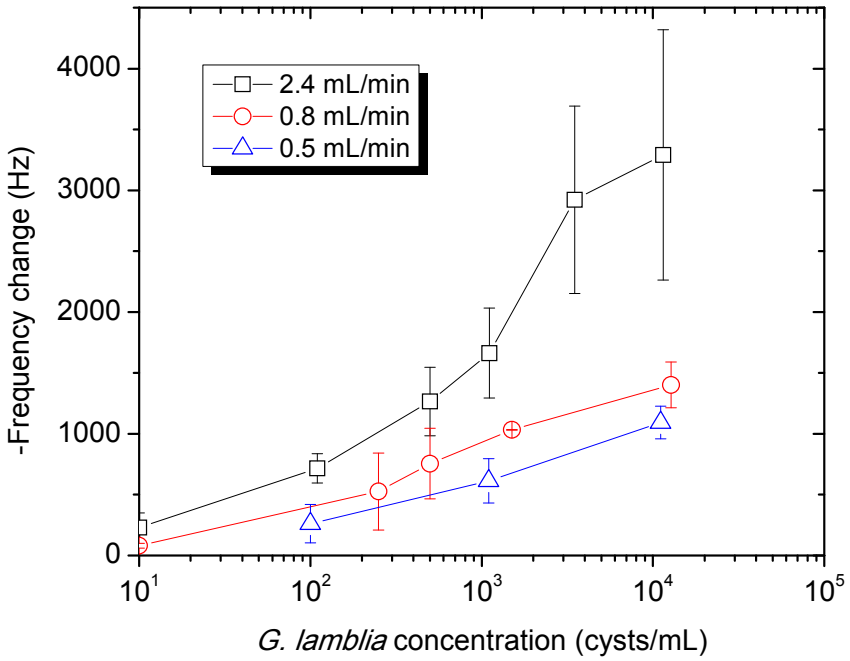

Figure 5-7. Quantification of sensor response using a group of PEMC sensors (m=10) at the flow rates of 0.5, 0.8 and 2.4 mL/min. Each data point represents an average of a minimum of three experiments. Error bars represent one standard deviation (n=3 to 5).

In Chapter 4, we observed sensor resonant frequency decrease correlated with analyte concentration by a log-linear function, $(-\Delta f) = A\ \mathrm{Log}(C) + B$. The term $(-\Delta f)$ is the steady-state resonant frequency response and C is the concentration of target analyte exposed to the sensor. The parameters A and B are sensor constants which depend on cantilever geometry, antibody-antigen binding constant, and antibody surface concentration. To examine whether the same relationship noted above holds true for *G. lamblia*, a plot of frequency response to *G. lamblia* cysts concentrations ranging from 10 to 12,500 cysts/mL at three different flow rates (0.5, 0.8 and 2.4 mL/min) using ten different sensors was prepared, and is given in Figure 5.7. Flow rate of 1.5 mL/min was also investigated, but data are not included here for clarity of presentation. From the plot

we see the frequency response obtained using different sensors correlated quite well with log of *G. lamblia* cysts concentration (n=3 for 0.5 mL/min, n=3 to 5 for 0.8 mL/min, n=3 to 4 for 2.4 mL/min). The results indicate good repeatability of experiments using a group of PEMC sensors (m=10). The experimental data were fitted to the log-linear relationship noted above, and the correlation properties are summarized in Table 5.2. We note the correlation coefficient decreased from R^2 = 0.99 at 0.5 mL/min to R^2 = 0.91 at 2.4 mL/min. Also standard deviation increased with flow rate indicating a higher variance in sensor response. The plot in Figure 5.7 shows higher flow rate enhanced transport of *G. lamblia* to sensor surface quite significantly. The enhancement in sensor response is seen in the value of the constant *A*, which increased from 405.7 to 435.4, 572.3 and 1055.0, for the increasing flow rates of 0.5 to 0.8, 1.5 and 2.4 mL/min, respectively.

Table 5-2. Sensor response correlation with *G. lamblia* concentration at various flow rates.

Flow rate (mL/min)	Correlation	R^2
0.5	$(-\Delta f) = 405.7 \text{ Log (C)} - 572.5$	0.99
0.8	$(-\Delta f) = 435.4 \text{ Log (C)} - 405.9$	0.98
1.5	$(-\Delta f) = 572.3 \text{ Log (C)} - 573.4$	0.92
2.4	$(-\Delta f) = 1055.0 \text{ Log (C)} - 1200.9$	0.91

5.4.4. Analysis of one liter sample at 5.0 mL/min

After confirming that a quantitative relationship between sensor response and *G. lamblia* concentration correlated well, an even higher flow rate (5.0 mL/min) was tested in a once-through flow mode for examining if a large one liter sample could be analyzed. The purpose of using higher flow rate is to explore the possibility of large sample processing in a short time without a pre-concentration step for detection. The frequency response of the sensor to 1,000 and 10,000 cysts in one liter at 5.0 mL/min is plotted in Figure 5.8 and compared with the response obtained at lower flow rates. On an average, the resonant frequency decreased by 3,800 ± 895 Hz (n=3) when one liter of 10 cysts/mL *G. lamblia* sample was tested in a once-through fashion. And the response for one liter of 1 cysts/mL *G. lamblia* was 1,950 ± 318 Hz (n=3). The magnitude of sensor response is larger than the response obtained at lower flow rates, which is consistent with the trend shown in Figure 5.7. Control experiments were carried out with 10,000 cysts with an unfunctionalized sensor and the responses were 42 ± 24 Hz, 54 ± 36 Hz, 58 ± 24 Hz, 65 ± 21 Hz and 194 ± 50 Hz at flow rate of 0.5, 0.8, 1.5, 2.4 and 5.0 mL/min, respectively. The higher response level at 5.0 mL/min may include some sensor drift as the length of experiment was longer than 4 h. One notes the sensor responses for 1,000 and 10,000 cysts at 5.0 mL/min are easily distinguishable from the controls. The tests showed detection feasibility of 1 cyst/mL in a one liter sample in 4 h at 5.0 mL/min. The data in Figure 5.8A can be normalized by considering the arrival rate of target cysts at the sensor by plotting sensor response against Ct where C is cyst concentration and t is time. Such a plot (Figure 5.9) nearly merges the two profiles into one suggesting that the binding rate when normalized for concentration gave nearly the same binding rate.

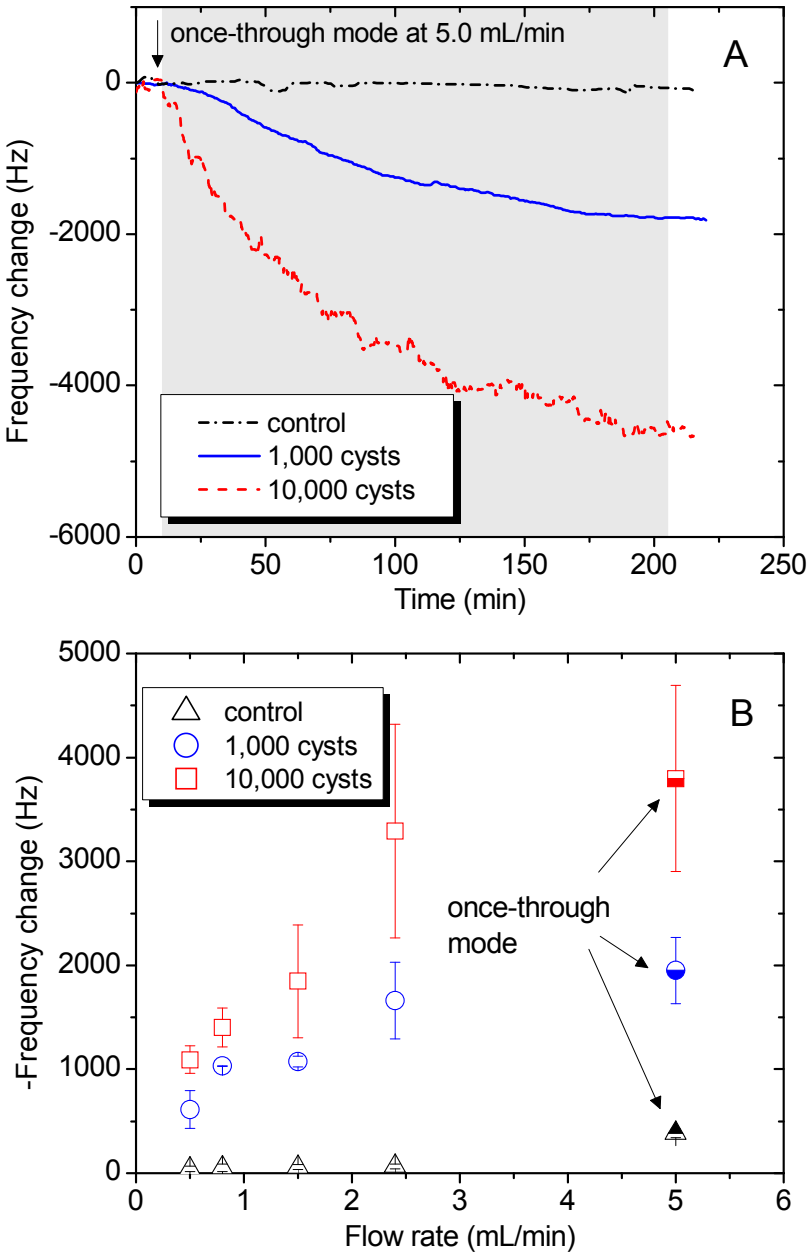

Figure 5-8. **(A)** Detection of 1 cyst/mL and 10 cysts/mL *G. lamblia* in one liter sample at 5.0 mL/min. The one liter sample containing either 1,000 or 10,000 cysts was introduced into the flow loop in a once-through mode followed by PBS rinse. Average responses for 1 and 10 cysts/mL were 1,950 ± 318 Hz and 3,800 ± 895 Hz, respectively. Control responses with 10,000 cysts were 380 ± 42 Hz. **(B)** PEMC sensors responses to 1,000 and 10,000 cysts as a function of flow rate. Once-through mode was used in detection at 5.0 mL/min, and the others were on a recirculation mode. Control experiments that exposed unfunctionalized sensor to 10,000 cysts were carried out at various flow rates. Error bars represent one standard deviation (n=3 to 5).

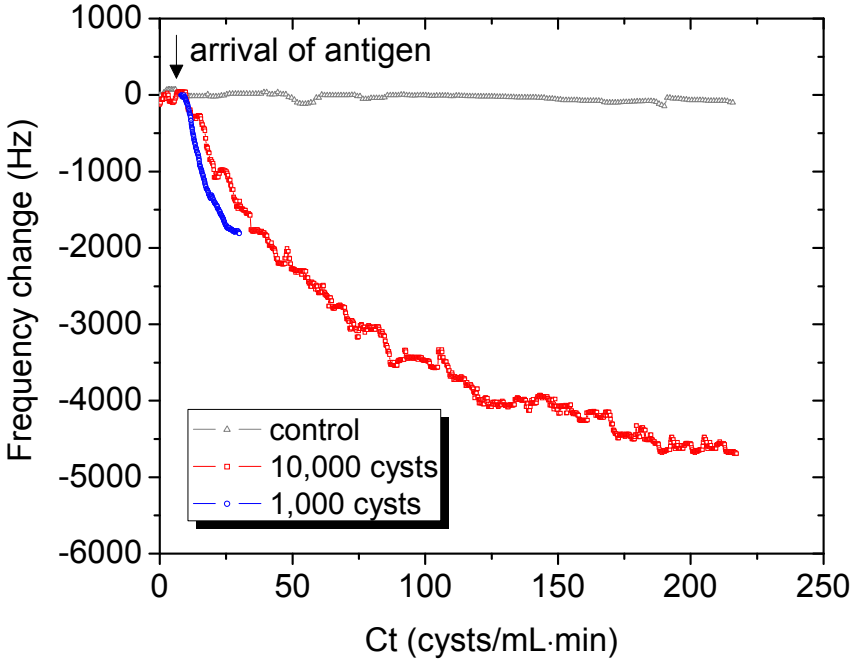

Figure 5-9. Frequency response to *Giardia*-spiked one liter PBS sample carried out at 5.0 mL/min. The two experiments were at concentrations of 1 and 10 cysts/mL. The sensor response data are plotted as a funciton of normalized time defined as *Ct* where *C* is the cyst concentration and *t* is time. The normalization takes into account the sensor exposure to equivalent number of cysts. The two profiles nearly overlap suggesting that the different sensor response kinetics shown in Figure 5.8A is due to the difference in arrival rate of target cysts.

The transport of cysts to the sensor surface is the first of a two-step process that leads to sensor response [208]. The second step is the binding reaction to surface-immobilized antibody. The transport step is governed by the flow field in the flow cell. In order to examine the reason for higher response at higher flow rate, we examined two questions. Namely: Is the sample flow velocity sufficient in the flow cell to carry the cysts to sensor surface? Qualitatively what is the difference in the flow field at the two extreme flow rates used (0.5 and 5.0 mL/min)?

Stokes settling velocity of the cysts (assuming average diameter = 10 μm, density = 1.02 g/cm^3) is ~0.000109 cm/s, and the average velocity of the fluid in the flow cell is

0.046 – 0.46 cm/s for the flow rate range of 0.5 to 5.0 mL/min. Thus the flow velocity is far higher than the settling velocity, and we expect the cyst to follow the fluid flow path through the flow cell. In order to examine the second question, a calculation of the flow field in the flow cell using 2-D Navier-Stokes equation was conducted and the resulting flow maps are given in Figure 5.10. Finite element simulation (COMSOL Multiphysics, Boston, MA) at various flow rates from 0.5 to 5.0 mL/min were analyzed. The significant difference observed in the flow map is the extent of flow adjacent to the sensor surface at the two flow rates. The vertical flow velocities adjacent to sensor was extracted from the finite element calculation at three representative sensor surface locations, and are plotted as a function of distance from the sensor. At a distance of 100 μm from the middle point of the sensor (point b), the vertical velocity was 0.044 cm/s at 5.0 mL/min, and was about five-times greater than 0.009 cm/s at 0.5 mL/min. A distance of 100 μm is approximately ten times the size of *Giardia* cysts, and to the first approximation is the region that the sensor samples. We believe that higher level of interaction of the sample with the sensor surface increases the probability of the cysts binding to it. Higher inlet velocity results in better exposure of *G. lamblia* cysts to the antibody on the sensor surface and accounts for the higher sensor response. Although an even higher flow rate can improve cysts interaction with the sensor surface, a higher noise level in resonant frequency occurs that compromises the measurement. Furthermore, higher flow rate will also cause higher shear stress at the sensor surface that potentially could dislodge bound cysts or impede binding of cysts to antibody.

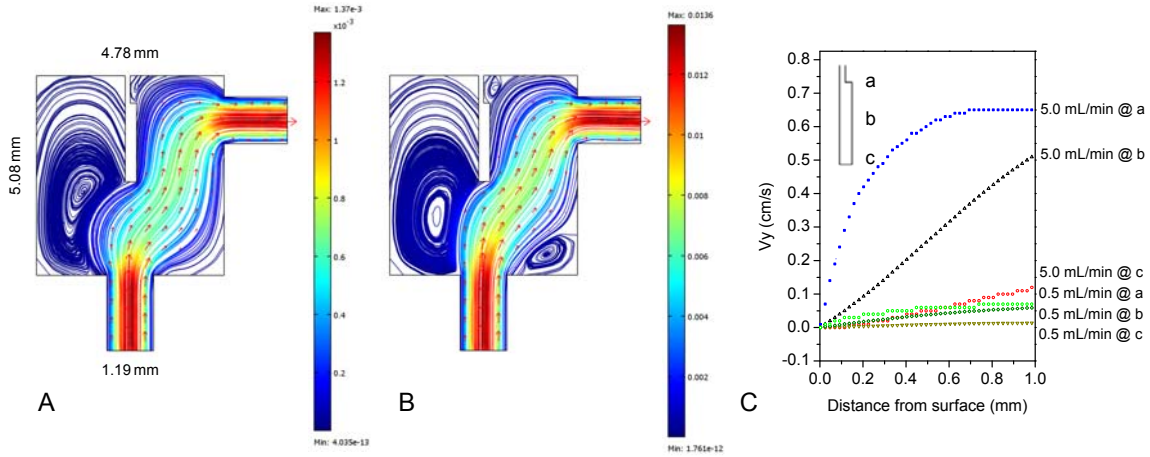

Figure 5-10. Effect of flow rate on the flow field. **(A)** 0.5 mL/min **(B)** 5.0 mL/min. The flow field was laminar and exhibited recirculation zones, but of different recirculation velocities. **(C)** Vertical velocities at three sensor locations (a, b, c) are plotted as a function of distance from sensor surface at the two flow rates 0.5 and 5.0 mL/min.

5.4.5. Detection of G. lamblia in tap water and river water

Having established detection feasibility at 1 cysts/mL in buffer background, we examined if similar level of sensitivity can be obtained in practical matrixes, namely tap water and river water. First set of experiments were designed to examine if the tap and river water samples contain any *Giardia* cysts. Antibody-immobilized sensors exposed to 50 mL of tap/river water in a once-through mode after stabilization in DI water showed no detectable response, which verified that no cysts were present in the tap/river water tested. Negative controls in PBS, tap and river water with antibody-immobilized sensors exposed to the three water samples showed 15 ± 6, 20 ± 5 and 39 ± 9 Hz response, respectively. Positive controls with unfunctionalized sensors exposed to 10,000 cysts spiked in the three water matrixes set in recirculation mode showed 20 ± 5, 18 ± 8 and 45 ± 12 Hz responses, respectively (data not plotted). Sensors for detection experiments were functionalized with anti-*G. lamblia* and installed in flow cell with tap water or river

water as running buffer. We initially used a flow rate of 2.4 mL/min as it gave good signal-to-noise ratio.

Table 5-3. Sensor responses to *G. lamblia* in various media.

	PBS		**Tap water**		**River water**	
Conc. (cysts/mL)	-Δf (Hz)	S.D. (Hz)	-Δf (Hz)	S.D. (Hz)	-Δf (Hz)	S.D. (Hz)
0	15	6	20	5	39	9
10	231	118	200	42	142	109
100	716	120	691	128	509	371
1,000	1,662	369	1,388	301	852	474
10,000	3,290	1,027	2,442	461	1,746	379

S.D.: standard deviation (n=3).

Spiked water samples containing 10 to 10,000 cysts were added to the flow loop following the same procedure as with the PBS samples. From the results summarized in Table 5.3 and illustrated in Figure 5.11, one notes that the response in tap water was 4-20 % lower than that obtained in PBS and the response to river water samples was 20-47 % lower at the concentrations tested. The control experiments verified that the positive responses to spiked samples were due to the cysts binding to sensor surface. We believe the lower sensor response compared to buffer samples is due to the interference of both biological and non-biological matters in the sample matrix.

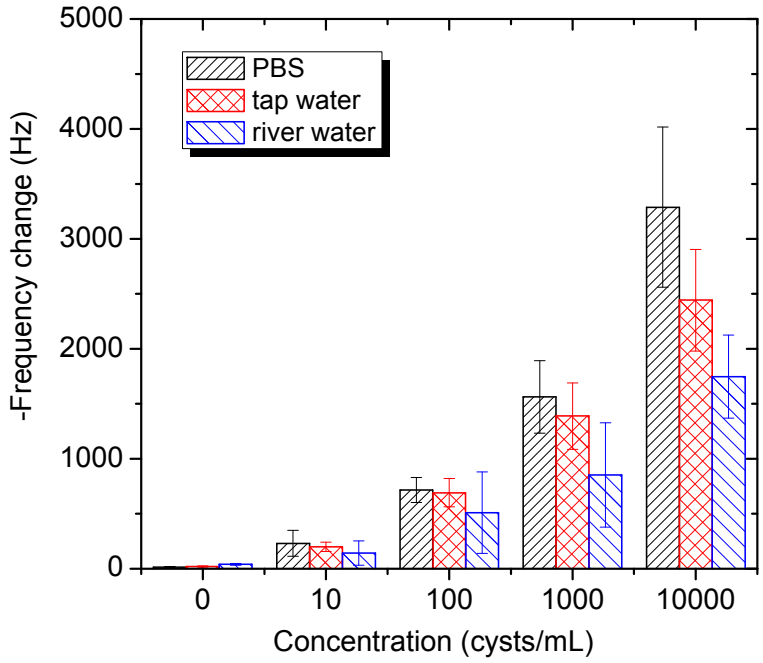

Figure 5-11. Comparison of sensor detection responses at 2.4 mL/min in the three water matrixes: PBS, tap water and river water. In all cases sample size was 1 mL. Both tap and river water samples gave lower sensor response at the same concentration. The decrease of response is attributed to weak binding of materials in water to cysts surface.

Masking of antigenic sites of immobilized antibodies by organic macromolecules such as humic and fulvic acids in river water has been suggested in the literature [182]. It is equally likely that antigenic sites on the cyst may weakly adsorb extraneous matter rendering then unrecognizable by surface-immobilized antibody. We believe the latter to be the dominant mechanism as our work on urine and serum samples show that proteinous matter in the sample matrix do not adsorb on PEMC sensors that are in continuous resonance in a flow field [97, 167, 209]. Another factor that may also contribute to lower sensor response is the pH at which detection was carried out. The pHs of tap and river waters were 6.7 ± 0.1 and 6.9 ± 0.1, respectively, and are lower than 7.4

at which the PBS experiments were conducted. In any case, the sensor exhibited sensitivity for detecting 10 cysts in tap and river water background.

5.5. Conclusions

We show for the first time a piezoelectric-excited millimeter-sized cantilever (PEMC) biosensor immobilized with a monoclonal antibody against *G. lamblia* exhibits selective and sensitive detection of *G. lamblia* cysts in several water matrixes (buffer, tap and river water) at a detection limit of 1 ~ 10 cysts/mL without a pre-concentration step. The antibody-immobilized sensor was exposed to 1 – 10,000 *G. lamblia* cysts/mL samples in a flow arrangement. When the cysts bind to the antibody on the sensor, the resonant frequency of the cantilever sensor decreased and was recorded continuously. Positive confirmation of sensor detection responses was obtained by environmental scanning electron microscope of sensor surface after detection experiments. Higher sample flow rates (0.5 to 5.0 mL/min) gave higher sensor detection response. Detecting as few as 10 cysts per mL was achieved in all three water matrixes tested, and significant sensor response was obtained in 15 min. Feasibility of analyzing at a low concentration of 1 cyst/mL in a one liter sample at a high flow rate of 5.0 mL/min was demonstrated.

CHAPTER 6 : SENSITIVE AND SELECTIVE DETECTION OF MYCOPLASMA IN CELL CULTURE SAMPLES

6.1. Introduction

Mycoplasmas are the smallest free-living bacteria with a size of 300 – 800 nm. They lack a rigid cell wall and thus are resistant to common antibiotics that target cell wall synthesis [210]. They have been found either attached to cell membrane or internalized within mammalian cells, causing compromised cell metabolic function. Among the over 100 species that have been discovered, about 20 species cause majority of cell culture contamination in both research laboratories and industrial processes [211]. About 15 – 35% of continuous human and animal cell lines in current use are infected with mycoplasmas [212]. Earlier surveys showed as high as 65 – 80% incidence of mycoplasma infection of cell culture [213]. The six species, *Mycoplasma orale*, *M. hyorhinis*, *M. arginini*, *M. fermentans, M. hominis* and *Acholeplasma laidlawii*, represent the majority of contaminating isolates [214, 215]. The contamination causes alternations in growth rates, morphology and cell viability. Both reduced antibody yield in hybridoma culture and total culture degradation have been reported. Therefore, routine assay of cell culture for possible contamination is an absolute requirement to ensure quality of biological products. The current industry standard for mycoplasma testing is specified in the Food and Drug Administration guideline [216].

Current method for detecting mycoplasma is by microbiological colony assay. Although this method is quite sensitive (1 – 10 CFU/mL), it requires a long incubation time (3 – 28 d) and experienced personnel for analysis [217]. PCR is sensitive (1 – 10 CFU/mL) for purified mycoplasma DNA, but its sensitivity deteriorates significantly to

10^3 CFU/mL in cell culture samples [211, 218-220]. ELISA is also used for routine mycoplasmas detection, but its sensitivity is poor (10^4 – 10^7 CFU/mL, depends on the species) [221]. Both PCR and ELISA rely on culturing as a first step for increasing mycoplasma concentration and such a step often requires several days, particularly for low concentration samples. PCR method has shortened the time to results greatly (1 – 2 d), but has been reported to give false positive/negative results for low counts ($<10^3$ CFU/mL) and is not readily implemented at production sites [222]. ELISA method is less expensive, but requires a laboratory and an instrumentation arrangement. Because of its low sensitivity, a long incubation step becomes necessary. Therefore, there is a great need for a rapid, sensitive, selective and inexpensive method for monitoring mycoplasma contamination in cell culture reactors.

Biosensors for cell culture systems have drawn lots of interest due to their rapid response, low cost and high sensitivity [223-227]. Various biosensors have been applied for real-time monitoring of glucose and acids level in a bioreactor. In this chapter, we used antibody immobilized PEMC sensors for detecting the mycoplasma, *A. laidlawii*, as it is one of the most common contaminant in cell culture systems. To the best of our knowledge, in spite of a very active biosensor research over the past decade, no publication on detecting mycoplasmas has appeared in the literature. Detection experiments were conducted with readily available positive control samples from a commercial mycoplasma ELISA detection kit as well as with specially grown and calibrated *A. laidlawii* samples. Selectivity of sensor response was also evaluated in cell culture medium (5% serum) samples containing mammalian and bacterial cells. Since mycoplasma is the smallest cell and has no cell wall, production of good quality

antibodies against them is difficult. Though a large amount of resources has been invested for antibody production to medical significant mycoplasmas, antibody production for cell line significant mycoplasmas is still an evolving process. Currently there is no antibody available with very good binding affinity. This also imposing a challenge for PEMC performance as the biorecognition element is extremely important for sensor performance.

6.2. Materials and methods

6.2.1. Experimental approach

Although a good number of antibodies for medically important pathogenic mycoplasmas are available, only a limited few are available for cell culture mycoplasma contaminants. An ELISA kit designed specifically for cell culture contaminants that recognizes the four species, *M. orale*, *M. hyorhinis*, *M. arginini* and *A. laidlawii*, is available from Roche. The kit contains a coating polyclonal antibody (*c*pAb) and a biotinylated polyclonal antibody (*b*pAb) against each of the four species, and a positive control containing a mixture of the four species at undisclosed concentrations. In this work, we used both antibodies for detecting *A. laidlawii* in separate experiments. Since the sensor does not require a labeled antibody, we used either the *c*pAb or *b*pAb for confirming sensor response in a sandwich format. It should be mentioned that experiments were conducted with immobilized *c*pAb as well as immobilized *b*pAb.

The positive control in the commercial kit was used initially for developing data on detection feasibility and sensitivity. The manufacturer would not provide the composition of the positive control and thus we report the concentration as a volume of

the positive control used. In order to obtain quantitative information on sensor limit of detection, we grew *A. laidlawii* cells, and prepared a standard inactivated stock sample so that the same biological sample can be used for sensor response comparison studies. To ensure integrity of *A. laidlawii* sample, periodic ELISA assays using the commercial kit were carried out, and the results showed no variation over a 14 d period. Thimerosal inactivated cells were used in all PEMC experiments. For evaluating sensor performance, simultaneous measurements were carried out using the ELISA kit with both live and inactivated mycoplasma samples.

6.2.2. Reagents

Cysteamine, glutaraldehyde solution, streptavidin and phosphate buffered saline (PBS, 10 mM, pH 7.4) and others were purchased from Sigma-Aldrich (St. Louis, MO). Calibrated *A. Laidlawii* (ATCC 23206, American Type Culture Collection, Manassas, VA) samples were prepared as described here. Mycoplasma positive control, biotinylated polyclonal antibody and coating polyclonal antibody were from Roche kit (#11296744001, Roche Diagnostics GmbH, Penzberg, Germany). Antibody and antigen solutions were prepared in PBS (with 0.05% sodium azide) and stored at 4℃ for use. Human epidermoid squamous carcinoma cells (A431) were obtained from another research laboratory at Drexel University and cultured in Dulbecco's Modified Eagle's Medium (DMEM, Mediatech, Inc., Manassas, VA) supplemented with 5% fetal bovine serum and grown at 37°C in 5% CO_2. *E. coli* JM 101 cells were grown in nutrient broth, killed in 1% Clorox®, centrifuged and re-suspended in PBS. Concentration was determined using a hemocytometer after staining with methylene blue.

6.2.3. Fabrication of PEMC sensor and flow cell design

A PEMC sensor consists of two layers: a PZT layer (lead zirconate titanate, Piezo Systems, Woburn, MA) and a quartz layer (SPI, West Chester, PA), bonded by a non-conductive adhesive. Two PEMC designs were used. One is a flush design with a 2.7 × 1.0 × 0.127 mm ($l \times w \times t$) PZT bonded to 2.0 × 1.0 × 0.160 mm quartz. The second is an overhang design in which a 4.5 × 1.0 × 0.127 mm PZT bonded a 4.0 × 1.0 × 0.160 mm glass. In both designs, the PZT end was anchored at one end. In the flush design, the glass layer was attached at the free-end with zero protrusion. In the overhang design, the glass layer protruded from the free-end by 1.0 mm. Wires (30 gauge) were soldered to electrodes of PZT layer and epoxy fixed in 6 mm glass tubing. The sensor was polyurethane (Wasser, Auburn, WA) spin-coated for providing electrical insulation. The two designs were shown to exhibit similar mass-change sensitivity [2, 3].

6.2.4. PEMC sensor surface functionalization and experimental procedures

Prior to immobilization, 2.0 mm^2 (flush design) or 1.8 mm^2 (overhang design) of the PEMC sensor tip surface was freshly sputter-coated with 100 nm gold. Two immobilization methods illustrated in Figure 6.1 were used in the experiments. In the first method (Figure 6.1A), the sensor was incubated in 2 mM cysteamine in PBS overnight at room temperature, and then immersed in 2.5% glutaraldehyde solution for 1 h followed by 1 h incubation in 100 μg/mL anti-*A. laidlawii*. The sensor was rinsed with DI water, and installed in a custom-made flow cell apparatus. In the second method (Figure 6.1B), sensor was incubated in 100 μg/mL streptavidin solution for 2 h, followed by 1 h in 100

µg/mL *b*pAb prior to installation in the flow cell. The detection experiments were done at sample flow rate of 0.5 mL/min in an incubator maintained at 28 ± 0.1℃.

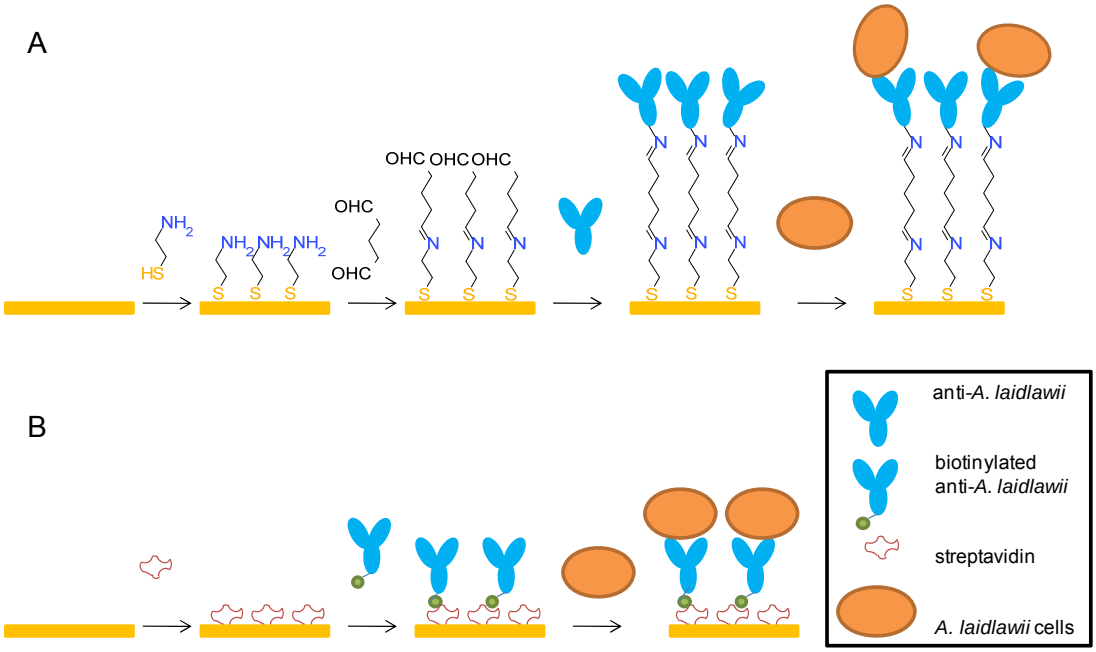

Figure 6-1. Illustration of antibody immobilization and immunoassays with PEMC sensor. **(A)** Surface functionalization using cysteamine/glutaraldehyde chemistry on gold surface. **(B)** Gold surface directly modified with streptavidin, and then biotinylated antibody was attached to the sensor surface via streptavidin/biotin binding.

6.2.5. Sensor calibration

Mass-change sensitivity of PEMC sensor were determined by depositing known mass of paraffin wax on the sensor surface and measuring the resulting change in resonant frequency after solvent evaporation [202]. All measurements were made at 28 ± 0.1℃. Sensor surface was deposited with known wax mass using a stock paraffin wax in hexane solution prepared at concentrations ranging from 0.3 pg/µL to 100 ng/µL.

6.2.6 A. laidlawii culture and ELISA detection

6.2.6.1. A. laidlawii propagation and enumeration

Frozen glycerol stock of *A. laidlawii* was inoculated into 25 mL tryptic soy broth (Northeast Laboratory Services, Winslow, ME) in a sterile flask and incubated at 37°C in a 7% CO_2 atmosphere for 24 h. Cultures were either used immediately or stored at 4°C for several days until needed. Serial dilutions at 1:10 of the culture were made to 10^{-5} in mycoplasma phosphate buffer (28 mM monobasic sodium phosphate, 72 mM dibasic sodium phosphate in Milli-Q water, pH 7.1 ± 0.3). Aliquots of 100 µL of the three highest dilutions were spread-plated onto 100 mm BBL tryptic soy agar plates (Becton, Dickinson & Co., Franklin Lakes, NJ) in triplicate. The plates were loosely plastic wrapped and incubated at 37°C in 7% CO_2 for 4 – 5 d until colonies were distinctly observable. The plates were then counted and the concentration of the source culture calculated by averaging colony counts accounting for the dilutions used.

6.2.6.2. Inactivation of A. laidlawii cultures with thimerosal

Cultures were treated by adding 10% aqueous (w/v) thimerosal solution to a final concentration of 0.0001% and then incubated at 37°C with shaking for 24 h. Killing of the culture was confirmed by spread-plating 100 µL of the undiluted and treated culture in triplicate. Plates were incubated at 37°C in 7% CO_2 for 4 – 5 d and visually examined. The treated culture was stored at 4°C until use (<14 d).

6.2.6.3. ELISA detection of A. laidlawii

ELISA detection of *A. laidlawii* was performed using the antibodies from Roche mycoplasma detection kit. Kit reagents were prepared according to the manufacturer instructions. Serial dilutions of viable and thimerosal-treated cells were prepared as described and then tested according to the vendor supplied protocol. The completed 96-well test plate was quantitated at 405 nm using a Wallac Victor 3 1420 Multi-label Counter (Perkin Elmer, Waltham, MA).

6.3. Results and discussion

6.3.1. PEMC sensor spectra and sensitivity calibration

The PEMC sensors used in this study have a resonant frequency near ~900 kHz. A number of fabricated sensors (n=23) gave similar resonant frequency values within ± 30 kHz of 900 kHz, and were used in all detection experiments. As shown in Figure 6.2A, the resonant frequency decreases from 924.75 kHz in air to 856.50 kHz in DI water (Δf = 68.25 kHz) due to density increase of fluid surrounding the sensor. Although *Q*-value decreased from 40.3 to 29.5, it was sufficiently high for detecting resonant frequency within ± 20 Hz in stagnant or flowing liquid samples.

Mass-addition (Δm) and resonant frequency change ($-\Delta f$) of a PEMC sensor is given by the following semi-log relationship:

$$\left(-\Delta f\right) = A\log\left(\Delta m\right) + B \tag{6.1}$$

where A and B are constants and depend on sensor geometry.

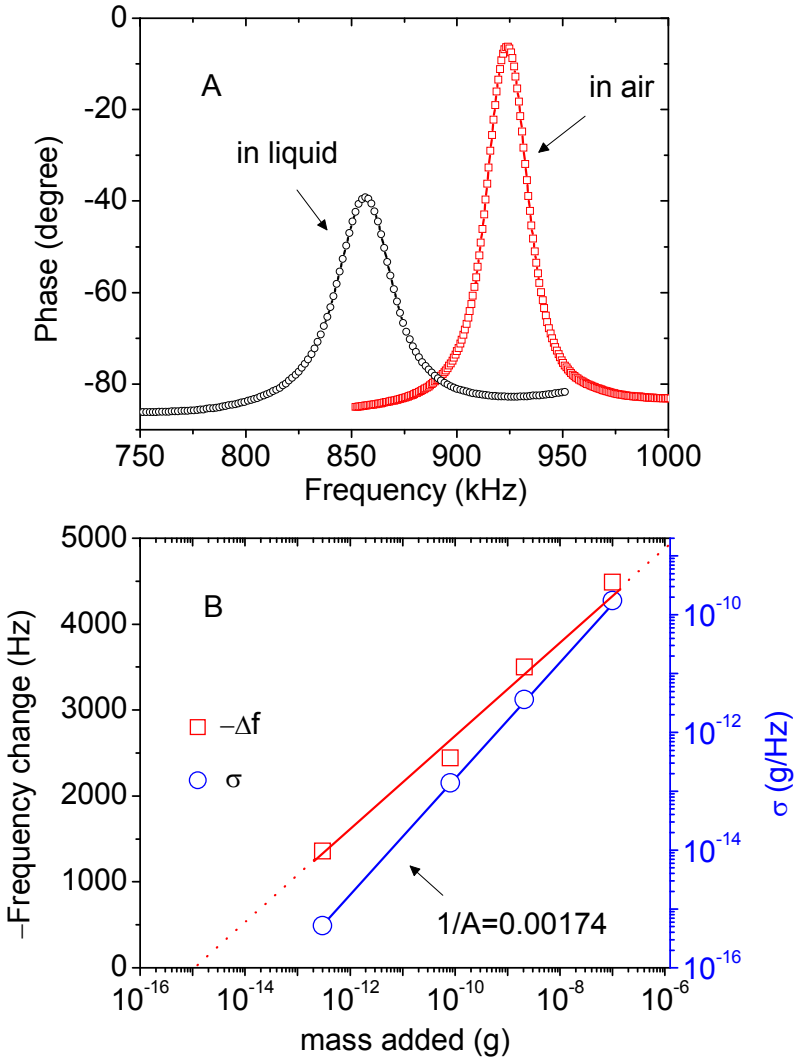

Figure 6-2. Typical sensor spectra and sensitivity calibration curve. **(A)** Typical sensor spectra in air (□) and in DI water (○), respectively. **(B)** Sensitivity calibration using diluted paraffin wax solutions. Sensor response ($-\Delta f$) is plotted as a function of log (mass added) (□), and log (σ) is plotted as a function of log (mass added) (○), respectively. PEMC sensor response to mass addition is log-linear, and is similar to previous results.

In principle, the parameter B should be ~0, but in practice we find it to have a non-zero intercept. Sensitivity, defined as mass that causes unit resonant frequency change can be determined from Eq. (6.1) as:

$$\sigma = \frac{\partial(\Delta m)}{\partial(-\Delta f)} = \frac{\Delta m}{A} \tag{6.2}$$

where σ is the sensitivity of PEMC sensor at mass-addition (Δm). Since A is a constant, σ depends linearly on the magnitude of Δm. The smaller the value of Δm is, the more sensitive the sensor is for a given sensor parameter A. Lower σ value indicates a higher mass-change sensitivity. Parameter σ is the mass of analyte that causes a unit resonant frequency decrease.

A typical sensitivity calibration result of flush design sensor is shown in Figure 6.2B, where resonant frequency response ($-\Delta f$) and log (σ) are plotted as function of log (mass added). The log-linear relationship between added mass and frequency response (R^2=0.99) confirms the validity of Eq. (6.1). The parameters are A = 573.9 Hz and B = 8442.2 Hz, with $(-\Delta f)$ in Hz and Δm in g. Sensitivity calculated using Eq. (6.2) is σ = 5.23 × 10^{-16} g/Hz, 1.40 × 10^{-13} g/Hz, 3.62 × 10^{-12} g/Hz and 1.75 × 10^{-10} g/Hz corresponding to the cumulative mass loading of 0.3 pg, 80.3 pg, 2.08 ng and 102 ng, respectively. One notes in Figure 6.2B that as added mass increased, the sensitivity becomes numerically larger, indicating a decrease in mass-change sensitivity. This is an intrinsic characteristic of PEMC sensor response and is quantitatively given by Eq. (6.1).

At the lowest added mass (300 fg) in the calibration experiments, the sensitivity was 5.23 × 10^{-16} g/Hz. If the noise level is ~20 Hz and we require a signal to noise ratio to be greater than 3, then a 60 Hz response would be caused by the attachment of ~30 mycoplasma cells. Average mass of a mycoplasma cell is ~1 fg. In liquid, resonant frequency change of PEMC sensor is directly attributable to mass change because the Reynolds number (Re) of PEMC at ~900 kHz is ~10^6. That is, the sensor responses are

due to inertial effects, and not due to viscous forces. If *Re* is low (~1), the dominant forces on the sensor are the viscous forces exerted by the surrounding liquid. Viscous damping not only reduces the *Q*-value, but also significantly reduces sensitivity to changes in mass. In an earlier study we showed mass-change sensitivity in liquid decreased by 3 to 5 times compared to in air using two calibration methods; namely a wax deposition method and bovine serum albumin (BSA) binding assay. The difference in sensitivity is due to the difference in surface geometries; for example, wax forms a uniform film, while bound BSA on the surface is non-uniform. Nevertheless, having a means to relate mass-change response in air gives us a reasonable framework for interpreting resonant frequency changes in liquids.

6.3.2. Detection of mycoplasma positive control and calibrated samples in PBS

Sensor responses to sequentially increasing concentration of *A. laidlawii* in PBS were first obtained (Figure 6.3A). We used the mycoplasma positive control directly from Roche mycoplasma detection kit prepared in PBS. Since the positive control contains four species, the sample analyzed contained the competing species and the antibody recognizes only *A. laidlawii*. The sensor was functionalized with *c*pAb via cysteamine-glutaraldehyde method in batch prior to the detection experiments. The sensor was installed in flow cell and resonant frequency was allowed to reach steady state with PBS as running buffer. Volumes of mycoplasma positive control sequentially introduced were 1 μL, 10 μL and 50 μL. At least 10 min steady state time was observed prior to the addition of a higher dose. The resonant frequency decreases resulting from mycoplasma positive control injections were 528 Hz, 606 Hz and 525 Hz, respectively. The main

responses for various doses were observed within the first 10 min after sample was injected.

Prior to conducting the detection experiments, responses to both positive and negative controls (*in here the positive control and negative control are terms used in experimental design, should not be mistaken as positive control from the Roche kit*) were obtained with the same sensor. Buffer control, which consisted of exposing unfunctionalized the sensor to running buffer produced no response. In a separate set of experiments, unfunctionalized sensor was exposed to positive control (100 μL) and yielded a very small response of -50 ± 15 Hz, which is slightly higher than the noise level. In a negative control experiment, the sensor was immobilized with anti-*A. laidlawii*, and the introduction of *A. laidlawii*-free PBS gave a small response of -37 ± 4 Hz. Comparing the detection responses with the three controls, we conclude the decrease of sensor resonant frequency as due to the binding of *A. laidlawii* cells to the sensor surface.

Besides the sequential addition of various positive control sample volumes, experiments of single volume injection to freshly prepared sensor were also carried out and a set of typical responses is shown in Figure 6.3B. For separate injection of 1 μL, 10 μL and 50 μL, the responses were 446 Hz, 997 Hz and 1,304 Hz, respectively. Experimentally we found that the accumulative resonant frequency response due to the addition of mycoplasma control were similar by either sequential injections in a single experiment or separate injections of single dose in different experiments. The correlation of sensor (m=10 for sensors used) response to mycoplasma positive control in PBS (n=3 to 5 at each separate volume) is shown in Figure 6.4.

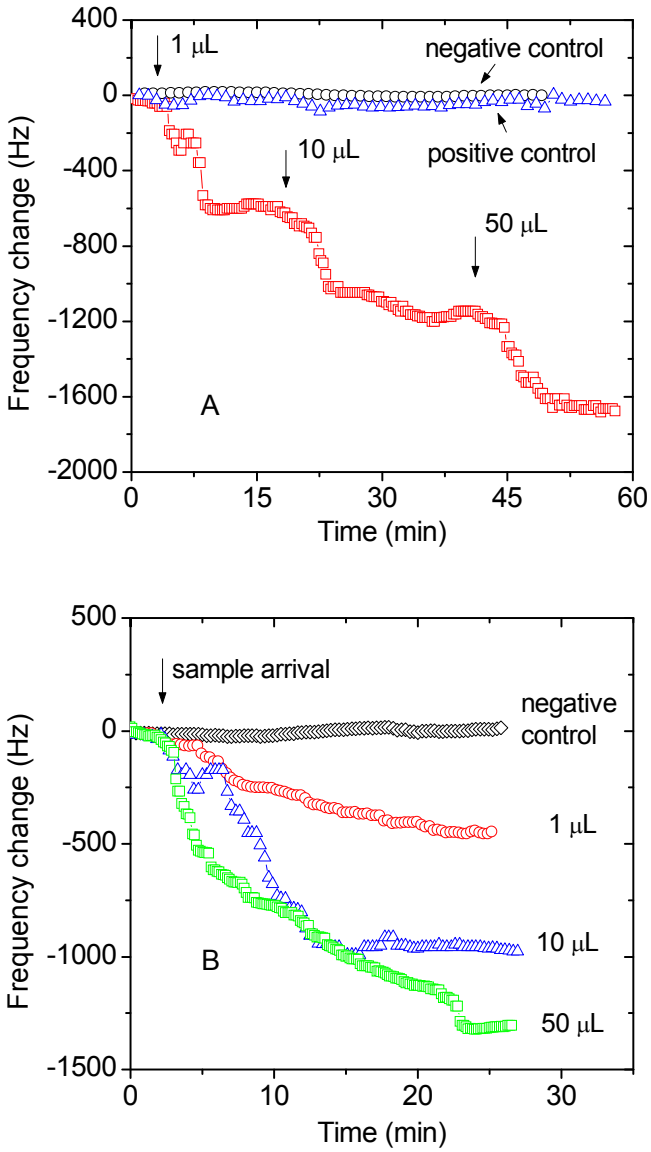

Figure 6-3. Detection of positive control in PBS. **(A)** Response to sequential addition of mycoplasma positive control from Roche kit. PEMC sensor was exposed to 1 μL, 10 μL and 50 μL positive controls. Sequential decreases of 528 Hz, 606 Hz and 525 Hz were obtained. **(B)** Response to injections of 1 μL, 10 μL and 50 μL positive control using fresh sensors in each experiment. The responses were 446 Hz, 997 Hz and 1,304 Hz, respectively. The injected samples were diluted by 1:4 in flow loop.

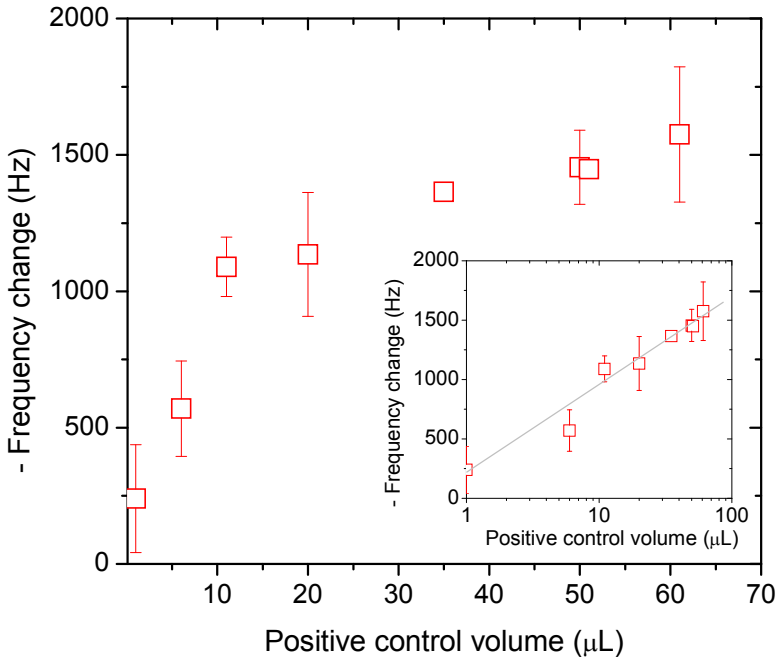

Figure 6-4. Resonant frequency change as a function of positive control volume injected. Inset shows resonant frequency response of as a log function of volume injected. PEMC sensors exhibit log-linear relationship for mycoplasma positive control detection.

Since the exact *A. laidlawii* cell numbers in the positive control is not known, we plot the sensor response as a function of volume (μL) added. One notes the sensor response exhibits lower sensitivity beyond 35 μL, which may indicate sensor saturation. That is, the available antibody sites on the surface are not sufficient for detection of a large number of cells. As seen in the inset, the response was plotted as a log function of volume added, which yielded $-\Delta f = 758.79 \log (C) + 174.78$ ($R^2 = 0.96$). The mycoplasma detection kit manual indicates a detection limit of *A. laidlawii* as $10^4 – 10^5$ CFU/mL. It is estimated that in ELISA the positive control contains two to three orders higher concentrations of *A. laidlawii* cells than detection limit value. Based on this approximation, we estimate the cells number in 1 μL sample as $\sim 10^3 – 10^5$. As seen in

Figure 6.3, the response to 1 μL sample was easily measurable. Since the sensor was not limited by sample volume, we expect detection sensitivity to be far better than $10^3 – 10^5$ *A. laidlawii* cells. By experiments with positive control from Roche kit, we established the feasibility of the surface chemistry as well as working ability of the antibodies.

6.3.3. Detection of calibrated A. laidlawii in PBS and cell culture medium

After accumulating good detection responses using positive control from the commercial kit, detection experiments with calibrated *A. laidlawii* cell samples were carried out. Spiked samples tested were in the concentration range of $10^3 – 10^7$ CFU/mL since the ELISA data showed detection limit as 10^7 CFU/mL.

In Figure 6.5, sensor responses to samples containing 1,100 and 88,000 *A. laidlawii* cells are shown. Introduction of the calibrated samples caused decrease in resonant frequency due to *A. laidlawii* binding. Injection of 1,100 cells caused a decrease of 895 Hz, as shown in Figure 6.5A. Since the volume of flow loop was ~4 mL, the effective concentration was diluted to 275 CFU/mL. In order to confirm that the response was due to *A. laidlawii* binding, 500 μL of the *c*pAb was introduced into the flow loop after a PBS rinse. The logic here is that the polyclonal antibody will bind to the *A. laidlawii* cells that were already bound to the first antibody immobilized on the sensor surface [228, 229]. Response to the antibody was strong and showed a decrease of 256 Hz, confirming the first sensor response was due to *A. laidlawii* binding. It is interesting to point out that the second antibody binding is akin to a sandwich assay in ELISA. Unlike in ELISA, both the first and second antibody contributes to detection signal and the second antibody provides for higher stringency.

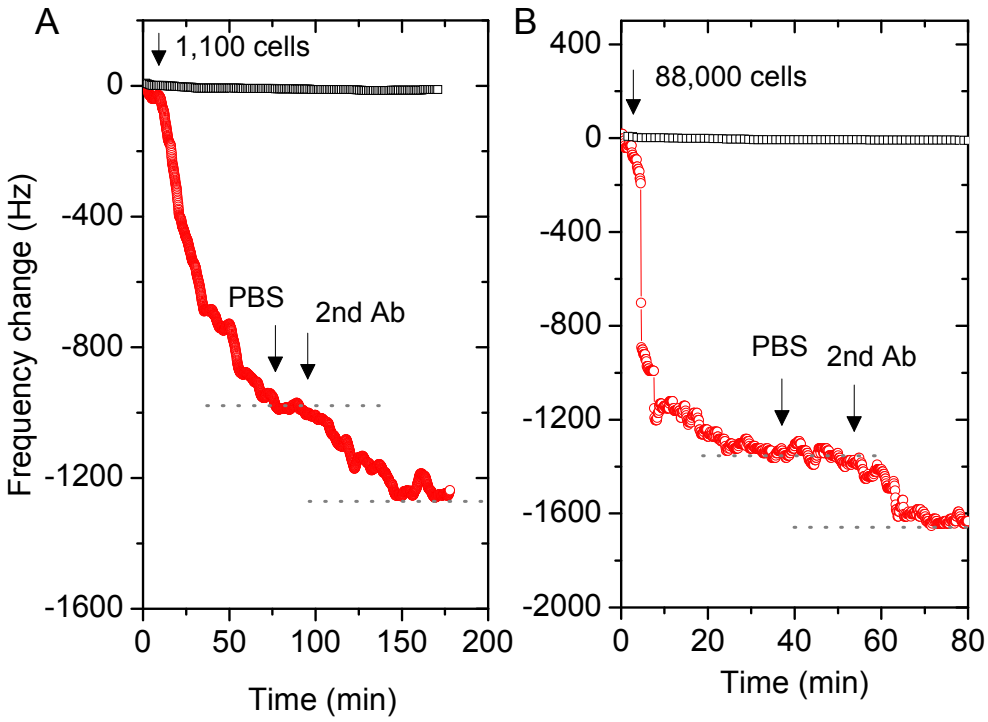

Figure 6-5. Detection of *A. laidlawii* in PBS and confirmation by a second antibody binding response. **(A)** The PEMC sensor was exposed to 1,100 cells *A. laidlawii* (effective concentration 275 CFU/mL) for 50 min, then stabilized in PBS for 30 min before injection of 500 µL polyclonal antibody from Roche kit. The initial attachment of *A. laidlawii* gave a frequency decrease of 895 Hz, and the second antibody caused a further decrease of 256 Hz. **(B)** The frequency response for injection of 88,000 cells (effective concentration 22,000 CFU/mL) was 1,512 Hz. After rinsing with PBS, a further 336 Hz decrease was obtained for 500 µL second antibody binding reaction.

In a similar experiment shown in Figure 6.5B, PEMC sensor was exposed to 88,000 calibrated *A. laidlawii* cells (effective concentration 22,000 CFU/mL) in the same fashion. The injection of *A. laidlawii* cells caused 1,512 Hz resonant frequency decrease. A further 336 Hz decrease was observed with the introduction of 500 µL *c*pAb. These two examples show the detection of *A. laidlawii* in PBS at as low a concentration as ~10^3 CFU/mL is feasible using PEMC sensors.

Since mycoplasma species are common contaminants in mammalian cell cultures, direct and rapid detection in cell culture containing serum without any pre-treatment is useful for evaluating practical performance of PEMC sensors. A detection experiment using PEMC sensor in cell culture medium is shown in Figure 6.6B. Sensor was functionalized with *b*pAb and stabilized in PBS. Cell culture medium containing serum (DMEM with 5% fetal calf serum, FCS) and A431 cells (5×10^6 CFU/mL; human skin cells) was introduced into flow loop in a once-through fashion so as to displace the flow loop with the new medium. A decrease of 330 Hz in frequency was observed due to higher density of the cell culture medium and was verified in a separate experiment (see Figure 6.6A). After sensor stabilized in the cell culture medium, 1 mL killed *E. coli* JM101 (10^7 CFU/mL) cells were introduced into the flow loop in recirculation mode. Although one sees an increase in noise level in resonant frequency, no significant decrease in resonant frequency occurred. After steady state was reached, the circulating fluid was DMEM-serum-A431 (1.2×10^6 CFU/mL) and *E. coli* JM101 (2.5×10^6 CFU/mL), which simulated a strongly contaminated cell culture medium environment. The absence of resonant frequency responses indicate that neither A431 nor *E. coli* JM101 attached to the sensor surface. In this background, *A. laidlawii* detection experiments were conducted. At 40 min, 1 mL 1,000 CFU/mL *A. laidlawii* (effective concentration 250 CFU/mL in flow loop) prepared in cell culture medium (DMEM with 5% FCS) was introduced into the flow loop. Note that the circulating fluid and the *A. laidlawii* sample were of the same composition except for the mycoplasma cells, and thus no density difference was introduced. Resonant frequency decrease of 692 Hz was

observed shortly after sample introduction. At 62 min, 1 mL of 100,000 CFU/mL *A. laidlawii* was further injected in and an additional decrease of 428 Hz was observed.

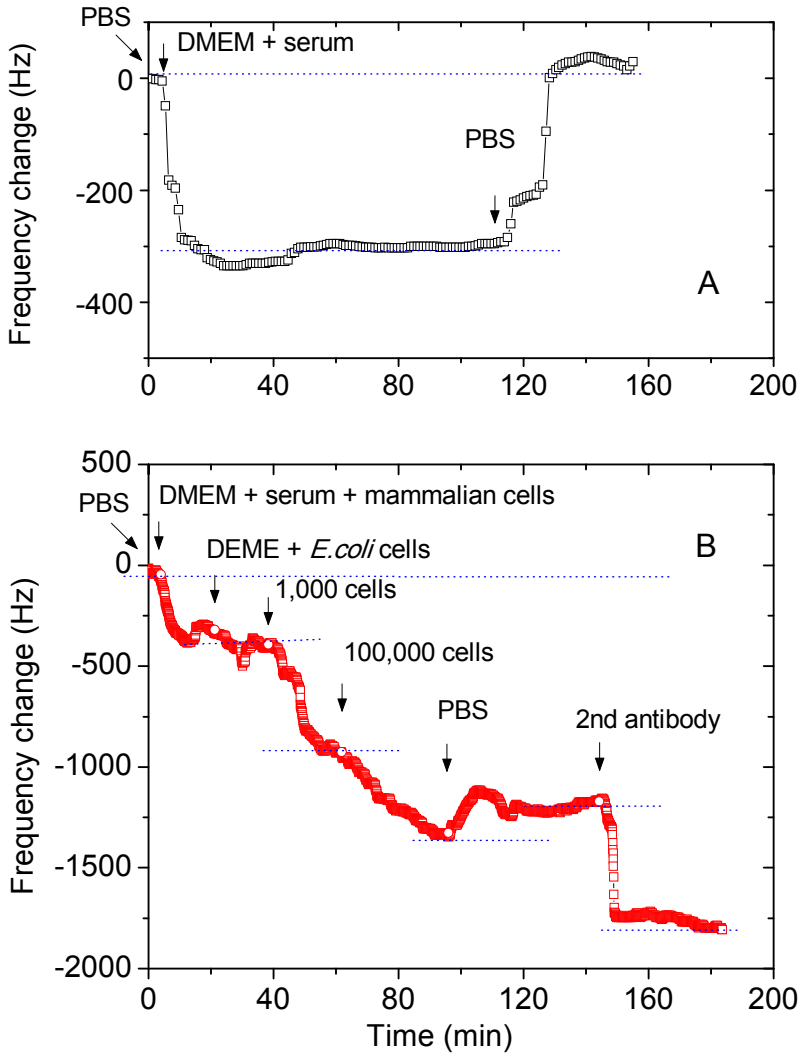

Figure 6-6. (A) PEMC responds to density when DMEM was introduced to replace the running buffer PBS; resonant frequency decreased by 315 Hz due to density. Upon replacing DMEM with PBS, the resonant frequency fully recovered back to the original value. (B) Detection experiment in DMEM containing serum (5% FCS), mammalian cells (5×10^6 cells A431 cells) and *E. coli* JM 101 cells (10^7 cells) as background. The PEMC sensor was functionalized with antibody prior to experiment. 692 Hz decrease was observed for 1,000 *A. laidlawii* cells, and a further 428 Hz decrease was seen for 100,000 cells. Second antibody binding gave a further decrease of 575 Hz.

PBS flush caused a recovery of 215 Hz and was slightly less than the initial density-induced decrease of 330 Hz, which may suggest an incomplete PBS rinse. After stabilization in PBS, 500 µL freshly prepared *c*pAb from was introduced and a significant resonant frequency decrease of 575 Hz was observed. The second antibody binding response confirmed that the initial sensor response was indeed due to *A. laidawii* attachment. A similar experiment where the sensor was not exposed to *A. laidawii* sample did not result in a resonant frequency response.

6.3.4. Quantification of sensor response

It is useful to examine if the response of PEMC sensor to various concentrations of *A. laidlawii* can be quantified. Sensor responses to various concentrations of calibrated *A. laidlawii* samples in PBS (n = 3 or 4) and DMEM (n = 3) are given in Figure 6.7. First order analysis indicates that the sensor response ($-\Delta f$) correlated well with *A. laidlawii* concentration (C_{Al}) with the relationship given in Eq. (6.1). This relationship has been tested true in other detection experiments for a pathogen [230] and a 30 kDa toxin [97]. For the case of *A. laidlawii* detection in PBS, the correlation was excellent ($-\Delta f = 310.14 \log (C_{Al}) - 77.212$, $R^2 = 0.98$). For experiments conducted in DMEM, sensor response was also proportional to *A. laidlawii* concentration. Comparing the results in PBS and DMEM, one notes the response in DMEM was consistently ~50% lower than in PBS, which suggests that the sensor is ~50% less sensitive in complex serum/mammalian cells/*E. coli* background than in PBS. Similar sensitivity decreases in complex matrix (serum or plasma) have also been reported in other biosensor platforms [192, 231-233].

We attribute reduced sensor response to reduced access to binding sites, as well as possible loss of available antibody sites.

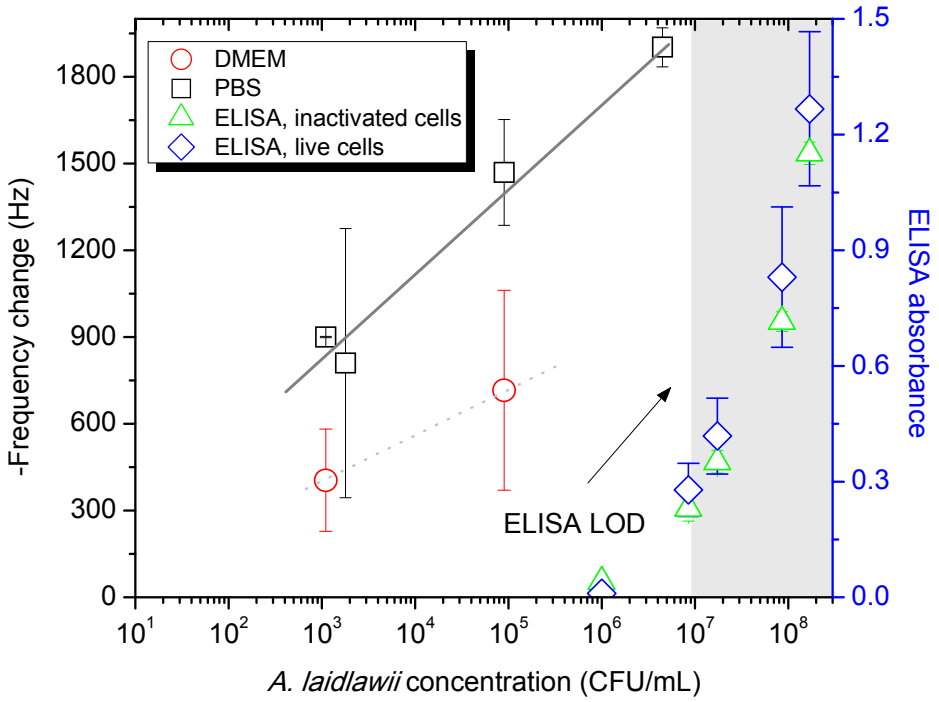

Figure 6-7. Comparison of PEMC and ELISA results. For PEMC sensor, resonant frequency response is plotted as a log function of *A. laidlawii* concentration with a detection limit of 10^3 CFU/mL in the dynamic range of 10^3 – 10^7 CFU/mL. Measurements in PBS (□) consistently gave higher response in comparison to cell culture medium (○). Detection limit by ELISA assay was 10^7 CFU/mL for both live cells (◊) and inactivated cells (Δ).

6.3.5. Comparison of PEMC sensor with ELISA

ELISA assays of thimerosal-inactivated and live A. laidlawii cells were within ~10-15 %. The inactivated cells gave a slightly lower absorbance value compared to live cells. Since binding in ELISA assay was only marginally compromised by using inactivated cells, we can compare PEMC sensor responses with the ELISA results conducted with both live and inactivated cells, and the latter is included in Figure 6.7. As

can be seen in Figure 6.7, detection limit of the freshly grown or thimerosal-treated A. laidlawii was ~10^7 CFU/mL. On the other hand, the LOD of the PEMC sensor was lower than 10^3 CFU/mL, which is four orders of magnitude lower than ELISA LOD. The results suggest PEMC sensors can significantly improve our ability to monitor contamination in cell culture systems. If one uses sample preparation steps such as centrifugation and resuspension in a buffer, a further improvement in LOD can potentially be achieved using PEMC sensors.

The FDA recommended positive control inoculation is 10 – 100 CFU/mL for testing cell culture samples. Although experiments at such a low concentration have not been carried out with PEMC sensors, it would be prudent to include a short incubation step to permit growth of contaminating mycoplasma cells prior to detection, as this will ensure detection of live cells. Because LOD is lower than 10^3 CFU/mL, the required incubation step would be shorter than that is required for plate-counting microbiological method or PCR approach. In a future report we will examine the applicability of the PEMC sensors at ultralow concentrations of 1 – 100 CFU/mL by using a second and probably a third antibody to amplify the sensor response.

6.4. Conclusions

In this chapter, we showed successful detection of *A. laidlawii* at 10^3 CFU/mL in both PBS and cell culture medium. Anti-*A. laidlawii* immobilized PEMC sensor showed positive responses for both positive control from the Roche mycoplasma detection kit and self-grown *A. laidlawii* cells. Detection of calibrated *A. laidlawii* samples showed positive response in the dynamic range of 10^3 – 10^7 CFU/mL in buffer medium. The

PEMC sensor showed about four orders higher sensitivity compared with ELISA method conducted in parallel using the same *A. laidlawii* stock and the same antibody reagents. Furthermore, the time required for positive detection signal using PEMC sensor was less than 1 h, which is attractive for timely determination of mycoplasma contamination.

CHAPTER 7 : SENSITIVE AND RAPID CELL VIABILITY MEASUREMENT USING BCECF-AM AND CANTILEVER SENSOR

7.1. Introduction

Rapid detection of live bacterial pathogens is important in monitoring food safety and water quality as well as in medical diagnostics. Selective plating and culturing is the current standard due to its high selectivity and sensitivity. However, the time-to-results (TTR) depends strongly on the growth rate of the pathogen. For the slow growers, confirmation of positive detection could take as long as 16 days [234]. PCR in combination with plating method can reduce TTR considerably. However, a significant time is still needed to enrich and grow the target microorganism, especially when it is present at low concentrations. PCR techniques without an enriching step do not distinguish between viable and non-viable cells because DNA is a stable molecule and is present in both dead and live cells. Similarly antibody-based biosensors suffer from the deficiency of not distinguishing viable from non-viable cells. Since only the viable cells are virulent, it is important to discern them in a sample. In situations where TTR is long, timely corrective decisions cannot be made. For example, it takes more than 5 h using real time PCR to detect the pathogen *E. coli* O157:H7 [235], and more than a day for *Salmonellae* [236] and two weeks for *Mycobacterium tuberculosis* [237]. The purpose of this investigation is to examine if a biosensor approach can improve TTR for live cell detection.

PEMC sensors have been shown to be very highly sensitive to mass change at femtogram levels [2]. Because of this property, any perturbation to cell environment that causes its mass to change in live cells and not in dead cells can be used for detecting live

cells. Candidate reagents that fit this requirement are the dyes used for measuring intracellular pH. Acetoxymethyl ester of 2',7'-bis(2-carboxyethyl)-5,6-carboxyfluorescein (BCECF-AM) is a fluorescent dye that has been extensively used for intracellular pH measurement since 1982 (structure is shown in Figure 7.1) [238]. Once it diffuses into the cell, it is hydrolyzed to fluorescent BCECF via the action of intracellular non-specific esterases known to be present only in live cells, and thus can be used as a viability indicator. BCECF carries 4-5 negative charges per molecule at cytosolic pH and thus accumulates within viable cells and over 80% of the loaded BCECF remains within the cell for at least 2 h [239]. A typical bacterium (~1 μm) weighs 1 picogram and if the uptake of BCECF-AM is ~0.1% of its mass, then a single live bacterium mass will increase by 1 femtogram, which is potentially measurable by a PEMC sensor. BCECF-AM readily diffuses into *E. coli* cells [240], but its transport rate and the amount of it taken up by a cell has not been reported.

In this chapter, live *E. coli* cells immobilized on the sensor were exposed to BCECF-AM and the resulting mass increase was measured via resonant frequency change. Although detecting viable pathogenic cells is our interest, a non-pathogenic strain *E. coli* JM 101 strain was used as a surrogate in the current study. The approach which combines BCECF accumulation and highly mass-change sensitive PEMC sensor is shown to be feasible experimentally. Further, live cells coated PEMC sensor can also be used as a cell based biosensor for environmental monitoring, especially for heavy metals and toxic gas detection.

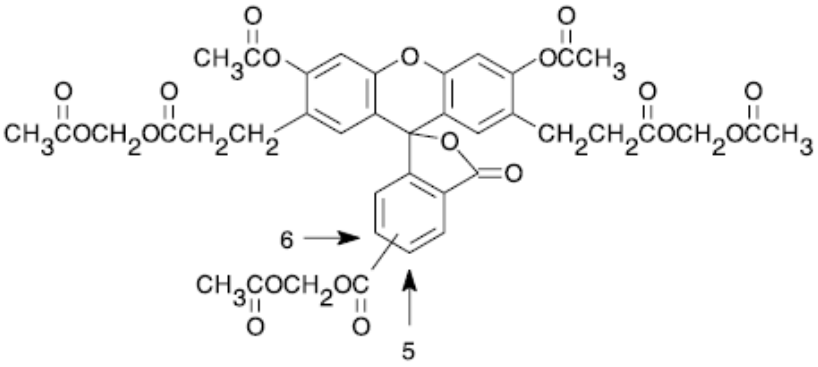

I (Molecular Weight = 820.7)

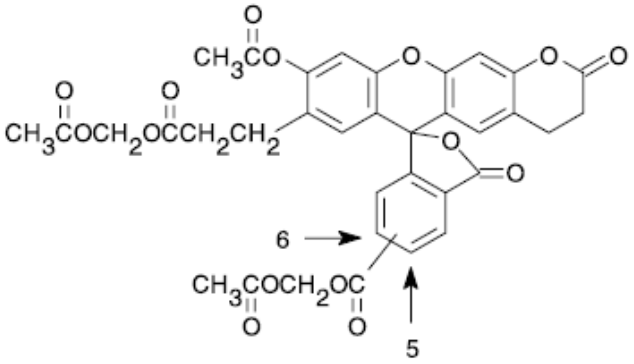

II (Molecular Weight = 688.6)

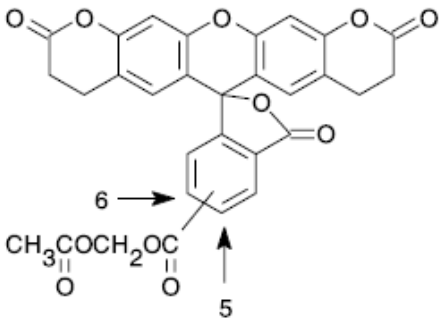

III (Molecular Weight = 556.5)

Figure 7-1. Molecular structures of BCECF-AM.

7.2. Experimental

7.2.1. Materials and reagents

Phosphate buffered saline (PBS, 10 mM, pH 7.4), Poly-L-lysine (PLL, 0.1% w/v in H_2O) and AC Broth were purchased from Sigma-Aldrich (St. Louis, MO). BCECF-AM (B1170) was purchased from Invitrogen (Eugene, OR) and stored at -20 ℃. De-ionized water (DI, 18 MΩ, Milli-Q system, Millipore, Billerica, MA) was obtained locally. *E. coli* JM101 was cultured in AC Broth (prepared as per vendor instructions) at 37 ℃ overnight. Harvested *E. coli* cells were centrifuged (×6,000 rpm for 3 min) and re-suspended in PBS twice. Live cell numbers were counted in a hemocytometer with 0.4% trypan blue. The desired cell concentration samples were prepared by dilution with PBS. E. coli culture was maintained in 37 ℃ hot room.

7.2.2. Sensor preparation

Sensors were fabricated as described previously. Briefly, the composite cantilever structure was fabricated with a quartz layer (SPI, West Chester, PA) bonded to a PZT layer (lead zirconate titanate, Piezo Systems, Woburn, MA) by an adhesive. Quartz layer (2.00 mm × 1.00 mm × 0.160 mm) was bonded to the PZT layer (2.70 mm × 1.00 mm × 0.127 mm) ($l \times w \times t$) by a non-conductive adhesive. A layer (10 μm) of Parylene-C was deposited on the sensor surface by chemical vapor deposition in a parylene coating machine (PDS 2010 LABCOTER® 2, SCS) to provide insulation for liquid environment application. A picture of fabricated sensor is shown in Figure 7.2B.

7.2.3. Experimental procedures

Sensor tip (2 mm^2) was freshly sputter-coated with 100 nm gold in a Desk IV sputtering system (Denton Vacuum, Moorestown, NJ). PLL droplets were applied to the gold surface and dried in chemical hood overnight prior to use [241]. PLL modified sensor was batch incubated in 1 mL *E. coli* JM101 cell solution (concentration range from 10^4 to 10^7 cells/mL) for 2 h at 37 ℃.

After incubation in live cell sample, the sensor was rinsed with PBS thoroughly and installed in a homemade flow cell (depicted in Figure 7.2B). The flow cell was placed in an incubator and the temperature was controlled at 30 ± 0.1℃. A peristaltic pump was used to provide a flow rate of 450 μL/min. The cantilever sensor was connected to an impedance analyzer (HP4192A, Hewlett-Packard) and a LabVIEW® program was used for collecting resonant frequency and impedance values in real-time. PBS was used as running buffer in flow experiments. Upon sensor resonant frequency stabilization in PBS, 100 μL 60 μM BCECF-AM aqueous solution was injected into the flow loop in recirculation mode. BCECF-AM aqueous solutions were freshly prepared from 10 mM anhydrous DMSO stock solution and diluted to the desired concentration (~1.5 μM final concentration in the flow loop) and used immediately. The volume of the flow loop was ~4 mL, thus requiring ~9 min to complete one circulation. The sensor response was assumed to have reached steady state when resonant frequency remained constant for at least 20 min. Subsequently PBS was introduced to rinse the system.

Fluorescence measurement was carried out in a spectrofluorometer (QuantaMaster™ 40, PTI, Birmingham, NJ). Glass slide cut to fit a cuvette size was incubated in 1 mL *E. coli* JM101 live cell samples (concentration from 10^4 to 10^7

cells/mL) for 2 h. Then the glass slides were rinsed with PBS and placed in a cuvette filled with 4 mL PBS; 100 µL 60 µM BCECF-AM was introduced and incubated for 1 h. After incubation, glass slide was removed, rinsed with PBS thoroughly and placed in cuvette for fluorescence measurement. The measurement was done with excitation at 505/439 nm and emission at 535 nm [242]. The ratio of fluorescence of BCECF at 505-439 nm is a function of pH. Slit width were 1 nm for excitation and 5 nm for emission. The cuvette was thermostated at 30 ℃ for measurement.

7.2.4. SEM examination of sensor surface

Sensors, following the BCECF experiments, were rinsed thoroughly with DI water and air dried. Subsequently, ~8 nm platinum/palladium (80/20) was deposited on the sensor surface and then examined in a Zeiss Supra 50VP or an FEI XL30 scanning electron microscope. Counting of the cells was typically done within 24 h of the flow experiments.

7.3. Results and discussion

A group of sensors with identical geometry was selected (m=20) from a large set that had nearly the same spectral and mass-change sensitivity properties. All sensors exhibited a dominant resonant mode in 940 ± 10 kHz region and showed an air-to-water frequency shift of 70.50 ± 4.50 kHz (m=20). The small standard deviation of 4.5 kHz suggests a sensitivity variation within 7%. Figure 7.2A shows the resonance spectra in air and under full immersion in DI water of a typical sensor. PEMC sensors do not suffer from damping in liquids because Reynolds number (Re) is high (~10^6), and the resonant

frequency can be measured with an accuracy of ± 20 Hz. This feature enables conducting continuous flow detection experiments in which sample can be changed conveniently and the resulting resonant frequency response is measured. Since the measurement is made *in situ* without removing the sensor from its housing, changes in measured resonant frequency is attributed to the detection response. This measurement format removes the ambiguity that plagues the dip-and-dry method used often with microcantilever sensors.

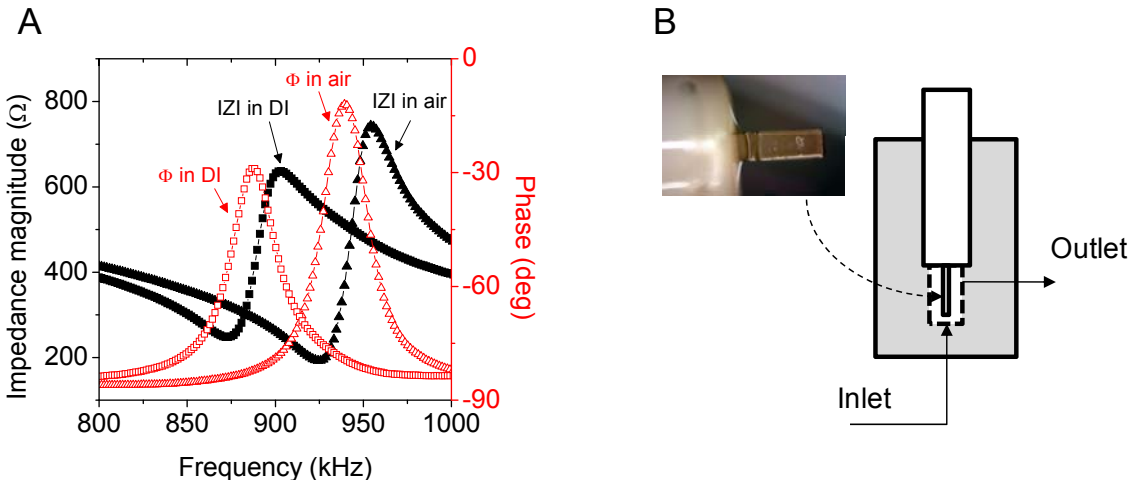

Figure 7-2. **(A)** Sensor spectra in air and in liquid. Solid symbols stand for impedance magnitude. Sensor exhibited resonant frequency at 940.71 kHz in air and 873.27 kHz in DI water, which gave a Δf = 67.44 kHz shift due to the difference in density of the surrounding medium. **(B)** Flow configuration of the flow cell.

The number of cells attached to the sensor surface increased with both incubation concentration and incubation time. The relationship between sample concentration and the cell number on the sensor surface bore a log-linear relationship ($y = 384.98\ ln(x) - 2309.9$, $R^2 = 0.98$) as shown in Figure 7.3. For incubation concentration of 10^4, 10^5, 10^6 and 10^7 cell/mL, sensor surface cell concentration was 1,090 ± 580, 2,360 ± 230, 2,950 ± 160, 3,960 ± 370 cells/mm^2 (n=5), respectively. As control, sensors coated

with gold at the sensor distal tip were exposed to 1 mL 10^7 cells/mL *E. coli* live cells and the attached cell was found to be very low (330 ± 100 cells/mm^2, n=5). In the following part of discussion, we correlate the sensor response with sensor surface cell concentration as it is the indicator of sensor sensitivity.

In a typical experiment, sensor was first incubated in 1 mL live *E. coli* samples (at various concentrations) in batch, and then exposed to BCECF-AM in the flow arrangement. The mass of the attached cells increase as BCECF accumulates within, and is measured by resonant frequency decrease.

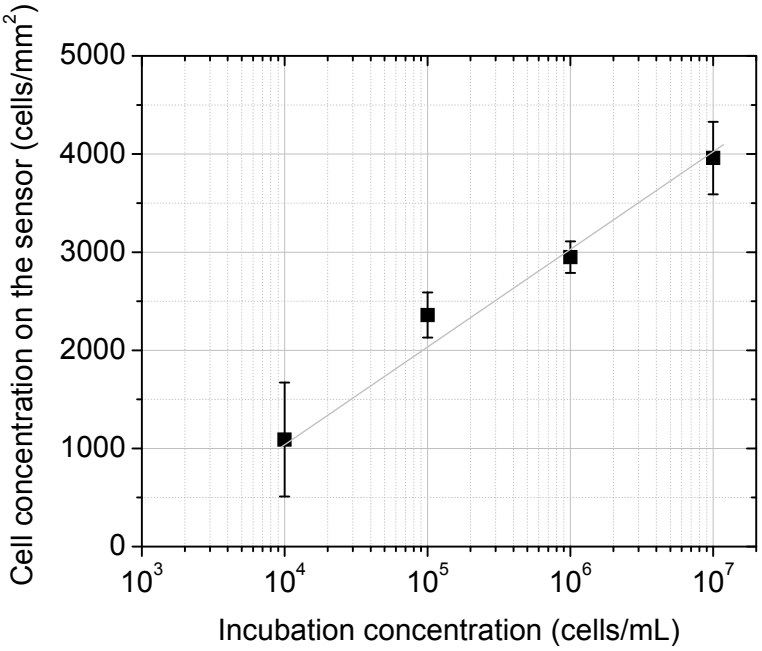

Figure 7-3. Correlation of cell concentration on the sensor surface with *E. coli* JM101 incubation concentration (n=5). A log-linear relationship is observed.

In Figure 7.4, we show the response of live *E. coli* JM 101 immobilized sensor to the addition of 100 µL 60 µM BCECF-AM (5 µg) to the flow loop. In all cases illustrated in Figure 7.4, the resonant frequency began to decrease ~5 – 10 min after the introduction

of BCECF-AM. The response took ~40-50 min to reach steady state. The time scale of sensor response is similar to previous reports on incubation time used (30-60 min) [237, 240]. As shown in Figure 7.4, resonant frequency decrease of 280 ± 10 Hz, 563 ± 21 Hz and 864 ± 15 Hz was obtained after BCECF-AM introduction corresponding to sensor surface cell concentration (measured by SEM) of 1,090 ± 580, 2,360 ± 230, 3,960 ± 370 cells/mm^2 (n=5), respectively. Impedance response of the sensor corresponding to these three experiments is given in Figure 7.5.

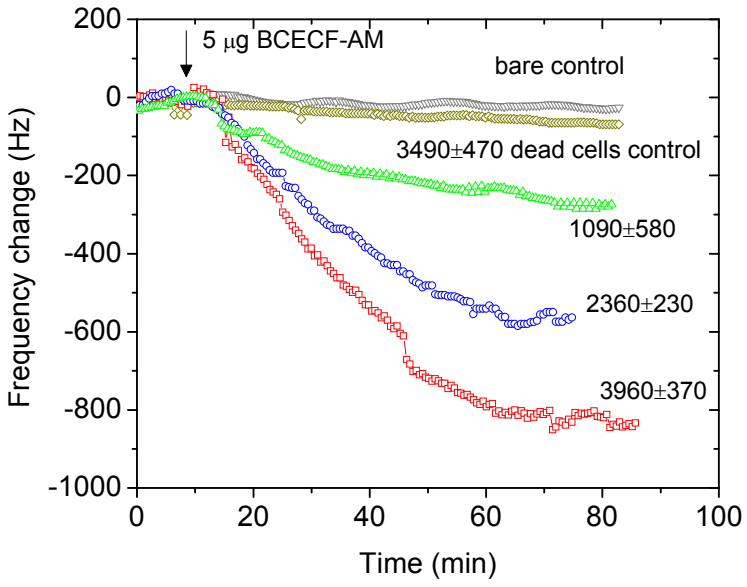

Figure 7-4. Resonant frequency response to the addition of 100 µL of 60 µM (5 µg) BCECF-AM to sensors with surface cell concentrations (1,090 ± 580, 2,360 ± 230, 3,960 ± 370 cells/mm^2 (n=5)). Sensor that was immobilized with 3,490 ± 470 cells/mm^2 (n=3) dead *E. coli* cells gave very small frequency decrease (62 ± 4 Hz). An additional control (labeled as bare control) with no *E.coli* incubation also yielded no observable response.

As expected, the response was larger for larger number of cells on the sensor, as total BCECF accumulation is proportional to cell number. Once the sensor response reached steady state, the flow was changed to PBS in a once-through mode. No further change in resonant frequency was observed over the subsequent 20 min period, suggesting BCECF leakage was small or none in that time window. Separate control experiments with PLL-prepared sensors without a cell incubation step showed no response to 100 µL 60 µM BCECF-AM (Figure 7.4 and 7.5). A second set of controls with killed cells (3,490 ± 470 cells/mm^2, n=3) immobilized on PLL-prepared sensor yielded a small resonant frequency decrease (62 ± 4 Hz) to the same BCECF-AM addition. The two control experiments indicate that the response observed with live cells to BCECE-AM is due to BCECF accumulation in live cells.

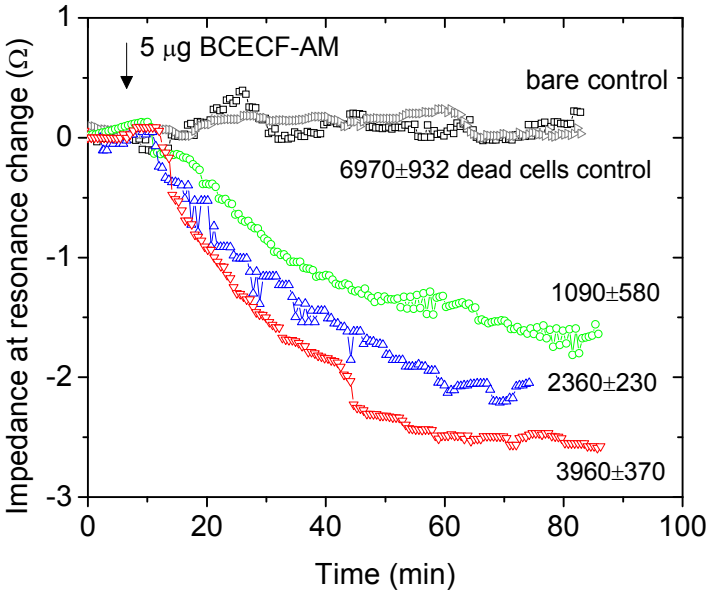

Figure 7-5. Impedance magnitude response at resonance to the addition of 100 µL of 60 µM (5 µg) BCECF-AM with the sensor surface cell concentrations at 1,090 ± 580, 2,360 ± 230, 3,960 ± 370 cells/mm^2 (n=5). Control experiments are the cases: (a) no cells (bare control), and (b) sensor immobilized with 3,490 ± 470 cells/mm^2 (n=3) dead *E. coli* cells. Both yielded essentially no impedance response.

We tested if the cells remained viable subsequent to the BCECF exposure. This was accomplished by introducing growth medium and then examining if sensor response decreased due to cell growth. The idea is that nutrients in the growth medium would stimulate growth of viable cells on the sensor surface. The growth medium, AC Broth, was introduced into the flow loop in recirculation mode after a detection experiment. The temperature of the flow cell was adjusted to 37 ℃ to facilitate growth. As shown in Figure 7.6, upon the introduction of 4 mL AC Broth, resonant frequency showed a higher density induced decrease of ~600 Hz and reached a new steady state value within 20 min [158, 168, 243]. The resonant frequency then began to decrease after a lag of ~50 min, and continued to decrease for a further 140 min, resulting in a total resonant frequency change of ~2,100 Hz. From the exponential growth phase one can calculate the growth rate (μ) as 2.1 h^{-1}, which is comparable to literature [99, 244]. Control experiments that exposed the sensor with no immobilized cells to AC Broth gave no response except the initial density response due to switching from PBS to AC Broth. From the cell growth experiments, we confirm that the cells in the BCECF experiments were alive and can be stimulated to grow if nutrients are supplied.

Practically, cell colony and plate counting is one of the most reliable method for bacteria detection as it has the merits of high accuracy, high sensitivity and ability to distinguish viable and non-viable cells. Bacterial pathogens doubling time generally is short (30 min to several hours depending on species), which making the growth observation a relatively easy and timely method for cell viability determination. In our cases, cell growth can be monitored on the sensor surface in real-time by resonant frequency changes, which can be another very useful method for cell viability

measurement. However, differentiating viable and non-viable cells depends on the growth rate of the particular species. For cells with long doubling time, growth method is not practical for sensor application.

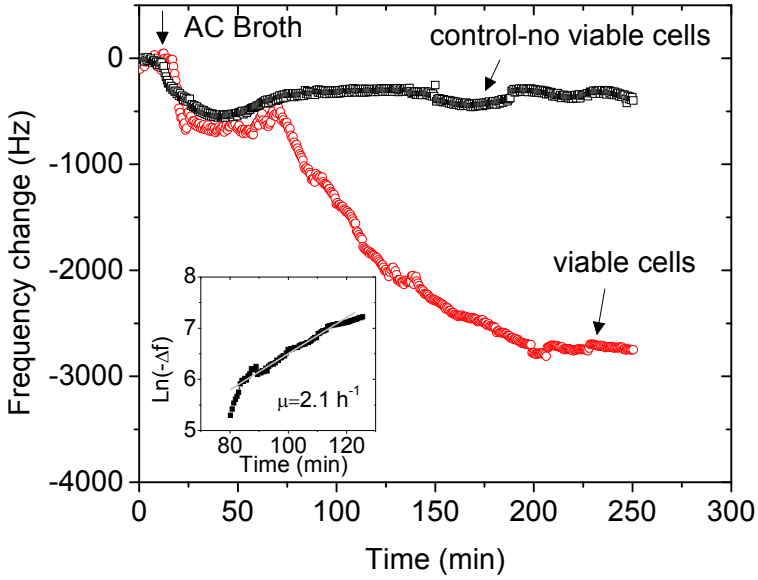

Figure 7-6. Sensor response upon introduction of AC Broth. Sensor at the end of BCECF experiment was exposed to growth medium, AC Broth. After an initial response due to density change, decrease in resonant freuqency is due to cell growth. Reasponse reaches a constatnt value, presumably due to stoppage of growth. Inset plot shows growth response was expoenential with specific growth rate of 2.1 h^{-1}. Control experiments without *E. coli* on the sensor surface gave no response.

It is of interest to investigate the relationship between the response of the sensor to BCECF-AM and the cell concentration on the sensor surface. As shown in Figure 7.7A, resonant frequency decrease in response to 100 μL 60 μM (5 μg) BCECF-AM correlated with cell concentration on the sensor surface in a log-linear fashion (*y=426.43 ln(x)-3003.2*, R^2=0.9115) in the range of 1,000 – 4,000 cells/mm^2. The quantification shows the potential of using BCECF-AM for measuring live cell concentrations directly in

liquid samples by measuring resonant frequency change since cell concentration on sensor surface is proportional to sample concentration.

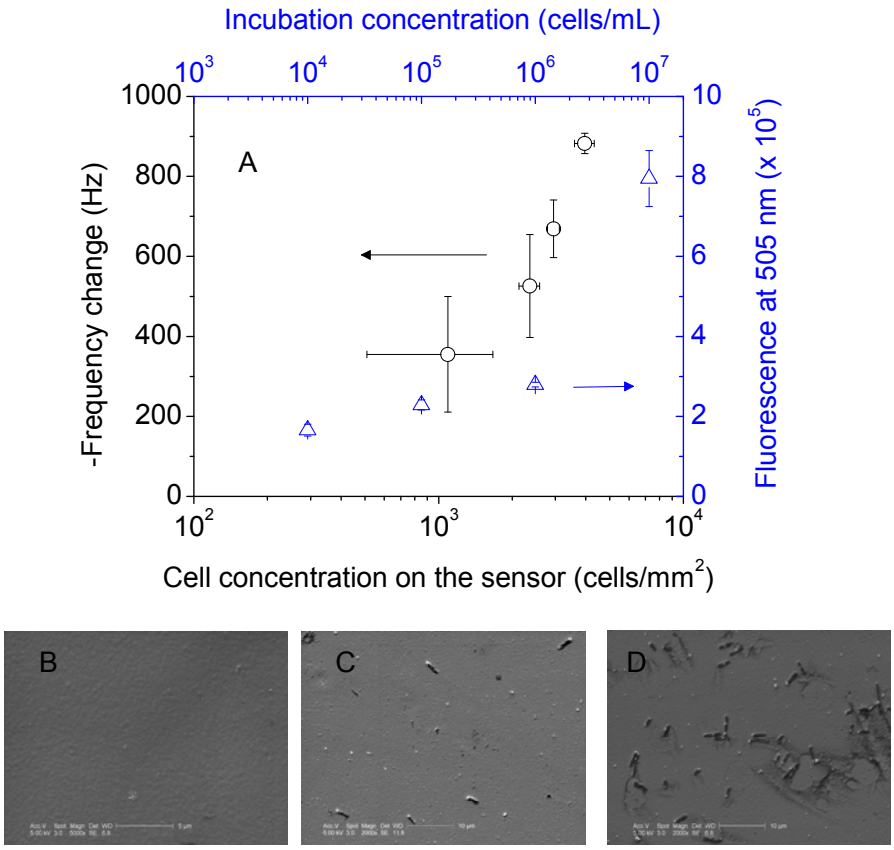

Figure 7-7. (A) Frequency response is compared with fluorescence response (505 nm) due to BCECF-AM injection. Sensor response to cell concentration on the surface (○) and fluorescence response to incubation concentration (Δ) are shown. **(B)**, **(C)**, **(D)** are the SEM micrographs of sensor surface after the associated experiments. They show sensor cell concentrations were 0, 1,090 ± 580, 3,960 ± 370 cells/mm^2 (n=5) corresponding to 1 mL 0, 10^4 and 10^7 cells/mL incubation, respectively. Scale bars in **(B)**, **(C)** and **(D)** are 5 µm, 10 µm and 10 µm, respectively.

Since BCECF is fluorescent, we measured fluorescence of incubated cells to confirm sensor response. Experimentally, glass slides (cut to fit in a cuvette diagonally) was immobilized with *E. coli* following the approach used in sensor experiments, and then was exposed to the same BCECF-AM (~1.5 µM in 4 mL) for 1 h showed higher fluorescence value with higher *E. coli* concentration, and is in the same direction as

resonant frequency change. The increase of fluorescence intensity is particularly significant when incubation concentration was increased to 10^6 and 10^7 cells/mL. This indicates accumulation of BCECF in viable *E. coli* cells, and verifies the PEMC sensor response to BCECF-AM.

Typical distribution of *E. coli* cells on the sensor surface is shown in Figure 7.7B, C and D, which are the SEM images after incubation in 1 mL 0, 10^4, 10^7 cells/mL samples, respectively. Sensor that was not incubated in *E. coli* was quite clean. Higher *E. coli* concentration yielded higher cell density on the sensor surface. For analysis of a pathogenic bacterium of interest, antibody specific to the pathogen can be immobilized on the sensor surface to capture the desired target through antibody-antigen binding. The sensor can then be exposed to BCECF-AM for examining if the bound cells are viable using the method developed in this study. Thus, both quantification and viability information of a sample can be obtained improving TTR.

7.4. Conclusions

Cantilever biosensor in combination with BCECF accumulation can be used for detecting viability of cells at a detection sensitivity of ~ 2,000 *E. coli* cells. Poly-L-lysine coated sensor immobilized with live *E. coli* JM101 (a surrogate for a pathogenic target) at various concentrations was exposed to BCECF-AM in a flow arrangement. Larger resonant frequency decrease to 100 μL 60 μM BCECF-AM was observed when sensor surface cell concentration was increased from 1,090 ± 580 to 3,960 ± 370 cells/mm^2 (n=5). A log-linear relationship between the sensor surface cell concentration and frequency response was obtained in the range of 1,000 – 4,000 cells/mm^2 and as low as

~2,000 viable *E. coli* cells was rapidly detected (<1 h). Because live cells respond to toxins, a live cell immobilized cantilever sensor would be useful in monitoring environmental toxic pollutants.

CHAPTER 8 : CONCLUSIONS AND RECOMMENDED FUTURE WORK

8.1. Summary and conclusions

The main results of this dissertation can be summarized as follows.

1. Impedance response of a PEMC sensor was found to be equivalent to resonant frequency response. Experimentally it was found that monitoring frequency for impedance change should be located within ± 1 kHz of resonant frequency. The proposed approach was experimentally verified using minute density change and antibody-based *E. coli* O157:H7 detection experiments. Flow experiments carried out using impedance method showed superior signal-to-noise ratio. The impedance approach is limited to responses where only small changes in *Q*-value occur, which is typical of biosensing applications using PEMC sensor.
2. Limit of detection for *C. parvum* in PBS or 25% milk background was found to be 5 oocysts/mL. The sensitivity of PEMC sensor was not compromised in milk matrix even though the frequency response magnitude decreased (~45%) and binding kinetics was slower. The second antibody binding method provided confirmation of sensor detection response. The sensor showed a semi-log relationship between resonant frequency change and *C. parvum* oocysts concentration with a dynamic range of 50 – 10^4 oocysts/mL.
3. Limit of detection for *G. lamblia* in several water matrixes (buffer, tap and river water) was found to be 10 cysts/mL without a pre-concentration step using a PEMC sensor immobilized with a monoclonal antibody. The dynamic detection range was 1 – 10,000 *G. lamblia* cysts/mL. Positive confirmation of sensor

detection responses was obtained by environmental scanning electron microscope of sensor surface after detection experiments. Higher sample flow rates (0.5 to 5.0 mL/min) gave higher sensor detection response. Feasibility of analyzing at a low concentration of 1 cyst/mL in a one liter sample at a high flow rate of 5 mL/min was demonstrated.

4. Detection of *A. laidlawii* at 10^3 CFU/mL was achieved in both PBS and cell culture medium with a dynamic range of 10^3 – 10^7 CFU/mL in buffer medium. Roche mycoplasma kit was also characterized using PEMC sensor. The PEMC sensor showed about four orders higher sensitivity compared with ELISA method conducted in parallel using the same *A. laidlawii* stock and the same antibody reagents.
5. PEMC sensor in combination with BCECF accumulation was used for detecting viability of *E. coli* cells at a detection sensitivity of ~ 2,000 cells. Poly-L-lysine coated sensor immobilized with live *E. coli* JM101 at various concentrations was exposed to BCECF-AM in a flow arrangement. Larger resonant frequency decrease to 100 μL 60 μM BCECF-AM was observed when sensor surface cell concentration was increased from 1,000 to 4,000 cells/mm^2. A log-linear relationship between the sensor surface cell concentration and frequency response was obtained. Further, BCECF accumulation can be extended for *C. parvum* viability assessment using fluorescence microscopy as well as PEMC sensor.

8.2. Recommended future work

Cantilever technology has been evolving in the past 15 years for chemical and biological detection. With the development of novel methods and understanding of their working principles, cantilever sensors might have a broader application in the future. Here a brief summary of problems encountered during the course of PhD work that appear worthy of further investigation.

8.2.1. Voltage-assisted non-specific binding reduction and analytes release

Non-specific binding is the technical issue plagues cantilever biosensors when used in liquids that contain extraneous biological entities. To address non-specific binding, several reports have emerged in the last few years that indicate increasing the oscillation magnitude of shear resonators (QCM and SAW) causes reduced binding of extraneous materials [245, 246]. For example, it was found that by increasing excitation voltage of a QCM from the normal 1 V to 5 V, 85% reduction in BSA adsorption to the sensor surface was obtained [245]. By further increasing the excitation voltage to 10 V, several studies found that ligand-receptor bond can be disrupted [247-249]. Flexural oscillation of a cantilever is normal to sensor surface while that of a QCM is in shear mode and thus parallel to sensor surface. Consequently disruption of binding is expected to be achieved at a much lower excitation voltage with a cantilever sensor. Analyte binding affinity can be measured in a single experiment by modulating excitation intensity. Using resonant-mode cantilever biosensors, one could excite the cantilever at the appropriate voltage level suitable for reduction of non-specific binding or disrupting ligand-receptor bond. This approach of measurement when fully developed may achieve

the goal of screening molecules based on the strength of binding. Binding energy assay using cantilever biosensors could provide a more rapid and direct measure of binding affinity.

8.2.2. Cell activity investigation

As discussed in Chapter 7, live cell coated PEMC sensor was able to respond to external disturbance. This leads to a very useful application in biological assays: investigation of cell activities and response to chemical reagents. Animal cells coated sensor would be able to respond to various reagents and can be monitored using resonant frequency or impedance method. In another case, reduction of cell volume, which can be used as an early indicator of apoptosis, can also be monitored on the sensor surface for biological process evaluation. This method can not only be used for providing useful information on cell activities, but also can be used as a cell-based sensor for environmental monitoring.

8.2.3. Cantilever sensor array development for high-throughput screening

Cantilever sensor array bares two advantages over single cantilever sensor: one is the ability to cancel out false positive response using one or more as a reference sensor; the other is the ability to screen a large library of candidates within a short period of time, i.e, will be able to provide means for high-throughput screening [250]. As discussed in Chapter 3, we have shown the impedance method can provide equivalent information as resonant frequency method and greatly reduce the cost for high-throughput screening from instrument point of view. Design and fabrication of cantilever arrays with 96 or up

to several thousand sensors and coupled with newly developed impedance method would provide a general platform for measurement of 100 to 1,000 interactions simultaneously with redundant measurements. These attractive and time-saving characteristics could potentially accelerate the drug discovery process.

LIST OF REFERENCES

1. Thevenot, D.R., et al., *Electrochemical biosensors: Recommended definitions and classification - (Technical Report).* Pure Appl. Chem., 1999. **71**(12): 2333-2348.

2. Maraldo, D., et al., *Method for label-free detection of femtogram quantities of biologics in flowing liquid samples.* Anal. Chem., 2007. **79**(7): 2762-2770.

3. Rijal, K. and R. Mutharasan, *Method for measuring the self-assembly of alkanethiols on gold at femtomolar concentrations.* Langmuir, 2007. **23**(12): 6856-6863.

4. Fritz, J., et al., *Translating biomolecular recognition into nanomechanics.* Science, 2000. **288**(5464): 316-318.

5. McKendry, R., et al., *Multiple label-free biodetection and quantitative DNA-binding assays on a nanomechanical cantilever array.* Proc. Natl. Acad. Sci. USA, 2002. **99**(15): 9783-9788.

6. Wu, G.H., et al., *Bioassay of prostate-specific antigen (PSA) using microcantilevers.* Nat. Biotechnol., 2001. **19**(9): 856-860.

7. Arntz, Y., et al., *Label-free protein assay based on a nanomechanical cantilever array.* Nanotechnology, 2003. **14**(1): 86-90.

8. Burg, T.P., et al., *Weighing of biomolecules, single cells and single nanoparticles in fluid.* Nature, 2007. **446**(7139): 1066-1069.

9. Davila, A.P., et al., *Microresonator mass sensors for detection of Bacillus anthracis Sterne spores in air and water.* Biosens. Bioelectron., 2007. **22**(12): 3028-3035.

10. Gupta, A., D. Akin, and R. Bashir, *Single virus particle mass detection using microresonators with nanoscale thickness.* Appl. Phys. Lett., 2004. **84**(11): 1976-1978.

11. Moulin, A.M., S.J. O'Shea, and M.E. Welland, *Microcantilever-based biosensors.* Ultramicroscopy, 2000. **82**(1-4): 23-31.

12. Campbell, G.A. and R. Mutharasan, *Use of piezoelectric-excited millimeter-sized cantilever sensors to measure albumin interaction with self-assembled monolayers of alkanethiols having different functional headgroups.* Anal. Chem., 2006. **78**(7): 2328-2334.

13. Campbell, G.A. and R. Mutharasan, *Monitoring of the self-assembled monolayer of 1-hexadecanethiol on a gold surface at nanomolar concentration using a piezo-excited millimeter-sized cantilever sensor.* Langmuir, 2005. **21**(25): 11568-11573.

14. EPA. *CCL list*. 2009 Jul.10th, 2009]; Available from: http://www.epa.gov/OGWDW/ccl/index.html.

15. Rogers, K.R., *Recent advances in biosensor techniques for environmental monitoring.* Anal. Chim. Acta, 2006. **568**(1-2): 222-231.

16. Rodriguez-Mozaz, S., M.J.L. de Alda, and D. Barcelo, *Biosensors as useful tools for environmental analysis and monitoring.* Anal. Bioanal. Chem., 2006. **386**(4): 1025-1041.

17. Wanekaya, A.K., W. Chen, and A. Mulchandani, *Recent biosensing developments in environmental security.* J. Environ. Monit., 2008. **10**(6): 703-712.

18. Nie, S.M. and R.N. Zare, *Optical detection of single molecules.* Annu. Rev. Biophys. Biomol. Struct., 1997. **26**: 567-596.

19. Ali, M.F., et al., *DNA hybridization and discrimination of single-nucleotide mismatches using chip-based microbead arrays.* Anal. Chem., 2003. **75**(18): 4732-4739.

20. Shi, J., et al., *Recent developments in nanomaterial optical sensors.* TrAC-Trends Anal. Chem. , 2004. **23**(5): 351-360.

21. Rosi, N.L. and C.A. Mirkin, *Nanostructures in biodiagnostics.* Chem. Rev., 2005. **105**(4): 1547-1562.

22. Boardman, A.D., ed. *Electromagnetic surface modes*. 1982, John Wiley and Sons: New York.

23. Ballantine, D.S.J., et al., eds. *Acoustic wave sensors - Theory, design, and physico-chemical applications*. 1997, Elsevier.

24. Homola, J., *Present and future of surface plasmon resonance biosensors.* Anal. Bioanal. Chem., 2003. **377**(3): 528-539.

25. Homola, J., *Surface plasmon resonance sensors for detection of chemical and biological species.* Chem. Rev., 2008. **108**(2): 462-493.

26. Shankaran, D.R., K.V. Gobi, and N. Miura, *Recent advancements in surface plasmon resonance immunosensors for detection of small molecules of biomedical, food and environmental interest.* Sens. Actuators B: Chem., 2007. **121**(1): 158-177.

27. Hecht, E., *Optics*. 4 ed. 2001: Addison Wesley.

28. Leung, A., P.M. Shankar, and R. Mutharasan, *A review of fiber-optic biosensors.* Sens. Actuators B: Chem., 2007. **125**(2): 688-703.

29. Kersey, A.D., et al., *Fiber grating sensors.* J. Lightwave Technol., 1997. **15**(8): 1442-1463.

30. Fan, X.D., et al., *Sensitive optical biosensors for unlabeled targets: A review.* Anal. Chim. Acta, 2008. **620**(1-2): 8-26.

31. Cush, R., et al., *The resonant mirror-A novel optical biosensor for direct sensing of biomolecular interactions. 1. Principle of operation and associated instrumentation.* Biosens. Bioelectron., 1993. **8**(7-8): 347-353.

32. Rowe-Taitt, C.A., et al., *Simultaneous detection of six biohazardous agents using a planar waveguide array biosensor.* Biosens. Bioelectron., 2000. **15**(11-12): 579-589.

33. Mouvet, C., et al., *Reflectometric interference spectroscopy for the determination of atrazine in natural water samples.* Environ. Sci. Technol., 1996. **30**(6): 1846-1851.

34. Ksendzov, A. and Y. Lin, *Integrated optics ring-resonator sensors for protein detection.* Opt. Lett., 2005. **30**(24): 3344-3346.

35. Gorton, L., ed. *Biosensors and modern biospecific analytical techniques*. Comprehensive Analytical Chemistry, ed. L. Gorton. Vol. XLIV 2005, Elsevier. 209-250.

36. Ligler, F.S. and C.A. Rowe-Taitt, eds. *Optical biosensors- present and future*. 2002, Elsevier.

37. Bashir, R., *BioMEMS: state-of-the-art in detection, opportunities and prospects.* Adv. Drug Deliv. Rev., 2004. **56**(11): 1565-1586.

38. Hanrahan, G., D.G. Patil, and J. Wang, *Electrochemical sensors for environmental monitoring: design, development and applications.* J. Environ. Monit., 2004. **6**(8): 657-664.

39. Guth, U., W. Vonau, and J. Zosel, *Recent developments in electrochemical sensor application and technology-a review.* Meas. Sci. Technol., 2009. **20**(4).

40. Abdel-Hamid, I., et al., *Flow-through immunofiltration assay system for rapid detection of E. coli O157:H7.* Biosens. Bioelectron., 1999. **14**(3): 309-316.

41. Abdel-Hamid, I., et al., *Highly sensitive flow-injection immunoassay system for rapid detection of bacteria.* Anal. Chim. Acta, 1999. **399**(1-2): 99-108.

42. Brewster, J.D., et al., *Immunoelectrochemical assays for bacteria: Use of epifluorescence microscopy and rapid-scan electrochemical techniques in development of an assay for Salmonella.* Anal. Chem., 1996. **68**(23): 4153-4159.

43. Zhang, F., et al., *A rapid competitive binding nonseparation electrochemical enzyme immunoassay (NEEIA) test strip for microcystin-LR (MCLR) determination.* Biosens. Bioelectron., 2007. **22**(7): 1419-1425.

44. Schnakenberg, U., et al., *Novel potentiometric silicon sensor for medical devices.* Sens. Actuators B: Chem., 1996. **34**(1-3): 476-480.

45. Gehring, A.G., D.L. Patterson, and S.-I. Tu, *Use of a light-addressable potentiometric sensor for the detection of Escherichia coli O157:H7.* Anal. Biochem., 1998. **258**(2): 293-298.

46. Tu, S.-I., et al., *The use of streptavidin coated magnetic beads for detecting pathogenic bacteria by light addressable potentiometric sensor (LAPS).* J. Rapid Methods Autom. Microbiol., 2000. **8**(2): 95-109.

47. Miranda-Castro, R., et al., *Hairpin-DNA probe for enzyme-amplified electrochemical detection of Legionella pneumophila.* Anal. Chem., 2007. **79**(11): 4050-4055.

48. Miranda-Castro, R., et al., *Stem-loop DNA probes for the voltammetric determination of Legionella pneumophila on disposable screen-printed gold electrodes.* Electroanalysis, 2009. **21**(3-5): 267-273.

49. Muhammad-Tahir, Z. and E.C. Alocilja, *A conductometric biosensor for biosecurity.* Biosens. Bioelectron., 2003. **18**(5-6): 813-819.

50. Muhammad-Tahir, Z. and E.C. Alocilja, *A disposable biosensor for pathogen detection in fresh produce samples.* Biosyst. Eng., 2004. **88**(2): 145-151.

51. Huang, X.J. and Y.Y. Zhang, *Electrical determination of E. coli O157 : H7 using tin-oxide nanowire coupled with microfluidic chip.* IEEE Sens. J., 2006. **6**(6): 1376-1377.

52. Star, A., et al., *Label-free detection of DNA hybridization using carbon nanotube network field-effect transistors.* Proc. Natl. Acad. Sci. USA, 2006. **103**(4): 921-926.

53. Dastagir, T., et al., *Electrical detection of Hepatitis C virus RNA on single wall carbon nanotube-field effect transistors.* Analyst, 2007. **132**(8): 738-740.

54. Patolsky, F., et al., *Electrical detection of single viruses.* Proc. Natl. Acad. Sci. USA, 2004. **101**(39): 14017-14022.

55. Cavic, B.A., G.L. Hayward, and M. Thompson, *Acoustic waves and the study of biochemical macromolecules and cells at the sensor-liquid interface.* Analyst, 1999. **124**(10): 1405-1420.

56. Ward, M.D. and D.A. Buttry, *In situ interfacial mass detection with piezoelectric transducers.* Science, 1990. **249**(4972): 1000-1007.

57. Konash, P.L. and G.J. Bastiaans, *Piezoelectric-cyrstals as detectors in liquid-chromatography.* Anal. Chem., 1980. **52**(12): 1929-1931.

58. Ogi, H., et al., *Concentration dependence of IgG-protein A affinity studied by wireless-electrodeless QCM.* Biosens. Bioelectron., 2007. **22**(12): 3238-3242.

59. Ogi, H., et al., *Effects of flow rate on sensitivity and affinity in flow injection biosensor systems studied by 55-MHz wireless quartz crystal microbalance.* Anal. Chem., 2008. **80**(14): 5494-5500.

60. Bottom, V.E., *Introduction to quartz crystal unit design*. 1982, New York Van Nostrand Reinhold.

61. Sauerbrey, G.Z., *Use of vibrating quartz for thin film weighting and microweighing (in German).* Z. Phys., 1959. **155**: 206-222.

62. Kanazawa, K.K. and J.G. Gordon, *The oscillation frequency of a quartz resonator in contact with a liquid.* Anal. Chim. Acta, 1985. **175**(SEP): 99-105.

63. Muramatsu, H., E. Tamiya, and I. Karube, *Computation of equivalent circuit parameters of quartz crystals in contact with liquids and study of liquid properties.* Anal. Chem., 1988. **60**(19): 2142-2146.

64. Hayward, G.L. and G.Z. Chu, *Simultaneous measurement of mass and viscosity using piezoelectric quartz crystals in liquid media.* Anal. Chim. Acta, 1994. **288**(3): 179-185.

65. Rodahl, M., et al., *Quartz crystal microbalance setup for frequency and Q-factor measurements in gaseous and liquid environments.* Rev. Sci. Instrum., 1995. **66**(7): 3924-3930.

66. Rodahl, M., F. Hook, and B. Kasemo, *QCM operation in liquids: An explanation of measured variations in frequency and Q factor with liquid conductivity.* Anal. Chem., 1996. **68**(13): 2219-2227.

67. Hook, F., et al., *Energy dissipation kinetics for protein and antibody-antigen adsorption under shear oscillation on a quartz crystal microbalance.* Langmuir, 1998. **14**(4): 729-734.

68. Hutter, J.L. and J. Bechhoefer, *Calibratioin of atomic-force microscope tips.* Rev. Sci. Instrum., 1993. **64**(7): 1868-1873.

69. Stony, G.G., *The tension of metallic films deposited by electrolysis.* Proc. R. Soc. London, Ser. A, 1909. **82**(553): 172-175.

70. Lee, J.H., et al., *Immunoassay of prostate-specific antigen (PSA) using resonant frequency shift of piezoelectric nanomechanical microcantilever.* Biosens. Bioelectron., 2005. **20**(10): 2157-2162.

71. Hansen, K.M., et al., *Cantilever-based optical deflection assay for discrimination of DNA single-nucleotide mismatches.* Anal. Chem., 2001. **73**(7): 1567-1571.

72. Ilic, B., et al., *Attogram detection using nanoelectromechanical oscillators.* J. Appl. Phys., 2004. **95**(7): 3694-3703.

73. Calleja, M., et al., *Low-noise polymeric nanomechanical biosensors.* Appl. Phys. Lett., 2006. **88**(11): 113901.

74. McFarland, A.W., et al., *Injection moulding of high aspect ratio micron-scale thickness polymeric microcantilevers.* Nanotechnology, 2004. **15**(11): 1628-1632.

75. Singamaneni, S., et al., *Bimaterial microcantilevers as a hybrid sensing platform.* Adv. Mater., 2008. **20**(4): 653-680.

76. Baker, G.A., R. Desikan, and T. Thundat, *Label-free sugar detection using phenylboronic acid-functionalized piezoresistive microcantilevers.* Anal. Chem., 2008. **80**(13): 4860-4865.

77. Baller, M.K., et al., *A cantilever array-based artificial nose.* Ultramicroscopy, 2000. **82**(1-4): 1-9.

78. Mukhopadhyay, R., et al., *Cantilever sensor for nanomechanical detection of specific protein conformations.* Nano Lett., 2005. **5**(12): 2385-2388.

79. Weeks, B.L., et al., *A microcantilever-based pathogen detector.* Scanning, 2003. **25**(6): 297-299.

80. Zhang, J. and H.F. Ji, *An anti E.coli O157 : H7 antibody-immobilized microcantilever for the detection of Escherichia coli (E-coli).* Anal. Sci., 2004. **20**(4): 585-587.

81. Betts, T.A., et al., *Selectivity of chemical sensors based on micro-cantilevers coated with thin polymer films.* Anal. Chim. Acta, 2000. **422**(1): 89-99.

82. Berger, R., et al., *Surface stress in the self-assembly of alkanethiols on gold.* Science, 1997. **276**(5321): 2021-2024.

83. Thundat, T., et al., *Thermal and ambient-induced deflections of scanning force microscope cantilevers.* Appl. Phys. Lett., 1994. **64**(21): 2894-2896.

84. Ilic, B., et al., *Enumeration of DNA molecules bound to a nanomechanical oscillator.* Nano Lett., 2005. **5**(5): 925-929.

85. Yang, Y.T., et al., *Zeptogram-scale nanomechanical mass sensing.* Nano Lett., 2006. **6**(4): 583-586.

86. Ekinci, K.L., X.M.H. Huang, and M.L. Roukes, *Ultrasensitive nanoelectromechanical mass detection.* Appl. Phys. Lett., 2004. **84**(22): 4469-4471.

87. Butt, H.J., et al., *Scan speed limit in atomic force microscopy.* J. Microsc.-Oxf., 1993. **169**: 75-84.

88. Mehta, A., et al., *Manipulation and controlled amplification of Brownian motion of microcantilever sensors.* Appl. Phys. Lett., 2001. **78**(11): 1637-1639.

89. Tamayo, J., et al., *Chemical sensors and biosensors in liquid environment based on microcantilevers with amplified quality factor.* Ultramicroscopy, 2001. **86**(1-2): 167-173.

90. Tamayo, J., et al., *High-Q dynamic force microscopy in liquid and its application to living cells.* Biophys. J., 2001. **81**(1): 526-537.

91. Hwang, K.S., et al., *In-situ quantitative analysis of a prostate-specific antigen (PSA) using a nanomechanical PZT cantilever.* Lab Chip, 2004. **4**(6): 547-552.

92. Kwon, T.Y., et al., *In situ real-time monitoring of biomolecular interactions based on resonating microcantilevers immersed in a viscous fluid.* Appl. Phys. Lett., 2007. **90**(22).

93. Campbell, G.A. and R. Mutharasan, *A method of measuring Escherichia coli O157 : H7 at 1 cell/mL in 1 liter sample using antibody functionalized piezoelectric-excited millimeter-sized cantilever sensor.* Environ. Sci. Technol., 2007. **41**(5): 1668-1674.

94. Campbell, G.A. and R. Mutharasan, *Detection of pathogen Escherichia coli O157: H7 using self-excited PZT-glass microcantilevers.* Biosens. Bioelectron., 2005. **21**(3): 462-473.

95. Zhu, Q., W.Y. Shih, and W.H. Shih, *In situ, in-liquid, all-electrical detection of Salmonella typhimurium using lead titanate zirconate/gold-coated glass cantilevers at any dipping depth.* Biosens. Bioelectron., 2007. **22**(12): 3132-3138.

96. Campbell, G.A. and R. Mutharasan, *Near real-time detection of Cryptosporidium parvum oocyst by IgM-functionalized piezoelectric-excited millimeter-sized cantilever biosensor.* Biosens. Bioelectron., 2008. **23**(7): 1039-1045.

97. Maraldo, D. and R. Mutharasan, *Detection and confirmation of staphylococcal enterotoxin B in apple juice and milk using piezoelectric-excited millimeter-sized cantilever sensors at 2.5 fg/mL.* Anal. Chem., 2007. **79**(20): 7636-7643.

98. Gfeller, K.Y., N. Nugaeva, and M. Hegner, *Micromechanical oscillators as rapid biosensor for the detection of active growth of Escherichia coli.* Biosens. Bioelectron., 2005. **21**(3): 528-533.

99. Detzel, A.J., G.A. Campbell, and R. Mutharasan, *Rapid assessment of Escherichia coli by growth rate on piezoelectric-excited millimeter-sized cantilever (PEMC) sensors.* Sens. Actuators B: Chem., 2006. **117**(1): 58-64.

100. Sithigorngul, P., et al., *A simple and rapid immunochromatographic test strip for detection of pathogenic isolates of Vibrio harveyi.* J. Microbiol. Methods, 2007. **71**(3): 256-264.

101. Nato, F., et al., *Dipstick for rapid diagnosis of Shigella flexneri 2a in stool.* PLoS ONE, 2007. **2**(4): e361.

102. Baeumner, A.J., et al., *RNA biosensor for the rapid detection of viable Escherichia coli in drinking water.* Biosens. Bioelectron., 2003. **18**(4): 405-413.

103. Esch, M.B., A.J. Baeumner, and R.A. Durst, *Detection of Cryptosporidium parvum using oligonucleotide-tagged liposomes in a competitive assay format.* Anal. Chem., 2001. **73**(13): 3162-3167.

104. Connelly, J., et al., *Human pathogenic Cryptosporidium species bioanalytical detection method with single oocyst detection capability.* Anal. Bioanal. Chem., 2008. **391**(2): 487-495.

105. Carter, D.J. and R.B. Cary, *Lateral flow microarrays: a novel platform for rapid nucleic acid detection based on miniaturized lateral flow chromatography.* Nucl. Acids Res., 2007. **35**(10): e74-.

106. Byrne, B., et al., *Antibody-based sensors: Principles, problems and potential for detection of pathogens and associated toxins.* Sensors, 2009. **9**(6): 4407-4445.

107. Conroy, P.J., et al., *Antibody production, design and use for biosensor-based applications.* Semin. Cell Dev. Biol., 2009. **20**(1): 10-26.

108. Ulman, A., *Formation and structure of self-assembled monolayers.* Chem. Rev., 1996. **96**(4): 1533-1554.

109. Weetall, H., *Preparation of immobilized proteins covalently coupled through silane coupling agents to inorganic supports.* Appl. Biochem. Biotechnol., 1993. **41**(3): 157-188.

110. Hermanson, G.T., *Bioconjugate Techniques*. 1st ed. 1996: Academic Press.

111. Narang, U., et al., *Fiber optic-based biosensor for ricin.* Biosens. Bioelectron., 1997. **12**(9-10): 937-945.

112. Orth, R.N., T.G. Clark, and H.G. Craighead, *Avidin-biotin micropatterning methods for biosensor applications.* Biomed. Microdevices, 2003. **5**(1): 29-34.

113. Love, J.C., et al., *Self-assembled monolayers of thiolates on metals as a form of nanotechnology.* Chem. Rev., 2005. **105**(4): 1103-1169.

114. Oh, B.K., et al., *Surface plasmon resonance immunosensor using self-assembled protein G for the detection of Salmonella paratyphi.* J. Biotechnol., 2004. **111**(1): 1-8.

115. Fowler, J.M., M.C. Stuart, and D.K.Y. Wong, *Self-assembled layer of thiolated Protein G as an immunosensor scaffold.* Anal. Chem., 2007. **79**(1): 350-354.

116. Oh, B.K., et al., *Surface plasmon resonance immunosensor for the detection of Salmonella typhimurium.* Biosens. Bioelectron., 2004. **19**(11): 1497-1504.

117. Hong, S.-R., et al., *Development of QCM biosensor to detect a marine derived pathogenic bacteria Edwardsiella tarda using a novel immobilisation method.* Biosens. Bioelectron., 2009. **24**(6): 1635-1640.

118. Brogan, K.L., et al., *Direct oriented immobilization of F(ab') antibody fragments on gold.* Anal. Chim. Acta, 2003. **496**(1-2): 73-80.

119. O'Brien, J.C., et al., *Immunosensing platforms using spontaneously adsorbed antibody fragments on gold.* Anal. Chem., 2000. **72**(4): 703-710.

120. Lucarelli, F., et al., *Electrochemical and piezoelectric DNA biosensors for hybridisation detection.* Anal. Chim. Acta, 2008. **609**(2): 139-159.

121. Herne, T.M. and M.J. Tarlov, *Characterization of DNA probes immobilized on gold surfaces.* J. Am. Chem. Soc., 1997. **119**(38): 8916-8920.

122. Diamandis, E. and T. Christopoulos, *The biotin-(strept)avidin system: principles and applications in biotechnology.* Clin. Chem., 1991. **37**(5): 625-636.

123. Caruso, F., et al., *In-situ measurement of DNA immobilization and hybridization using a 27 MHz quartz crystal microbalance.* Colloids Surf. B Biointerfaces, 1998. **10**(4): 199-204.

124. Su, X.D., et al., *Detection of point mutation and insertion mutations in DNA using a quartz crystal microbalance and MutS, a mismatch binding protein.* Anal. Chem., 2004. **76**(2): 489-494.

125. Zhou, X.C., L.Q. Huang, and S.F.Y. Li, *Microgravimetric DNA sensor based on quartz crystal microbalance: comparison of oligonucleotide immobilization methods and the application in genetic diagnosis.* Biosens. Bioelectron., 2001. **16**(1-2): 85-95.

126. Bruno, J.G. and J.L. Kiel, *In vitro selection of DNA aptamers to anthrax spores with electrochemiluminescence detection.* Biosens. Bioelectron., 1999. **14**(5): 457-464.

127. Wang, C., et al., *Single-stranded DNA aptamers that bind differentiated but not parental cells: subtractive systematic evolution of ligands by exponential enrichment.* J. Biotechnol., 2003. **102**(1): 15-22.

128. Huizenga, D.E. and J.W. Szostak, *A DNA aptamer that binds adenosine and ATP.* Biochemistry, 1995. **34**(2): 656-665.

129. Boiziau, C., et al., *DNA aptamers selected against the HIV-1 trans-activation-responsive RNA element form RNA-DNA kissing complexes.* J. Biol. Chem., 1999. **274**(18): 12730-12737.

130. Wiegand, T., et al., *High-affinity oligonucleotide ligands to human IgE inhibit binding to Fc epsilon receptor I.* J. Immunol., 1996. **157**(1): 221-230.

131. Jeon, S.H., et al., *A DNA aptamer prevents influenza infection by blocking the receptor binding region of the viral hemagglutinin.* J. Biol. Chem., 2004. **279**(46): 48410-48419.

132. Vianini, E., M. Palumbo, and B. Gatto, *In vitro selection of DNA aptamers that bind-tyrosinamide.* Bioorg. Med. Chem., 2001. **9**(10): 2543-2548.

133. Miyake, Y., et al., *MercuryII-mediated formation of thymine-Hg^{II}-thymine base pairs in DNA duplexes.* J. Am. Chem. Soc., 2006. **128**(7): 2172-2173.

134. Santoro, S.W. and G.F. Joyce, *A general purpose RNA-cleaving DNA enzyme.* Proc. Natl. Acad. Sci. USA, 1997. **94**(9): 4262-4266.

135. Balamurugan, S., et al., *Surface immobilization methods for aptamer diagnostic applications.* Anal. Bioanal. Chem., 2008. **390**(4): 1009-1021.

136. Liu, J., Z. Cao, and Y. Lu, *Functional nucleic acid sensors.* Chem. Rev., 2009. **109**(5): 1948-1998.

137. Balasubramanian, S., et al., *Lytic phage as a specific and selective probe for detection of Staphylococcus aureus - A surface plasmon resonance spectroscopic study.* Biosens. Bioelectron., 2007. **22**(6): 948-955.

138. Gervais, L., et al., *Immobilization of biotinylated bacteriophages on biosensor surfaces.* Sens. Actuators B: Chem., 2007. **125**(2): 615-621.

139. Shabani, A., et al., *Bacteriophage-modified microarrays for the direct impedimetric detection of bacteria.* Anal. Chem., 2008. **80**(24): 9475-9482.

140. Campas, M. and J.-L. Marty, *Enzyme sensor for the electrochemical detection of the marine toxin okadaic acid.* Anal. Chim. Acta, 2007. **605**(1): 87-93.

141. Campas, M., et al., *Enzyme inhibition-based biosensor for the electrochemical detection of microcystins in natural blooms of cyanobacteria.* Talanta, 2007. **72**(1): 179-186.

142. Villatte, F., et al., *A disposable acetylcholinesterase-based electrode biosensor to detect anatoxin-a(s) in water.* Anal. Bioanal. Chem., 2002. **372**(2): 322-326.

143. Alfonta, L., et al., *Electrochemical and quartz crystal microbalance detection of the cholera toxin employing horseradish peroxidase and GM1-functionalized liposomes.* Anal. Chem., 2001. **73**(21): 5287-5295.

144. Suresh, S., et al., *Detection of ricin in water samples using disposable screen-printed electrodes.* Def. Sci. J., 2007. **57**(6): 839-844.

145. Fritz, J., *Cantilever biosensors.* Analyst, 2008. **133**(7): 855-863.

146. Goeders, K.M., J.S. Colton, and L.A. Bottomley, *Microcantilevers: Sensing chemical interactions via mechanical motion.* Chem. Rev., 2008. **108**(2): 522-542.

147. Waggoner, P.S. and H.G. Craighead, *Micro- and nanomechanical sensors for environmental, chemical, and biological detection.* Lab Chip, 2007. **7**(10): 1238-1255.

148. Xu, S. and R. Mutharasan, *Cantilever biosensors in drug discovery.* Expert Opin. Drug Discov., 2009. **4**(12): 1237-1251.

149. Buttry, D.A. and M.D. Ward, *Measurement of interfacial processes at electrode surfaces with the electrochemical quartz crystal microbalance.* Chem. Rev., 1992. **92**(6): 1355-1379.

150. Janshoff, A., H.J. Galla, and C. Steinem, *Piezoelectric mass-sensing devices as biosensors - An alternative to optical biosensors?* Angew. Chem.-Int. Edit., 2000. **39**(22): 4004-4032.

151. Kim, G.H., A.G. Rand, and S.V. Letcher, *Impedance characterization of a piezoelectric immunosensor Part I: Antibody coating and buffer solution.* Biosens. Bioelectron. , 2003. **18**(1): 83-89.

152. Kim, G.-H., A.G. Rand, and S.V. Letcher, *Impedance characterization of a piezoelectric immunosensor part II: Salmonella typhimurium detection using magnetic enhancement.* Biosens. Bioelectron. , 2003. **18**(1): 91-99.

153. Su, X.-L. and Y. Li, *A QCM immunosensor for Salmonella detection with simultaneous measurements of resonant frequency and motional resistance.* Biosens. Bioelectron. , 2005. **21**(6): 840-848.

154. Xie, Q., et al., *A Study of Depletion Layer Effects on Equivalent Circuit Parameters Using an Electrochemical Quartz Crystal Impedance System.* Anal. Chem., 1999. **71**(20): 4649-4656.

155. Xie, Q.J., et al., *Simultaneous impedance measurements of two one-face sealed resonating piezoelectric quartz crystals for in situ monitoring of electrochemical processes and solution properties.* Anal. Chim. Acta, 2005. **533**(2): 213-224.

156. Wegener, J., et al., *Analysis of the Composite Response of Shear Wave Resonators to the Attachment of Mammalian Cells.* Biophys. J., 2000. **78**(6): 2821-2833.

157. Heitmann, V. and J. Wegener, *Monitoring Cell Adhesion by Piezoresonators: Impact of Increasing Oscillation Amplitudes.* Anal. Chem., 2007. **79**(9): 3392-3400.

158. Rijal, K. and R. Mutharasan, *Piezoelectric-excited millimeter-sized cantilever sensors detect density differences of a few micrograms/mL in liquid medium.* Sens. Actuators B: Chem., 2007. **124**(1): 237-244.

159. Sader, J.E., *Frequency response of cantilever beams immersed in viscous fluids with applications to the atomic force microscope.* J. Appl. Phys., 1998. **84**(1): 64-76.

160. Maraldo, D. and R. Mutharasan, *10-minute assay for detecting Escherichia coli O157 : H7 in ground beef samples using piezoelectric-excited millimeter-size cantilever sensors.* J. Food Prot. , 2007. **70**(7): 1670-1677.

161. Maraldo, D. and R. Mutharasan, *Preparation-free method for detecting Escherichia coli O157 : H7 in the presence of spinach, spring lettuce mix, and ground beef particulates.* J. Food Prot. , 2007. **70**(11): 2651-2655.

162. Weast, R.C., *CRC Handbook of Chemistry and Physics*. 1982, Boca Raton, FL: CRC Press.

163. Maraldo, D. and R. Mutharasan, *Mass-change sensitivity of piezoelectric-excited millimeter-sized cantilever (PEMC) sensors: Model and experiments.* Sens. Actuators B: Chem. , 2008. **132**(1): 140-148.

164. Chu, W.-H., *Technical Report No.2*, in *DTMB, Contract NObs-86396(X)*. 1963, Southwest Research Institute: San Antonio, Texas.

165. Campbell, G.A. and R. Mutharasan, *Detection of Bacillus anthracis spores and a model protein using PEMC sensors in a flow cell at 1 mL/min.* Biosens. Bioelectron. , 2006. **22**(1): 78-85.

166. Sabot, A. and S. Krause, *Simultaneous quartz crystal microbalance impedance and electrochemical impedance measurements. Investigation into the degradation of thin polymer films.* Anal. Chem., 2002. **74**(14): 3304-3311.

167. Rijal, K. and R. Mutharasan, *PEMC-based method of measuring DNA hybridization at femtomolar concentration directly in human serum and in the presence of copious noncomplementary strands.* Anal. Chem., 2007. **79**(19): 7392-7400.

168. Lakshmanan, R.S., S. Xu, and R. Mutharasan, *Impedance change as an alternate measure of resonant frequency shift of piezoelectric-excited millimeter-sized cantilever (PEMC) sensors.* Sens. Actuators B: Chem., 2010. **145**(1): 601-604.

169. Campbell, G.A., et al., *Detect of Escherichia coli O157 : H7 in ground beef samples using piezoelectric excited millimeter-sized cantilever (PEMC) sensors.* Biosens. Bioelectron. , 2007. **22**(7): 1296-1302.

170. Fayer, R., U. Morgan, and S.J. Upton, *Epidemiology of Cryptosporidium: transmission, detection and identification.* Int. J. Parasitol., 2000. **30**(12-13): 1305-1322.

171. Mead, P.S., et al., *Food-related illness and death in the United States.* Emerging Infect. Dis., 1999. **5**(5): 607-625.

172. Okhuysen, P.C., et al., *Virulence of three distinct Cryptosporidium parvum isolates for healthy adults.* J. Infect. Dis., 1999. **180**(4): 1275-1281.

173. Lisle, J.T. and J.B. Rose, *Cryptosporidium contamination of water in the USA and UK-A minireview.* J. Water Supp. Res. Technol., 1995. **44**(3): 103-117.

174. Mons, C., et al., *Monitoring of Cryptosporidium and Giardia river contamination in Paris area.* Water Res., 2009. **43**(1): 211-217.

175. USEPA, *Method 1623: Cryptosporidium and Giardia in Water by Filtration/IMS/FA 2005.* http://www.epa.gov/microbes/1623de05.pdf, 2005.

176. Johnson, D.W., et al., *Development of a PCR protocol for sensitive detection of Cryptosporidium oocysts in water samples.* Appl. Environ. Microbiol., 1995. **61**(11): 3849-3855.

177. Xiao, L.H., et al., *Molecular characterization of Cryptosporidium oocysts in samples of raw surface water and wastewater.* Appl. Environ. Microbiol., 2001. **67**(3): 1097-1101.

178. Rosenblatt, J.E. and L.M. Sloan, *Evaluation of an enzyme-linked immunosorbent assay for detection of Cryptosporidium spp in stool specimens* J. Clin. Microbiol., 1993. **31**(6): 1468-1471.

179. Lindergard, G., et al., *Detection of Cryptosporidium oocysts in soil samples by enzyme-linked immunoassay.* Vet. Parasitol., 2001. **94**(3): 163-176.

180. Kang, C.D., et al., *Performance enhancement of real-time detection of protozoan parasite, Cryptosporidium oocyst by a modified surface plasmon resonance (SPR) biosensor.* Enzyme Microb. Technol., 2006. **39**(3): 387-390.

181. Kang, C.D., et al., *Surface plasmon resonance-based inhibition assay for real-time detection of Cryptosporidium parvum oocyst.* Water Res., 2008. **42**(6-7): 1693-1699.

182. Poitras, C., J. Fatisson, and N. Tufenkji, *Real-time microgravimetric quantification of Cryptosporidium parvum in the presence of potential interferents.* Water Res., 2009. **43**(10): 2631-2638.

183. Xu, S. and R. Mutharasan, *Detection of Cryptosporidium parvum in buffer and in complex matrix using PEMC sensors at 5 oocysts mL^{-1}.* Anal. Chim. Acta, 2010. **699**(1-2): 81-86.

184. Baeumner, A.J., et al., *Detection of viable oocysts of Cryptosporidium parvum following nucleic acid sequence based amplification.* Anal. Chem., 2001. **73**(6): 1176-1180.

185. Kozwich, D., et al., *Development of a novel, rapid Integrated Cryptosporidium parvum detection assay.* Appl. Environ. Microbiol., 2000. **66**(7): 2711-2717.

186. Wang, J., et al., *Electrochemical biosensor for detecting DNA sequences from the pathogenic protozoan Cryptosporidium parvum.* Talanta, 1997. **44**(11): 2003-2010.

187. Zhu, L., et al., *Filter-based microfluidic device as a platform for immunofluorescent assay of microbial cells.* Lab Chip, 2004. **4**(4): 337-341.

188. Elmer, F.-J. and M. Dreier, *Eigenfrequencies of a rectangular atomic force microscope cantilever in a medium.* J. Appl. Phys., 1997. **81**(12): 7709-7714.

189. Li, M., H.X. Tang, and M.L. Roukes, *Ultra-sensitive NEMS-based cantilevers for sensing, scanned probe and very high-frequency applications.* Nat. Nanotechnol., 2007. **2**(2): 114-120.

190. Adams, J.D., et al., *Nanowatt chemical vapor detection with a self-sensing, piezoelectric microcantilever array.* Appl. Phys. Lett., 2003. **83**(16): 3428-3430.

191. Campbell, G.A. and R. Mutharasan, *Detection and quantification of proteins using self-excited PZT-glass millimeter-sized cantilever.* Biosens. Bioelectron., 2005. **21**(4): 597-607.

192. Hwang, K.S., et al., *Quantification of disease marker in undiluted serum using an actuating layer-embedded microcantilever.* J. Appl. Phys., 2009. **105**(10): 102017.

193. Adam, R.D., *Biology of Giardia lamblia.* Clin. Microbiol. Rev., 2001. **14**(3): 447-475.

194. Caccio, S.M., et al., *Unravelling Cryptosporidium and Giardia epidemiology.* Trends Parasitol., 2005. **21**(9): 430-437.

195. Savioli, L., H. Smith, and A. Thompson, *Giardia and Cryptosporidium join the 'Neglected Diseases Initiative'.* Trends Parasitol., 2006. **22**(5): 203-208.

196. Rochelle, P.A., et al., *Comparison of primers and optimization of PCR conditions for detection of Cryptosporidium parvum and Giardia lamblia in water.* Appl. Environ. Microbiol., 1997. **63**(1): 106-114.

197. Guy, R.A., et al., *Real-time PCR for quantification of Giardia and Cryptosporidium in environmental water samples and sewage.* Appl. Environ. Microbiol., 2003. **69**(9): 5178-5185.

198. Rosenblatt, J.E., L.M. Sloan, and S.K. Schneider, *Evaluation of an enzyme-linked-immunosorbent-assay for the detection of Giardia lamblia in stool specimens* Diagn. Microbiol. Infect. Dis., 1993. **16**(4): 337-341.

199. Maraha, B. and A.G.M. Buiting, *Evaluation of four enzyme immunoassays for the detection of Giardia lamblia antigen in stool specimens.* Eur. J. Clin. Microbiol. Infect. Dis., 2000. **19**(6): 485-487.

200. Rule, K.L. and P.J. Vikesland, *Surface-enhanced resonance Raman spectroscopy for the rapid detection of Cryptosporidium parvum and Giardia lamblia.* Environ. Sci. Technol., 2009. **43**(4): 1147-1152.

201. Li, X.X., et al., *Detection of pathogen based on the catalytic growth of gold nanocrystals.* Water Res., 2009. **43**(5): 1425-1431.

202. Campbell, G.A. and R. Mutharasan, *Method of measuring Bacillus anthracis spores in the presence of copious amounts of Bacillus thuringiensis and Bacillus cereus.* Anal. Chem., 2007. **79**(3): 1145-1152.

203. Garcia, L. and R. Shimizu, *Evaluation of nine immunoassay kits (enzyme immunoassay and direct fluorescence) for detection of Giardia lamblia and Cryptosporidium parvum in human fecal specimens.* J. Clin. Microbiol., 1997. **35**(6): 1526-1529.

204. Garcia, L.S., et al., *Commercial assay for detection of Giardia lamblia and Cryptosporidium parvum antigens in human fecal specimens by rapid solid-phase qualitative immunochromatography.* J. Clin. Microbiol., 2003. **41**(1): 209-212.

205. Oster, N., et al., *Evaluation of the immunochromatographic CORIS Giardia-Strip test for rapid diagnosis of Giardia lamblia.* Eur. J. Clin. Microbiol. Infect. Dis., 2006. **25**(2): 112-115.

206. Xu, S. and R. Mutharasan, *Rapid and sensitive detection of Giardia lamblia using a piezoelectric cantilever biosensor in finished and source waters.* Environ. Sci. Technol., 2010. **44**(5): 1736-1741.

207. Huang, D.B. and A.C. White, *An updated review on Cryptosporidium and Giardia.* Gastroenterol. Clin. North Am., 2006. **35**(2): 291-314.

208. Squires, T.M., R.J. Messinger, and S.R. Manalis, *Making it stick: convection, reaction and diffusion in surface-based biosensors.* Nat. Biotechnol., 2008. **26**(4): 417-426.

209. Xu, S., H. Sharma, and R. Mutharasan, *Sensitive and selective detection of mycoplasma in cell culture samples using cantilever sensors.* Biotechnol. Bioeng., 2010. **105**(6): 1069-1077.

210. Taylor-Robinson, D. and C. Bebear, *Antibiotic susceptibilities of mycoplasmas and treatment of mycoplasmal infections.* J. Antimicrob. Chemother., 1997. **40**(5): 622-630.

211. Rawadi, G. and O. Dussurget, *Advances in PCR-based detection of mycoplasmas contaminating cell cultures.* PCR Methods Appl., 1995. **4**(4): 199-208.

212. Drexler, H.G. and C.C. Uphoff, *Mycoplasma contamination of cell cultures: Incidence, sources, effects, detection, elimination, prevention.* Cytotechnology, 2002. **39**(2): 75-90.

213. Rottem, S. and M.F. Barile, *Beware of mycoplasmas.* Trends Biotechnol., 1993. **11**(4): 143-151.

214. McGarrity, G.J., *Detection of mycoplasma infection of cell cultures*, in *Advances in cell cultures*, K. Maramorosch, Editor. 1982, Academic Press, Inc.: New York. p. 99-131.

215. Uphoff, C.C. and H.G. Drexler, *Comparative PCR analysis for detection of mycoplasma infections in continuous cell lines.* In Vitro Cell Dev. Biol., 2002. **38**(2): 79-85.

216. FDA, *Points to consider in the characterization of cell lines used to produce biological products*. 1993.

217. Masover, G.K. and F.A. Becker, *Methodology for detection of mycoplasmas in cell cultures used to produce human pharmaceuticals*, in *Automated microbial identification and quantitation*, W. Olsen, Editor. 1996, Interpharm Press: Grove, IL. p. 149-177.

218. Eldering, J.A., et al., *Development of a PCR method for mycoplasma testing of Chinese hamster ovary cell cultures used in the manufacture of recombinant therapeutic proteins.* Biologicals, 2004. **32**(4): 183-193.

219. Tang, J., et al., *A polymerase chain reaction based method for detecting Mycoplasma/Acholeplasma contaminants in cell culture.* J. Microbiol. Methods, 2000. **39**(2): 121-126.

220. Wirth, M., et al., *Detection of mycoplasma contaminations by the polymerase chain reaction.* Cytotechnology, 1994. **16**(2): 67-77.

221. Garner, C.M., L.M. Hubbold, and P.R. Chakraborti, *Mycoplasma detection in cell cultures: a comparison of four methods.* Br. J. Biomed. Sci., 2000. **57**(4): 295-301.

222. Timenetsky, J., et al., *Detection of multiple mycoplasma infection in cell cultures by PCR.* Braz. J. Med. Biol. Res., 2006. **39**: 907-914.

223. Woolley, D.E., et al., *Electrochemical monitoring of cell behaviour in vitro: A new technology.* Biotechnol. Bioeng., 2002. **77**(7): 725-733.

224. Park, T.H. and M.L. Shuler, *Integration of cell culture and microfabrication technology.* Biotechnol. Prog., 2003. **19**(2): 243-253.

225. Jordan, J.L. and E.J. Fernandez, *QCM-D sensitivity to protein adsorption reversibility.* Biotechnol. Bioeng., 2008. **101**(4): 837-842.

226. Campbell, C.E., et al., *Monitoring viral-induced cell death using electric cell-substrate impedance sensing.* Biosens. Bioelectron., 2007. **23**(4): 536-542.

227. Kintzios, S., et al., *Development of a novel, multi-analyte biosensor system for assaying cell division: Identification of cell proliferation/death precursor events.* Biosens. Bioelectron., 2006. **21**(7): 1365-1373.

228. De Palma, R., et al., *The optimization of magnetosandwich assays for the sensitive and specific detection of proteins in serum.* Anal. Chem., 2007. **79**(19): 7540-7548.

229. Teramura, Y. and H. Iwata, *Label-free immunosensing for α-fetoprotein in human plasma using surface plasmon resonance.* Anal. Biochem., 2007. **365**(2): 201-207.

230. Campbell, G.A. and R. Mutharasan, *Piezoelectric-excited millimeter-sized cantilever (PEMC) sensors detect Bacillus anthracis at 300 spores/mL.* Biosens. Bioelectron., 2006. **21**(9): 1684-1692.

231. Cao, C., et al., *A strategy for sensitivity and specificity enhancements in prostate specific antigen-α_1-antichymotrypsin detection based on surface plasmon resonance.* Biosens. Bioelectron., 2006. **21**(11): 2106-2113.

232. Cui, X., et al., *Real-time immunoassay of ferritin using surface plasmon resonance biosensor.* Talanta, 2003. **60**(1): 53-61.

233. Oshima, K., et al., *Quartz crystal microbalance assay for determination of plasma vitellogenin.* Sens. Actuators B: Chem., 2005. **105**(2): 473-478.

234. Lazcka, O., F.J.D. Campo, and F.X. Muñoz, *Pathogen detection: A perspective of traditional methods and biosensors.* Biosens. Bioelectron., 2007. **22**(7): 1205-1217.

235. Fu, Z., S. Rogelj, and T.L. Kieft, *Rapid detection of Escherichia coli O157 : H7 by immunomagnetic separation and real-time PCR.* Int. J. Food Microbiol., 2005. **99**(1): 47-57.

236. Perelle, S., et al., *Comparison of PCR-ELISA and LightCycler real-time PCR assays for detecting Salmonella spp. in milk and meat samples.* Mol. Cell. Probes, 2004. **18**(6): 409-420.

237. Ashworth, M., et al., *Use of PCR-Based Mycobacterium tuberculosis Genotyping To Prioritize Tuberculosis Outbreak Control Activities.* J. Clin. Microbiol., 2008. **46**(3): 856-862.

238. Rink, T.J., R.Y. Tsien, and T. Pozzan, *Cytoplasmic pH and free Mg^{2+} in lymphocytes.* J. Cell Biol., 1982. **95**(1): 189-196.

239. Wierda, W.G., D.S. Mehr, and K. Yoon Berm, *Comparison of fluorochrome-labeled and 51Cr-labeled targets for natural killer cytotoxicity assay.* J. Immunol. Methods, 1989. **122**(1): 15-24.

240. Heo, J., et al., *A Microfluidic Bioreactor Based on Hydrogel-Entrapped E. coli: Cell Viability, Lysis, and Intracellular Enzyme Reactions.* Anal. Chem., 2003. **75**(1): 22-26.

241. Chabot, V., et al., *Biosensing based on surface plasmon resonance and living cells.* Biosens. Bioelectron., 2009. **24**(6): 1667-1673.

242. Ozkan, P. and R. Mutharasan, *A rapid method for measuring intracellular pH using BCECF-AM.* Biochim. Biophys. Acta, 2002. **1572**(1): 143-148.

243. Xu, S. and R. Mutharasan, *A novel method for monitoring mass-change response of piezoelectric-excited millimeter-sized cantilever (PEMC) sensors.* Sens. Actuators B: Chem., 2009. **143**(1): 144-151.

244. Fujikawa, H., A. Kai, and S. Morozumi, *A new logistic model for Escherichia coli growth at constant and dynamic temperatures.* Food Microbiol., 2004. **21**(5): 501-509.

245. Meyer, G.D., et al., *Nonspecific binding removal from protein microarrays using thickness shear mode resonators.* IEEE Sens. J., 2006. **6**(2): 254-261.

246. Cular, S., et al., *Removal of nonspecifically bound proteins on microarrays using surface acoustic waves.* IEEE Sens. J., 2008. **8**(3-4): 314-320.

247. Dultsev, F.N., V.P. Ostanin, and D. Klenerman, *"Hearing" bond breakage. Measurement of bond rupture forces using a quartz crystal microbalance.* Langmuir, 2000. **16**(11): 5036-5040.

248. Cooper, M.A., et al., *Direct and sensitive detection of a human virus by rupture event scanning.* Nat. Biotechnol., 2001. **19**(9): 833-837.

249. Yuan, Y.J., et al., *Bond rupture of biomolecular interactions by resonant quartz crystal.* Anal. Chem., 2007. **79**(23): 9039-9044.

250. Yue, M., et al., *Label-free protein recognition two-dimensional array using nanomechanical sensors.* Nano Lett., 2008. **8**(2): 520-524.

VITA

Sen Xu was born in Changsha, China in 1984. He attended Donghua University in Shanghai, China, and received a Bachelor of Engineering degree in Polymer Science and Engineering with highest honors in 2006. Then he flew over the ocean to the United States to pursue a Ph.D. degree in Chemical Engineering at Drexel University.

Since 2006, Sen has been doing research on biosensors development for biological contaminants detection, under the supervision of Dr. Raj Mutharasan. He was supported by Teaching Assistantship and Research Assistantship during the stay in Drexel. His research was funded by the Environmental Protection Agency and the National Science Foundation. During the course of studies, he has published seven peer-reviewed papers, one invited book chapter in *Environmental Microbiology*, and presented research results in national and international meetings 1-2 times every year. He has also co-filed two patent applications. He is a member of the American Institute of Chemical Engineers and the American Chemical Society.